学位論文

A Modeling Study on Coupling between Westerly Wind Events and ENSO

(西風イベントとENSOの結合に関するモデル研究)

平成27年12月博士 (理学) 申請

東京大学大学院理学系研究科
地球惑星科学専攻

林 未知也

Doctoral Dissertation

A Modeling Study on Coupling between Westerly Wind Events and ENSO

by

Michiya Hayashi

Department of Earth and Planetary Science

Graduate School of Science

The University of Tokyo

December, 2015

Abstract

Westerly wind events (WWEs), defined as strong surface westerly wind anomalies that persist for a few days to weeks over the western-central equatorial Pacific, are observed frequently during El Niño. Despite the short timescale, the WWE has been considered as an important factor for the El Niño-Southern Oscillation (ENSO) phenomenon having a typical period of 3–7 years. WWEs act to increase sea surface temperature (SST) in the central-eastern equatorial Pacific, and the warmer SST in turn favors the occurrence of WWEs. These potentially serve as a positive feedback between WWEs and ENSO. However, the detailed mechanisms of the interaction between them are not fully unraveled yet. It is particularly important to clarify (i) processes responsible for the response of the atmosphere and ocean to WWEs in the presence of annual cycle, (ii) state dependence and asymmetry of WWEs and their easterly counterpart called easterly wind events (EWEs), and (iii) role of the state dependence of WWEs in generating the complexity of ENSO. The purpose of this study is to advance understanding of the WWE-ENSO coupling using a hierarchy of coupled atmosphere-ocean models and observational data.

In Chapter 2, responses of the atmosphere-ocean coupled system to WWEs were examined by ensemble experiments using a coupled atmosphere-ocean general circulation model (CGCM) with a prescribed single WWE imposed at several different timings and locations. It is found that the lagged responses of the atmosphere and ocean to WWEs depend much on the timings of the imposed WWEs as an interaction with the annual cycle in the atmosphere and ocean is crucial. WWEs in May warm the eastern Pacific initially through the oceanic equatorial Kelvin wave propagating on a seasonally steeper thermocline tilt in the east. The warming then induces the equatorward shift of the rain belt over the Pacific, causing further warming in the equatorial Pacific by weakening easterly trade winds and poleward surface currents. On the other hand, WWEs in March increase SST only in the easternmost Pacific since the thermocline is flatter and the rain belt is not active when the response occurs. The above model experiments enable us to identify a

favorable set of combinations of timing and location that maximize the impact of WWEs on El Niño in the subsequent winter. By repeating the ensemble experiments with ocean initial states in El Niño and La Niña years, it is shown that WWEs are more efficient to amplify El Niño but are not efficient to suppress La Niña.

Chapter 3 showed the characteristics of WWEs and EWEs. Their state dependence and asymmetry are analyzed by using observational daily data of atmosphere and ocean fields. By referring to the surface zonal wind anomalies over the equatorial Pacific for 1982–2013 as reference, 101 WWEs and 23 EWEs are detected. Both types of events tend to appear over the Pacific warm pool, where SST is sufficiently high for active deep convection, with a similar seasonality, and they favorably occur with increasing SST in the Niño4 region (160 °E–150 °W, 5 °S–5 °N). The relationship of the occurrence of both events with the Madden-Julian oscillation is also identified. However, the occurrence frequency of EWEs is much less than that of WWEs, confirmed from a comparison of their characteristics based on different criteria for the event detection. The asymmetry in the occurrence frequency between WWEs and EWEs is caused by different local development processes associated with intraseasonal low-level zonal winds. The importance of both local and remote anomalous convections in exciting these events is demonstrated by using linear baroclinic model experiments.

In Chapter 4, role of coupling between WWEs and ENSO in the complexity of ENSO was examined using a coupled atmosphere-ocean model with an intermediate complexity. The model produces an ENSO-like oscillation by tuning a parameter (γ) that controls efficiency of the thermocline feedback. By referring to the observational statistics shown in Chapter 3 as the basis, WWEs are parameterized as state-dependent stochastic noise in surface zonal stress anomalies. Numerical experiments without the noise (denoted as NO) produce a regular ENSO-like oscillation with a period of 6 years, with its variance increasing with γ. When additive (purely stochastic) noise is given to the model over the western Pacific (experiment AD), oscillations become irregular with the dominant

period of about 5 years and the increase of its variance relative to NO depends on γ. When the state-dependent noise is incorporated (experiment SD), the oscillatory solution is also irregular besides its variance and asymmetry increase irrespective of the value of γ. Both the additive and state-dependent noises help to produce two types of ENSO-like oscillation, corresponding to the eastern-Pacific (EP) and central-Pacific (CP) El Niños. The noise tends to produce CP El Niño in boreal winter and to trigger EP El Niño in early summer even in AD due to the seasonally varying response to the noise (cf. Chapter 2). EP El Niño is magnified in SD due to the eastward shift of the noise location caused by the warm pool expansion. CP El Niño is even favored by the state-dependent stochastic noise, which enhances the zonal advection to warm the central Pacific, and in turn the warmer Niño4 SST increases the probability of occurrence of the noise. This positive feedback ensures the existence of CP El Niño regardless of γ in SD, while the number of CP El Niño declines with larger γ in AD. The above results thereby suggest that the state dependence of WWEs may play a crucial role in the asymmetry and diversity of ENSO in nature.

This study shows the crucial roles of the coupling between the atmosphere-ocean annual cycle and the response to WWEs (Chapter 2), and of the state-dependent WWEs in the rich behavior of ENSO (Chapter 4). The uneven occurrence probability of WWEs and EWEs, although they both have the similar state dependence and seasonality, emphasizes the relative importance of WWEs on El Niño (Chapter 3). This study also advocates that the WWE-SST feedback ensures the ENSO asymmetry and the existence of CP El Niño in nature. From the above results, it is clear that the ENSO mechanism is considerably affected by the background annual cycle, state-dependent high-frequency atmospheric disturbances, and interaction among them. This suggests that the reproducibility of these factors greatly influences the El Niño prediction skills and future projections of ENSO in CGCMs.

Acknowledgment

I would like to express the deepest appreciation to Prof. Masahiro Watanabe, the supervisor, for his patient guidance, constructive suggestions, and thoughtful supports.

I am deeply grateful to the members of this dissertation committee, Profs. Yukari Takayabu, Masahide Kimoto, Hiroaki Miura, and Tomoki Tozuka, for their many important suggestions and encouragements. I would particularly thank to Prof. Fei-Fei Jin at the University of Hawaii for his constructive comments and warm encouragements in my visiting to his laboratory. I would also like to thank Prof. Masaki Satoh at the University of Tokyo, Prof. Shoshiro Minobe at Hokkaido University, Drs. Shuhei Maeda and Yukiko Imada at Meteorological Research Institute, Prof. Axel Timmermann at the University of Hawaii, Prof. Matthieu Lengaigne and Dr. Jérôme Vialard at Institut de Recherche pour le Développement, Prof. Soon-Il An at Yonsei University, Prof. Sarah M. Kang at Ulsan National Institute of Science and Technology, and Dr. Shayne McGregor at the University of New South Wales for their helpful discussions. ZC-mLBM used in Chapter 4 was provided by Profs. Soon-Il An and Masahiro Watanabe. MIROC5 used in Chapter 2 was provided by Drs. Koji Ogochi, Tatsuo Suzuki, and Hiroaki Tatebe at Japan Agency for Marine-Earth Science and Technology. Prof. Harry H. Hendon at Bureau of Meteorology kindly provided me with MJO index data used in Chapter 3 and helpful suggestions. This work was supported by JSPS KAKENHI Grant Number 25-5379.

Special thanks are given to Prof. Hisanori Itoh at Kyuhsu University, the supervisor in my master course, for his encouragements. I also thank Drs. Masato Mori, Lestari R. Kartika, Chiharu Takahashi, Takahito Kataoka, Ms. Natsumi Yamamoto, and all members of Division of Climate System Research for their useful comments. I am particularly grateful for the assistance given by Ms. Kazuki Matsumoto and Ms. Hisae Tamura. I want to thank Mr. Kei Kawamura for his encouragement at Iwakuni Senior High School. Finally, I would like to express my gratitude to my friends, family, and parents, Masayuki and Hatsumi, for their kind supports.

Contents

Chapter 1

General introduction

The El Niño-Southern Oscillation (ENSO) phenomenon is the most energetic coupled atmosphere-ocean variability in the equatorial Pacific with typical period of 3–7 years. ENSO is usually characterized by sea surface temperature (SST) anomaly in the eastern equatorial Pacific (e.g., Niño3 region, 90 °–150 °W, 5 °S–5 °N) and its warm and cold phases are called El Niño and La Niña, respectively. The temporal SST variation in the equatorial Pacific is shown in Figs. 1.1a and 1.2a. It is seen that extremely strong El Niños occurred in 1982/83 and 1997/98, relatively weak El Niños in 1986/87, 1991/92, and 2002/03, and La Niñas in 1984/85, 1988/89, and 1998–2000.

In classical theories (e.g., Schopf and Suarez 1988; Battisti and Hirst 1989; Jin 1997a), the ENSO cycle has been interpreted as an unstable oscillatory solution of the coupled system. For instance, positive SST anomaly during El Niño is accompanied by anomalous westerly (Figs. 1.1b and 1.2b), which induces anomalous eastward surface currents and deepens thermocline. Then, the eastward surface currents advect warm water to the east, while the subsurface warm water associated with the deepened thermocline (Figs. 1.1c and 1.2c) is entrained into the surface due to mean equatorial upwelling. Therefore, both the processes act as positive feedbacks to further increase the SST. On the other hand, off-equatorial cyclonic curl associated with the anomalous westerly causes a slow poleward heat transport in the subsurface layer, and results in a shoaling of the zonal mean

thermocline. This acts as a delayed negative feedback by entraining cold water below the thermocline into the surface, and La Niña begins to develop. The turn about from La Niña to El Niño is vise versa. This oscillation cycle can explain the heart of ENSO mechanism. However, as shown in Fig. 1.1, the observed ENSO cycle is not purely periodic, but has a diverse structure, or the El Niño flavor (e.g., Yeh et al. 2014); 1997/98 El Niño has the SST maximum in the eastern Pacific (called eastern-Pacific (EP) El Niño) similar to conventional El Niño, while 2002/03 El Niño has the SST maximum in the central Pacific (called central-Pacific (CP) El Niño, Kao and Yu 2009), also named dateline El Niño (Larkin and Harrison 2005), El Niño Modoki (Ashok et al. 2007), or warm-pool El Niño (Kug et al. 2009). These diversity and irregularity of ENSO indicate that nonlinearity and external factors may modulate ENSO in nature.

Relationship between high-frequency atmospheric disturbances and ENSO can be detected in the temporally finer structures of El Niños in 1997/98 and 2002/03 (Figs. 1.3 and 1.4). While anomalous westerlies have the interannual components correlated with the SST anomalies, short-term strong westerlies that accompany active deep convections occur sporadically (Figs. 1.3b, c and 1.4b, c). These high-frequency westerly anomalies are called westerly wind events (WWEs) or westerly wind bursts (WWBs), defined as strong surface westerly wind anomalies that persist for a few days to weeks over the western and central equatorial Pacific (Luther et al. 1983; Hartten 1996; Harrison and Vecchi 1997; Seiki and Takayabu 2007a,b). WWEs may be associated with internal atmospheric variability in the tropics, such as the Madden-Julian oscillation (MJO), convectively-coupled Rossby wave, cold surge, and twin cyclones. Several criteria have been used to detect WWEs in surface wind datasets (Hartten 1996; Harrison and Vecchi 1997; Seiki and Takayabu 2007a; Chiodi et al. 2014). McPhaden (1999, 2004) indicated that successive occurrences of WWEs triggered and amplified El Niños in 1997 and 2002. Contrary, episodic easterly winds (easterly wind events, EWEs) may help terminate El Niño, as indicated by Takayabu et al. (1999) and Lengaigne et al. (2004, 2006). Takayabu et al. (1999)

showed a crucial role of the EWE, related with the atmospheric equatorial Kelvin wave coupled with deep convection, in the termination of 1997/98 El Niño. Using intraseasonal wind stress fields, Puy et al. (2015) characterized the spatio-temporal distribution of WWEs and EWEs, and suggested that occurrence probability of both WWEs and EWEs is affected by the MJO and convectively-coupled Rossby waves. However, their use of wind stress anomalies may affect the characteristics of atmospheric events since the wind stress nonlinearly depends on the surface wind.

WWEs tend to warm the equatorial Pacific in one direction through the ocean dynamics (Vecchi and Harrison 2000; Lengaigne et al. 2002; Belamari et al. 2003; Chiodi et al. 2014), and sometimes trigger El Niño (McPhaden 1999). That is, eastward wind stresses associated with WWEs advect warm water to the east, and also induce downwelling oceanic Kelvin waves, which deepen the thermocline in the eastern equatorial Pacific. These two dynamical processes can increase the SST. However, previous studies have suggested that the ocean response to WWEs depends on many factors: the longitudinal location of WWEs (Vecchi and Harrison 2000; Chiodi et al. 2014), zonal SST gradient (Harrison and Schopf 1984), tropical instability waves (TIWs) (Harrison and Giese 1988), mean state of zonal wind stresses and thermocline depth (Fedorov 2002), and phase of ENSO (Fedorov 2002; Hu et al. 2014; Fedorov et al. 2015). Latif et al. (1988) examined the oceanic response in a coupled atmosphere-ocean general circulation model (CGCM) to WWEs, and attempted to show the dependence of the response on seasonal timings of WWEs. However, no clear difference was observed in the model between experiments forced by WWEs in January and July due to unrealistic annual cycle in the precipitation. Recently, Chiodi and Harrison (2015) examined ocean response to EWEs using observational data and an ocean general circulation model (OGCM) forced by the climatological plus EWE wind stresses, and showed that EWEs cool the SST in the eastern equatorial Pacific in the following 2–3 months through ocean dynamics. These previous studies indicate that a robust picture of how WWEs impact the coupled system

is not obtained yet.

In many theoretical ENSO studies, high-frequency atmospheric disturbances have been simplified to stochastic additive noise. This treatment is justified by a far different time scale of WWEs against ENSO. The typical timescale of each WWE episode is shorter than a month, while that of ENSO is a few years. However, previous studies showed that WWEs are dependent on ENSO, namely, multiplicative. The state dependence of WWEs is supported by the observational fact that they occur frequently during El Niño and rarely occur during La Niña (Vecchi and Harrison 2000). In other words, the likelihood of the occurrence of WWEs increases when the warm pool expands to the east in association with the zonal contrast of SST (Lengaigne et al. 2003; Eisenman et al. 2005; Miyama and Hasegawa 2014) and sea level pressure (Yu et al. 2003). This can be dynamically interpreted as a high-frequency energy accumulation caused by the low-level background westerly, suggested either by observational analysis (Seiki and Takayabu 2007b) or by a modeling study (Sooraj et al. 2009). Using observational data, Kug et al. (2008) showed a significant increase of the noise variance during El Niño, and the interdecadal change in the state-dependent noise, which has been more energetic since the late 1970's. Gushchina and Dewitte (2012) reported the difference of the noise between EP and CP El Niños by separating the low-level intraseasonal zonal wind into the MJO and equatorial Rossby and Kelvin waves. State dependence of EWEs was also examined recently, but it is still unclear. Although frequent occurrence of EWEs during La Niña was suggested by Chiodi and Harrison (2015) using wind stress anomalies relative to the annual cycle, Puy et al. (2015) showed that, unlike the state dependence of WWEs, there was no dependence of EWEs on the ENSO cycle when focusing on intraseasonal wind stress fields. They further emphasized that WWEs and EWEs should be defined after removing the interannual component not to alter their relationship with ENSO. Levine and Jin (2015) confirmed that the state dependence of atmospheric noise remains even in the residual after both the linear and low-order nonlinear parts of the deterministic ENSO signal were removed.

Assuming a two-way interaction between WWEs and ENSO, the potential importance of their coupling on the ENSO cycle has been suggested by modeling studies. Perez et al. (2005) used a coupled atmosphere-ocean model with intermediate complexity forced by external noise. They showed that, while the irregular and symmetric ENSO cycle was produced by the additive stochastic noise, the state-dependent noise caused positively-skewed ENSO in the model. Eisenman et al. (2005) also investigated the coupling between WWEs and ENSO using an intermediate coupled model that has been stabilized by reducing the drag coefficient in wind stresses. They parameterized the WWE forcing in the central equatorial Pacific as a function of the warm pool extension, and indicated that low-frequency tail of occurrence of WWEs, corresponding to the envelop of episodic westerlies, was responsible for amplifying ENSO in the model (see also Zavala-Garay et al. 2005). They noted that the WWE modulation by the large-scale SST field is qualitatively equivalent to an increase in the atmosphere-ocean coupling strength controlled by the drag coefficient. Similar results were obtained using CGCMs (Lopez et al. 2013) and Zebiak-Cane (ZC) model (Zebiak and Cane 1987) with different noise parameterizations (Kapur et al. 2012; Kapur and Zhang 2012). Gebbie et al. (2007) parameterized state-dependent WWEs in an OGCM coupled with a statistical atmosphere model, and showed that the eastward shift of WWEs associated with the warm pool extension is important for the ENSO asymmetry via enhancing the eastward advection.

Coupling between the noise and ENSO has also been examined in the conceptual recharge oscillator model developed by Jin (1997a,b). Jin et al. (2007) and Levine and Jin (2010) introduced the stochastic forcing modulated by ENSO-related SST anomalies in their low-order model, and showed that the state-dependent noise enhances the instability of ENSO and its ensemble spreads besides increases the probability of occurrence of extremely large El Niños. Levine and Jin (2010) emphasized, as in Eisenman et al. (2005), that the low-frequency variability in the noise was necessary to influence ENSO in their model. Overall, the state-dependent noise tends to increase the variance and positive

skewness of ENSO, and the slow component of the noise is of importance to modulate ENSO.

The impact of WWEs on the El Niño flavor has also been focused in recent studies. Hu et al. (2014) and Fedorov et al. (2015) imposed a single WWE to a CGCM, and indicated that the initial state of the ocean was a key factor in the El Niño flavor in their model. When the initial ocean heat content is higher than normal, the WWE tends to excite an EP El Niño by warming the central and eastern Pacific via zonal advective and thermocline feedbacks. On the other hand, when the heat content is nearly normal, the WWE can produce a CP El Niño since the anomalous SST in the eastern Pacific is still negative and easterly wind anomaly persists there (see also, Xiang et al. 2013). Lian et al. (2014) and Chen et al. (2015) used a modified version of the ZC model with a parameterization of WWEs, and suggested that CP and extremely strong EP El Niños can be generated by the state-dependent WWEs. Lian et al. (2014) implied that the timing of occurrence of WWEs is crucial for the El Niño flavor, consistent with suggestions by Hu et al. (2014) and Fedorov et al. (2015). However, the role of the state-dependent WWEs in generating CP El Niño is still unclear since the previous studies did not compare their results with experiments with stochastic additive noise. Lopez and Kirtman (2013) showed the contributions of additive and multiplicative WWEs to the El Niño flavor in two CGCMs with a WWE parameterization. Their results depended on CGCMs, whose reproducibility of ENSO was different from each other. While WWEs affected both types of El Niño in one CGCM, they modified only EP El Niño in the other model. Although the above studies suggest the importance of WWEs on the El Niño flavor, the essential role of state dependence of WWEs in the coexistence of CP and EP El Niños should be clarified further.

Importance of coupling between atmospheric noise and ENSO on the ENSO cycle has so far been presented. However, as discussed above, several problems still remain.

- The dependence of the atmosphere-ocean coupled response to WWEs on the annual

cycle in both the ocean and atmosphere basic states should be clarified.

- The characteristics of atmospheric noise, i.e., WWEs and EWEs, should be assessed using both surface wind and wind stress data with careful definition of the events.

- Mechanism of the ENSO modulation due to atmospheric noise in a coupled system having a different stability needs to be elaborated. Role of the state dependence of WWEs in generating the El Niño flavor should also be clarified.

The objective of this study is to advance understanding of the coupling of WWEs with ENSO using a hierarchy of coupled atmosphere-ocean models and observational data. In particular, this study focuses on

- processes responsible for the response of the atmosphere and ocean to WWEs in the presence of annual cycle,

- observational evidence of the state dependence of WWEs and EWEs, as well as their asymmetry, and

- roles of the state dependence of WWEs in generating the complexity of ENSO.

In Chapter 2, the importance of annual cycle in the atmosphere-ocean coupled system for its response to WWEs is investigated using a CGCM forced by imposed WWEs. In short, the response of the coupled system to WWEs is shown to be influenced strongly by the annual cycle of the ocean subsurface temperature and the rain belt over the Pacific. A favorable set of combinations of timing and location that maximize the impact of WWEs on El Niños in the subsequent winter will be suggested.

In Chapter 3, the state dependence of WWEs and EWEs and their asymmetry are analyzed by using observational daily data of atmosphere and ocean fields. The atmospheric events are detected from zonal surface wind anomalies which retain intraseasonal component. A comparison of the characteristics of the events following different criteria for their detection shows the robustness of the state dependence and asymmetry between WWEs

and EWEs. Local and remote influences in the developing process of WWEs and EWEs are identified.

In Chapter 4, roles of coupling between WWEs and ENSO in the complexity of ENSO are examined using an intermediate coupled atmosphere-ocean model that produces ENSO-like oscillations. The model incorporates a parameterization of state-dependent WWEs by referring to the observational statistics in Chapter 3 as the basis. The annual cycles of both atmosphere and ocean are prescribed in the model given its importance on the ENSO cycle (Chapter 2). By perturbing a parameter controlling the model's ENSO stability, we qualify the ENSO modulation due to additive and state-dependent WWEs in stable and unstable regimes.

Chapter 5 summarizes the results in Chapters 2, 3, and 4, and provides conclusions of this study. Relationship among these chapters and comparisons with previous studies are also given there.

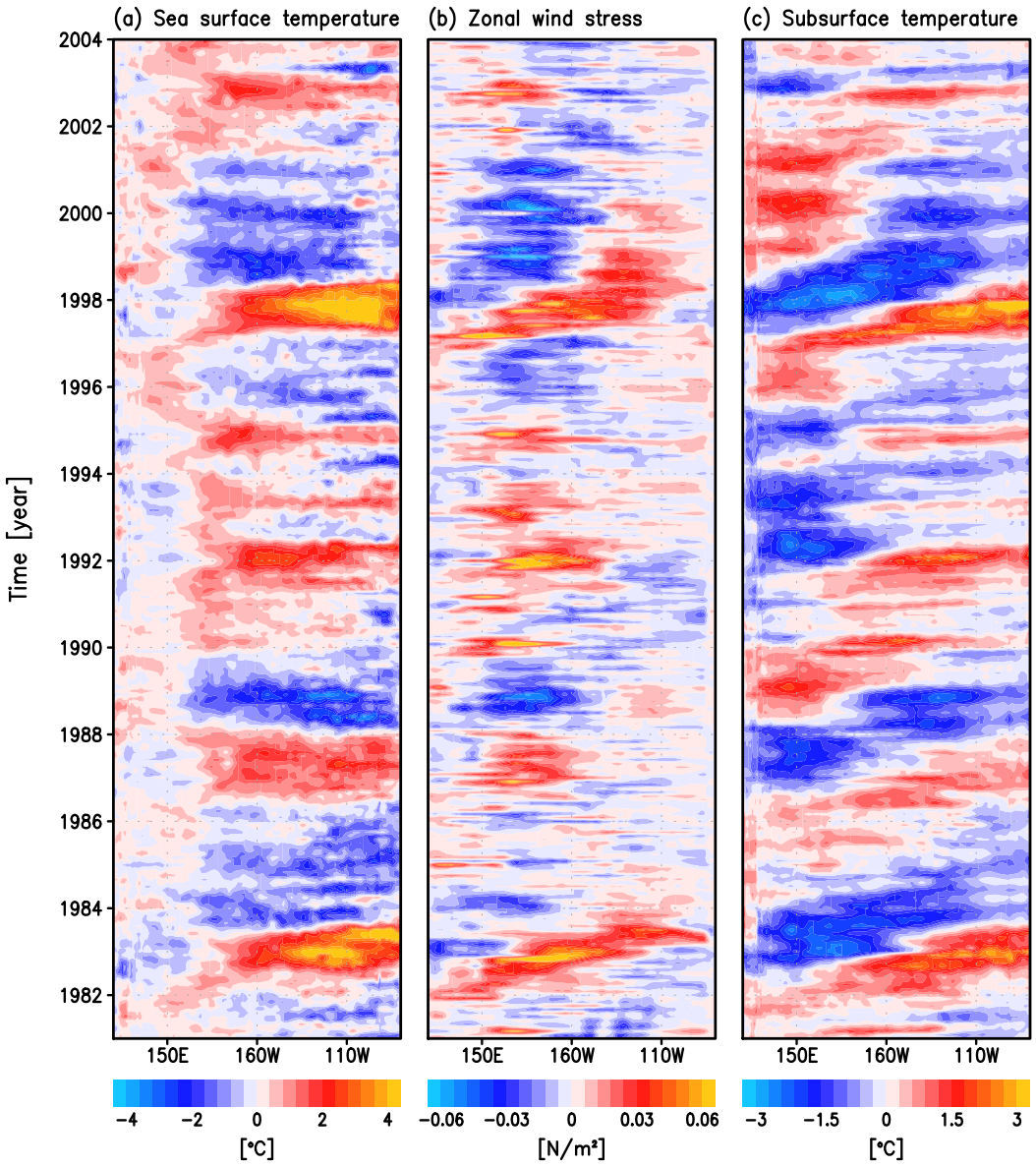

Figure 1.1: Time-longitudinal monthly plot of anomalies in (a) SST [°C], (b) zonal wind stress [N m^{-2}], and (c) subsurface temperature (ocean temperature averaged for 50–300 m depth) [°C] averaged between 2 °S and 2 °N in the Pacific from 1981 to 2003, derived from simple ocean data assimilation (SODA) data (Giese and Ray 2011). Climatology is defined as the monthly average for 1971–2000.

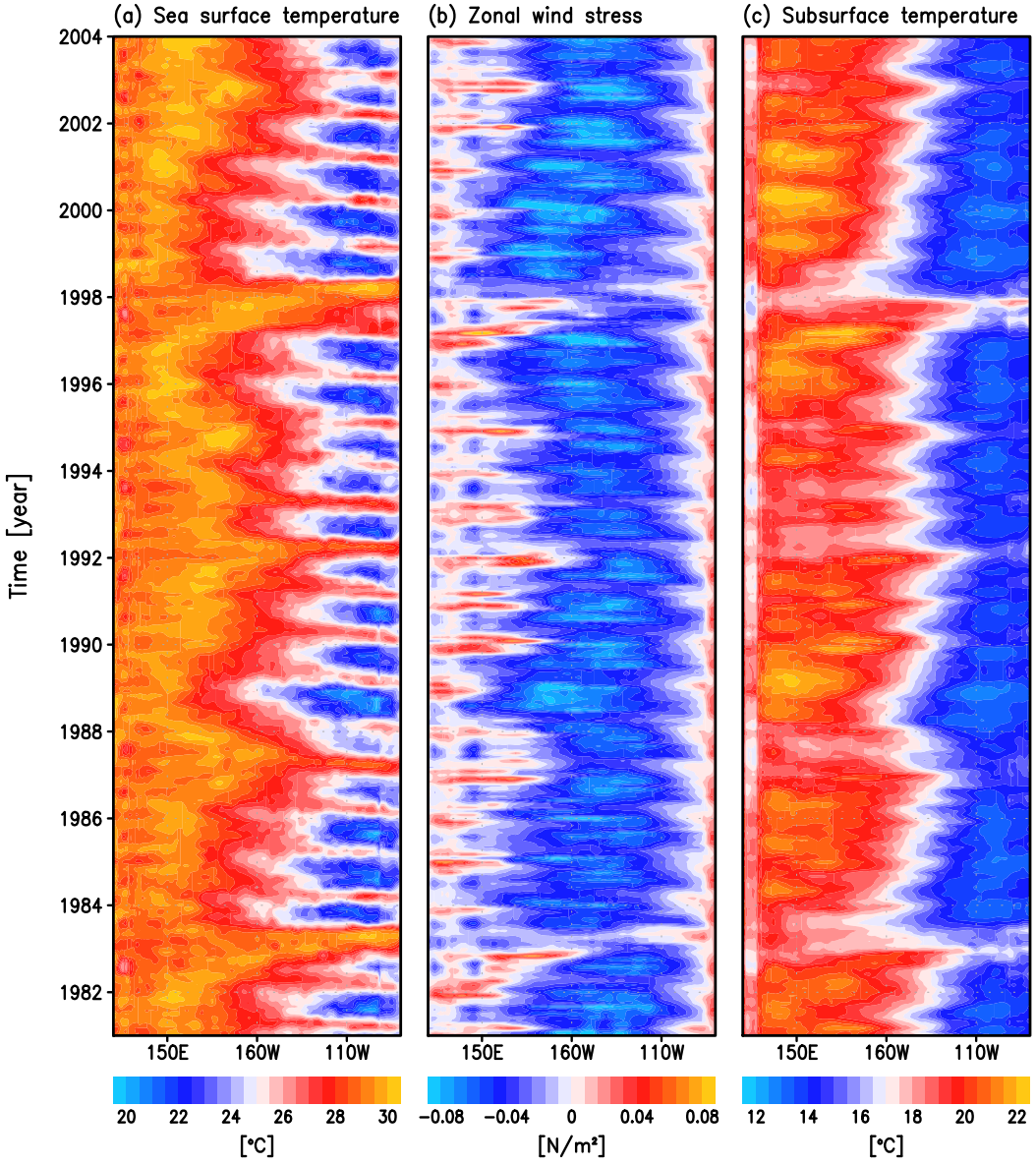

Figure 1.2: Same as Fig. 1.1, except for their absolute values.

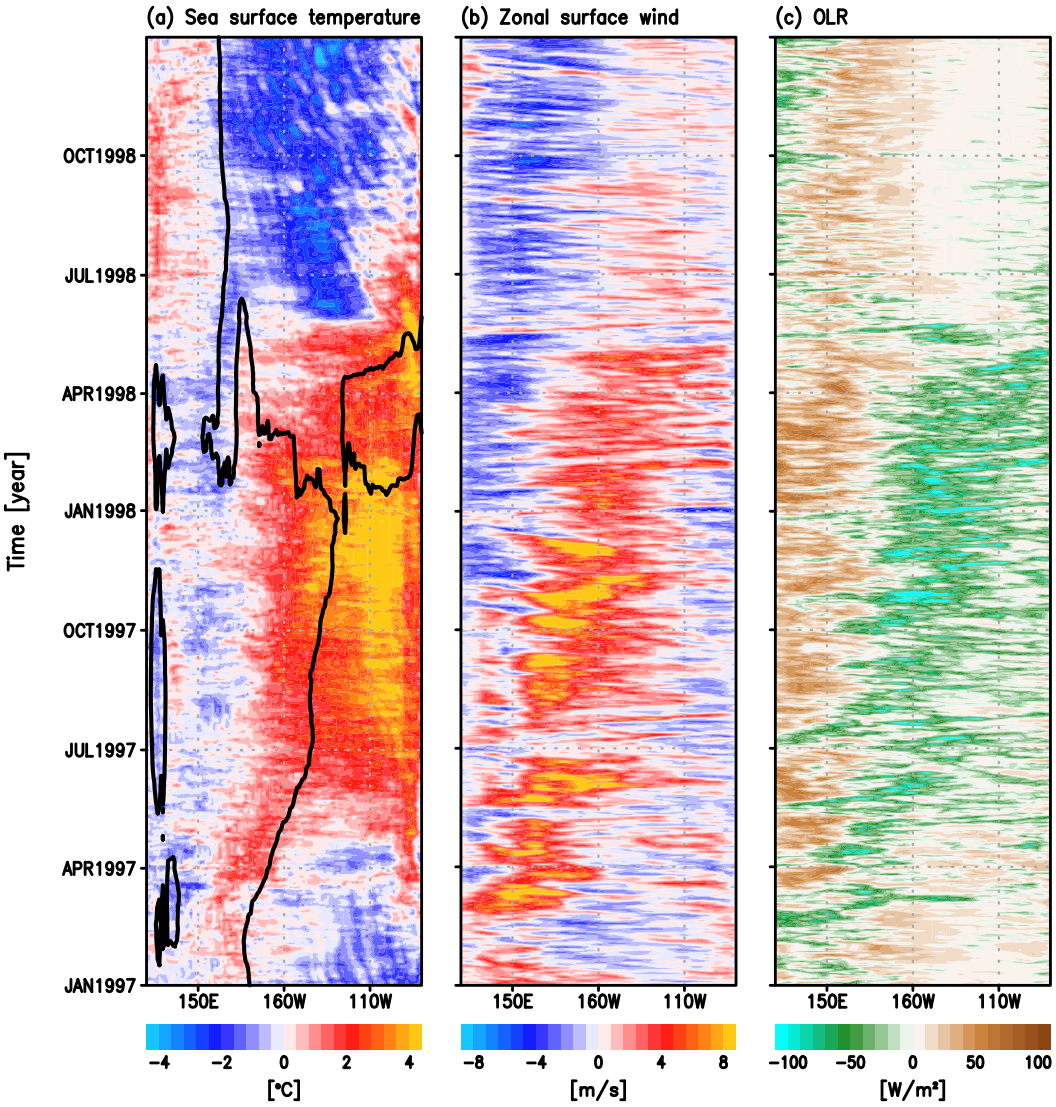

Figure 1.3: Time-longitudinal daily plot of (a) the SST anomaly and 3-month running averaged 28.5 °C isotherm [°C] averaged between 2 °S and 2 °N, (b) zonal surface wind anomalies [m s^{-1}], and (c) OLR anomalies [W m^{-2}] averaged between 5 °S and 5 °N in the Pacific from 1997 to 1998, derived from NOAA High Resolution SST data (Reynolds et al. 2007), surface zonal wind of the Japanese Re-Analysis 55 Years (JRA-55) data (Kobayashi et al. 2015), and interpolated OLR data (Liebmann and Smith 1996). Climatology is defined as the monthly average for 1982–2013 (see Chapter 3).

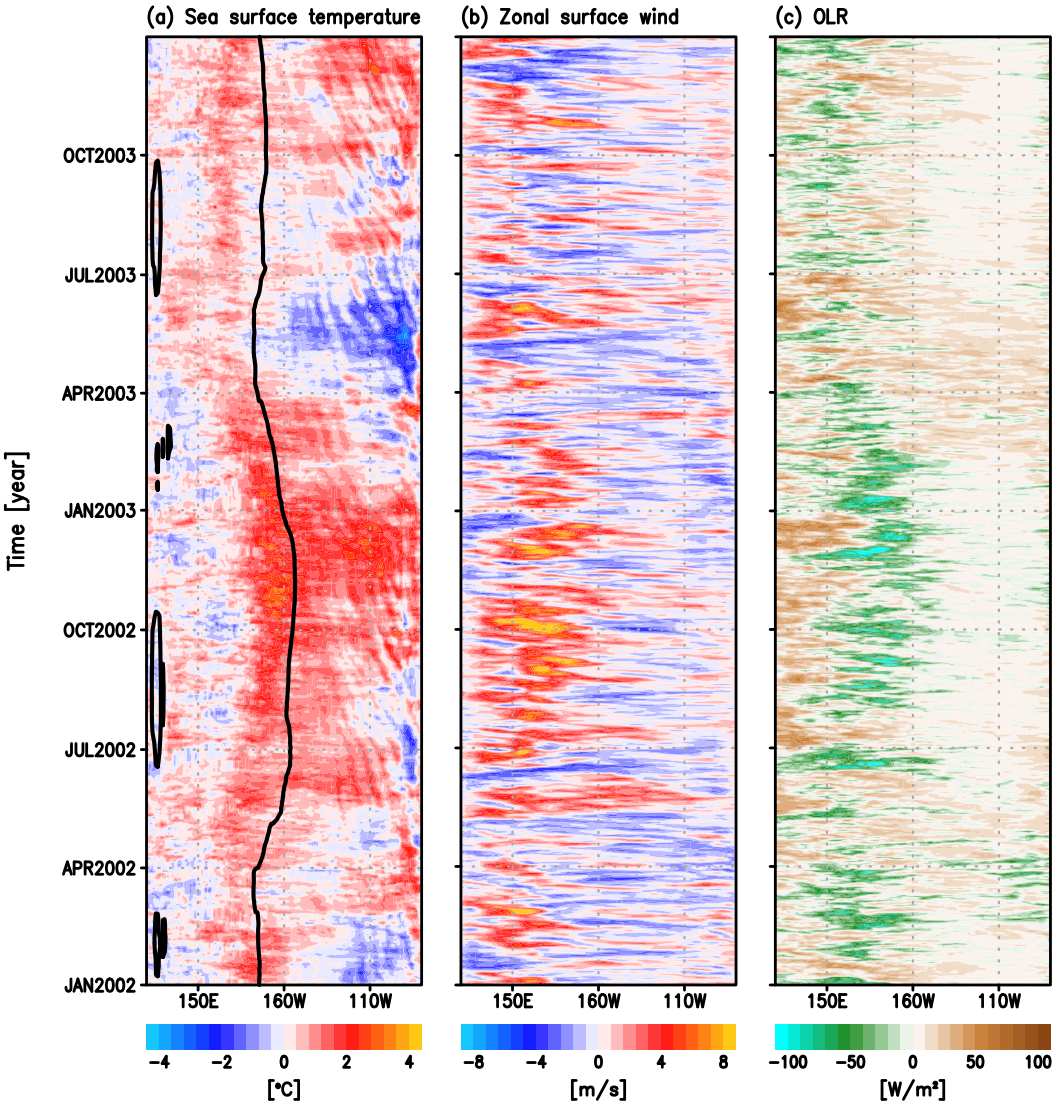

Figure 1.4: Same as Fig. 1.3, except for the period from 2002 to 2003.

Chapter 2

Importance of background seasonality over the eastern equatorial Pacific in a coupled atmosphere-ocean response to westerly wind events

Abstract

A coupled atmosphere-ocean response to westerly wind events (WWEs), which sometimes trigger El Niños, was investigated using a coupled general circulation model with particular attention paid to the dependence on the seasonal timing of WWEs. Twelve sets of 20-member ensembles were made with an idealized WWE pattern imposed in different months from January to July and in different longitudes from 160 °E to 160 °W. The initial ocean states are set to be near neutral so that the lagged response to WWEs can be isolated.

The results show that sea surface temperature (SST) in the Niño3.4 region (170 °–120 °W, 5 °S–5 °N) increases largely and persistently when a WWE is imposed in May,

which is favorable for El Niño growth. In contrast, a WWE imposed in March induced an SST increase only in the easternmost equatorial Pacific. In both cases, oceanic signal induced by the WWE in the subsurface propagates eastward and warms the surface in the eastern equatorial Pacific. When forced by the WWE in May, a positive SST anomaly appears in boreal summer when it can strongly interact with the atmospheric circulation and convective activity, which amplify the SST anomaly spreading toward the central equatorial Pacific. The above mechanism works conditioned by the seasonal march of both the atmosphere and ocean background states, and therefore the coupled response is sensitive to the timing of the WWEs. A favorable set of combinations of timing and location that maximize the role of WWEs in triggering El Niños in the subsequent winter is suggested. Other experiment sets with ocean initial states in El Niño and La Niña years showed that WWEs in May are efficient to amplify El Niño similar to the neutral case, but are not efficient to suppress La Niña.

2.1 Introduction

Strong equatorial westerly winds that persist for several days to weeks over the western-central Pacific are called westerly wind events (WWEs). Various atmospheric phenomena such as the Madden-Julian oscillation (MJO), tropical cyclones, and cold surges are thought to cause WWEs stochastically (Luther et al. 1983; Hartten 1996; Harrison and Vecchi 1997; Vecchi and Harrison 2000) or state dependently (Seiki and Takayabu 2007a,b; Chapter 3). Despite their short duration, WWEs are important elements with respect to the variability of tropical climate as they sometimes trigger El Niño events (Wyrtki 1975; McPhaden 1999; McPhaden and Yu 1999).

WWEs can excite oceanic downwelling Kelvin waves that warm the eastern Pacific. In addition, they can expand the edge of the western Pacific warm pool eastward and induce sequential WWEs, resulting in a further eastward shift of a large-scale convection

over the western Pacific, and potentially contribute to El Niño development (Lengaigne et al. 2002, 2003, 2004; Eisenman et al. 2005; Vecchi et al. 2006; Drushka et al. 2014; Fedorov et al. 2015). A typical example is the historic El Niño event of 1997/98. The sea surface temperature (SST) in the eastern Pacific rapidly increased after the sequential occurrence of WWEs from late-1996 to mid-1997. In contrast, two strong WWEs occurred from January to March in 2014, but El Niño growth did not follow—outcomes that were not well predicted by most operational centers (McPhaden et al. 2015). Menkes et al. (2014) suggested that subsequent WWEs were required after April 2014 for El Niño to start growing. Chen et al. (2015) implied that warm water volume (WWV) during the developing phase was not large enough for subsequent possible WWEs, although McPhaden (2015) showed the WWV in early 2014 was higher than any time since 1997. Another example was observed in 1974/75, when El Niño had been predicted, but warming occurred only in the far eastern Pacific (Niño1+2) in April 1975 (McPhaden et al. 2015). Thus, the coupled response to WWEs may be sensitive to the stochastic atmospheric behavior (Lengaigne et al. 2004) and oceanic heat content anomalies (Lian et al. 2014; Hu et al. 2014; Fedorov et al. 2015).

Oceanic variation observed in the eastern Pacific associated with the WWEs was examined by Vecchi and Harrison (2000). Using observational data obtained during the period 1986-98, they composited the SST anomaly (SSTA) related with WWEs. On the whole, warming was observed in the central and eastern Pacific relative to a composite SSTA without any WWEs. Beneath the WWE region, the sea surface was cooled in response to WWEs located to the west of the dateline, whereas it was warmed in response to WWEs located to the east of the dateline, implying a dependency of the oceanic response on the longitudinal location of WWEs (see also Chiodi et al. 2014). However, the ocean response to WWEs also depends on the basic state of the atmosphere and ocean (e.g., Harrison and Schopf 1984; Latif et al. 1988).

The ocean response to WWEs has been investigated using ocean general circulation

models. For instance, Harrison and Giese (1988) and Giese and Harrison (1991) examined the ocean variability associated with a WWE in May imposed on an ocean model with a realistic basic state. They showed that the Kelvin waves induced by WWEs not only warmed the surface locally due to zonal advection, but also introduced the modulations of tropical instability waves (TIWs) into the eastern Pacific, which initially enhance the warmer SSTA and then damp it out due to the meridional advection of heat related with the modulated TIWs (Hansen and Paul 1984). A volume-averaged nonlinear heat flux convergence in the mixed layer represents the influence of TIWs (An 2008). Moreover, Giese and Harrison (1991) indicated that the warming caused by WWE-induced Kelvin waves occurs most efficiently when the easterly trade winds are strongest. On the other hand, based on the observational data by Qiao and Weisberg (1995), a downwelling Kelvin wave reduces the TIW activity by temporally halting the South Equatorial Current, indicating the lack of consensus of the TIW response to WWEs. In either way, the atmospheric state strongly depends on the sea surface conditions in nature; therefore, it is reasonable to discuss the response to WWEs in a coupled atmosphere-ocean system, not only the oceanic responses.

Latif et al. (1988) examined the response of a coupled general circulation model (CGCM) to WWEs. Their coupled model consisted of a regional ocean model of the tropical Pacific and a global atmospheric model having a low resolution, and they imposed a WWE over the western Pacific for 1 month in January. They found that the warm SSTA response persisted for about 12 months associated with an eastward shift of the Walker circulation, whereas it disappeared after 4 months without the atmosphere-ocean coupling. They conducted the same experiment again, except for imposing the WWE in July; however, no clear difference was observed between the two experiments, although it was expected that WWE-induced variations would interact with the seasonal variabilities of the intertropical convergence zone (ITCZ) and South Pacific convergence zone (SPCZ). This insensitivity to the seasons was attributed to the fact that the atmospheric

model used did not realistically reproduce the background seasonality, although Tziperman et al. (1997) showed the importance of the prescribed seasonality of the ITCZ to destabilize an ENSO-like oscillation in a simple CGCM during boreal winter. Fedorov (2002) investigated the dependency of a coupled response to WWEs on the strength of background trade winds and background thermocline depth using a simple linear CGCM on an equatorial β plane. The response was found to be highly sensitive to the background state, with the temporal evolution of the SSTA varying greatly for tiny differences in the initial values (see also, Fedorov et al. 2003). Although they concluded that WWEs occurring 6 to 10 months prior to the peak of El Niño could strengthen El Niño significantly, the assumption of meridional symmetry is not valid when considering the seasonal march of the background precipitation.

In this chapter, the coupled atmosphere-ocean response to an idealized WWE is examined by using a state-of-the-art CGCM. Specifically, the relationship of the response to WWE and background seasonality is investigated by imposing the wind stress forcing in various timings and locations. To extract the response isolated from the El Niño-Southern Oscillation (ENSO) cycle, we suppress the ENSO perturbations in the model by employing a near-neutral ocean initial state. In addition, we discuss the impact of a WWE on the ENSO cycle using the same CGCM, but with the initial ocean state including ENSO perturbations.

The rest of this chapter is structured as follows. The experimental designs, data sets, and annual cycle in the model are described in section 2.2. In section 2.3, we show the various response of the coupled system to WWEs and background seasonal variations. The process of WWE-induced coupled response is examined by means of a heat budget analysis in the ocean mixed layer, and the generality of the process and the impacts on the ENSO cycle are explained in section 2.4. The relationship with observed situations is discussed in section 2.5, and conclusions are given in section 2.6.

2.2 Method and data

2.2.1 Model

An updated version of the Model for Interdisciplinary Research on Climate version 5 (MIROC5, Watanabe et al. 2010) is used for all the experiments. The modification from the original version is mainly in the ocean component model, which has replaced the horizontal coordinates with a tripolar grid having finer vertical resolution (see the supplementary information of Watanabe et al. 2014). For the ocean component model over the tropics, the zonal resolution is fixed as 1° longitude, whereas the meridional and vertical resolutions become finer toward the equator and the surface with 63 levels, and the meridional resolution is around 0.5° latitude. For ease of analysis, the model outputs are interpolated onto a 1° grid in the zonal and meridional directions. The atmospheric model is the same as MIROC5, having a spatial resolution of T85 with 40 vertical levels up to 3 hPa. The radiative forcing and other boundary conditions follow the Coupled Model Intercomparison Project phase 5 (CMIP5; Taylor et al. 2012) Representative Concentration Pathways 4.5 (RCP4.5) scenario, and values after January 1, 2014, are used. The integration period for each experiment is 18 months starting on January 1, until June 30 of the following year.

To determine the initial values for the experiments, we conducted a centennial run from 1850 with the radiative forcing and other boundary conditions following CMIP5 historical and RCP4.5 scenario runs before and after 2006, respectively (referred to as the "historical run"). The number of ensemble members in each experiment is 20. Whereas the climatological values are used for the initial states of the atmosphere and land, the initial values of the ocean include tiny perturbations obtained by averaging 29 out of 30 ocean fields, chosen from the historical run during the period 1981–2010. That is, the ocean initial values are near-neutral with respect to the ENSO cycle so that the response of the coupled system to WWEs can be isolated from the ENSO dynamics.

In our numerical experiments, zonal wind stress on the ocean (τ_x) is replaced, following the equation:

$$\tau_x = \tau_x^{model} + \tau_x^{WWE}, \tag{2.1}$$

where τ_x^{model} and τ_x^{WWE} are the wind stresses (unit: N m^{-2}) calculated in the model and representing an imposed WWE having the longitude (x), latitude (y), and time (t) dimensions:

$$\tau_x^{WWE} \equiv F(x,y,t) \times 0.2 \times \exp\left\{-\frac{(x-x_0)^2}{(20^\circ)^2}\right\} \times \exp\left\{-\frac{y^2}{(5^\circ)^2}\right\}. \tag{2.2}$$

A stepwise function F indicates that $F(x,y,t) = 1$ if $x_0 - 20^\circ \le x \le x_0 + 20^\circ$, $-5^\circ \le y \le 5^\circ$, and $t_0 - 6 \le t \le t_0 + 6$ [day] , otherwise $F = 0$. Figure 2.1a shows the structure of the imposed WWE, approximately following the composite structure of the observed WWEs in Fig. A2 (see appendix A). The maximum magnitude of τ_x^{WWE} averaged between 5 °S and 5 °N is about 0.14 N m^{-2} (Fig. 2.1), assuming strong events. The other parameters in Eq. (2.2) are the center longitude (x_0) and center date (t_0) of the imposed WWE; we set x_0 at 160 °E, 180 °, and 160 °W to capture various locations over the Pacific with t_0 set to the 15th of January, March, May, and July, assuming the typical season of El Niño onsets. In other words, we conduct 12 sets of ensemble experiments in addition to a reference experiment without the imposed WWE (referred to as "REF"). The names of these experiments are summarized in Table 2.1. Since the WWE occurrence is concentrated over the western Pacific (Fig. A1 top in appendix A), we focus on WWE-160E experiments. Note that τ_x^{WWE} is set to zero where the grid overlaps land in the model; the area is very limited and does not affect the results.

The background climatology is defined as the average of REF each time, and hereafter, an anomaly is defined by the difference between the climatology and each ensemble member of the experiments forced by the WWE. The difference between the anomalies of each ensemble member of WWE experiments and REF is called "WWE contribution."

Although all the results necessarily include model drift (i.e., systematic change of model background), the anomaly has no effect of the drift because the model climatology has been subtracted.

2.2.2 Observational data

To confirm how the background seasonality is consistent with observations, we use two observation-based monthly data sets. Ocean temperature data are derived from Ishii and Kimoto (2009). GPCP precipitation data provided by the NOAA/OAR/ESRL PSD, Boulder, Colorado, USA, from their web site at http://www.esrl.noaa.gov/psd/ (Adler et al. 2003) are also used. The horizontal resolutions of these two data sets are 1° and 2.5°, respectively, and the base period for deriving the climatological monthly values is during the period 1981–2010.

2.2.3 Model climatology

Figures 2.2 and 2.3 compare annual cycles between the observations and model. The model reproduces the seasonal intensification of the eastern Pacific cold tongue, represented by 24 °C SST isotherms (Fig. 2.2a, b), although it extends too far to the west than the observation. This bias may result in the eastern edge of the western Pacific warm pool migrating to the west after June farther than observed one (Fig. 2.2a, b). Figures 2.2c and 2.2d show the annual cycles of the climatological precipitation averaged over the eastern Pacific (170 °–120 °W). Although the amplitude of the precipitation associated with the ITCZ is larger in the model, its annual cycle and overall structure (e.g., no "double ITCZ," Li and Xie 2014; Zhang et al. 2015) are remarkably reproduced.

Figure 2.3 shows the vertical structures of the ocean temperature averaged for the first and second halves of the year along the equator. The thermocline, represented by isotherms of 20–24 °C, deepens from January to June and shoals after July in the eastern Pacific in both the observation and model. This annual cycle may result in the seasonal

difference of the ocean response to WWEs as pointed out by Harrison and Schopf (1984). The main error occurs in the western Pacific, where the warm water is shifted back to the west during the second half year in the model. The diffuse thermocline in the ocean model is a common bias in conventional ocean models (Tatebe and Hasumi 2010).

The model captures annual cycle of the ocean temperature and precipitation realistically, except for the error in the western Pacific warm pool associated with a bias in the easterly trade wind stronger than observations (cf. Zhang and Sun 2014). This may cause the less frequent WWEs over the central Pacific in the model (Fig. A1 bottom in appendix A). Nevertheless, in the historical run, the model is able to produce moderate ENSO events and extreme El Niños, accompanied by sequential WWEs similar to 1997/98 El Niño (cf. subsection 2.4.3).

Table 2.1: List of the names of experiments (left column), and the centers of month (middle column) and longitude (right column) for the imposed WWE in each experiment.

Experiment name	Month	Longitude
REF	(No WWE)	
WWE1-160E	January	160 °E
WWE1-180	January	180 °
WWE1-160W	January	160 °W
WWE3-160E	March	160 °E
WWE3-180	March	180 °
WWE3-160W	March	160 °W
WWE5-160E	May	160 °E
WWE5-180	May	180 °
WWE5-160W	May	160 °W
WWE7-160E	July	160 °E
WWE7-180	July	180 °
WWE7-160W	July	160 °W

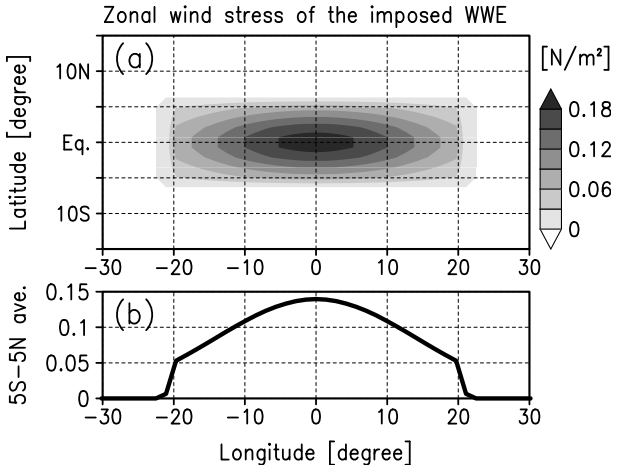

Figure 2.1: (a) Horizontal structure of the eastward zonal wind stress [unit: N m^{-2}] of the imposed WWE and (b) its average between 5 °S and 5 °N.

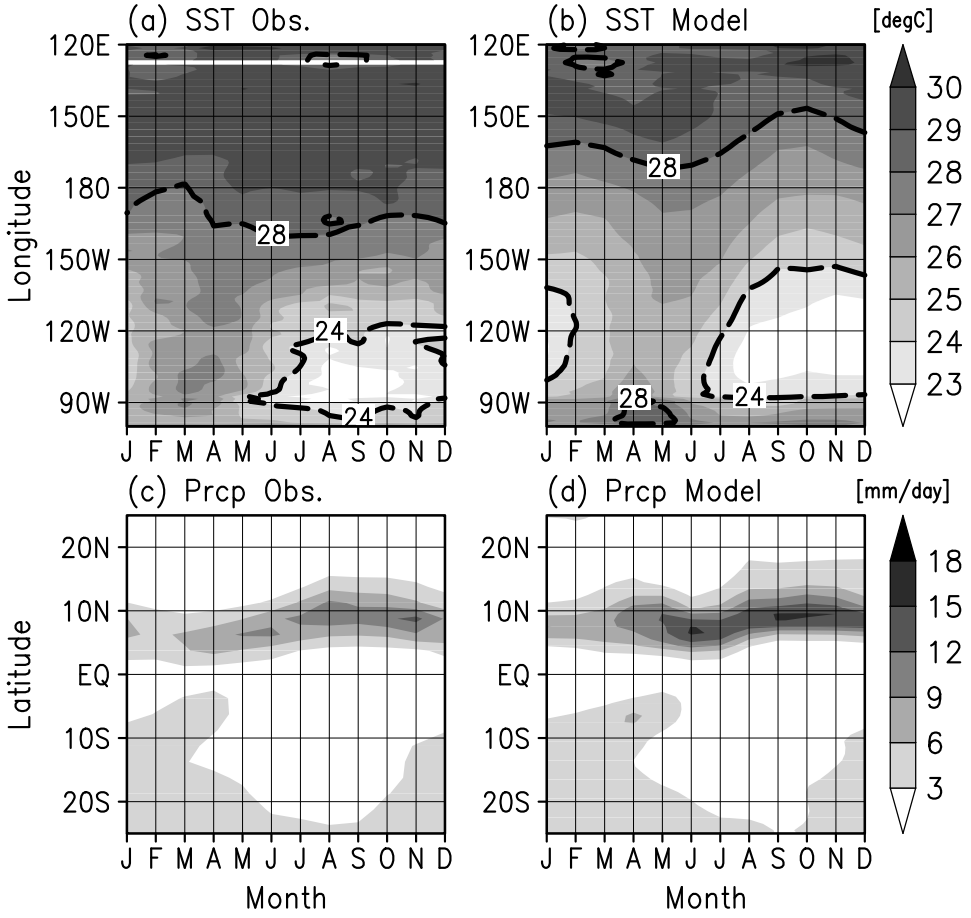

Figure 2.2: Annual cycles of SST of the (a) observation and (b) model along the equator (2 °S–2 °N) [unit: °C] and climatological precipitation of the (c) observation and (d) model averaged over the eastern Pacific (170 °–120 °W) [unit: mm day^{-1}]. Dashed lines in (a) and (b) indicate 24 and 28 °C SST isotherms.

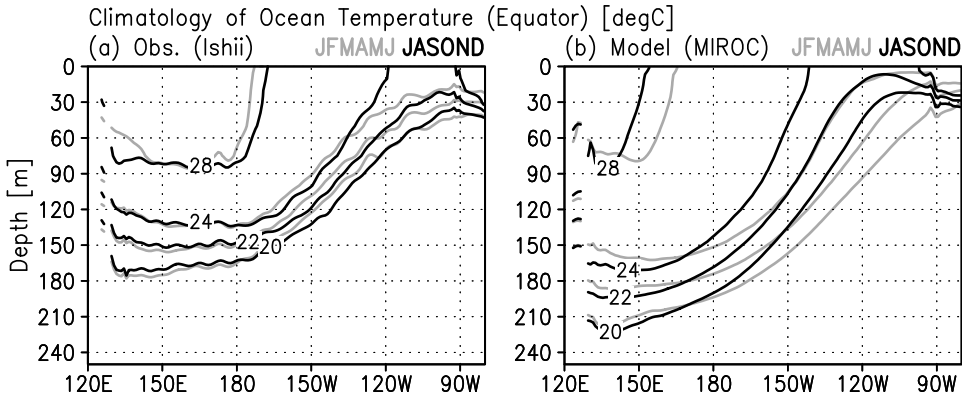

Figure 2.3: Climatology of ocean temperature of the (a) observation and (b) model along the equator (2 °S–2 °N) averaged from January to June (gray) and from July to December (black). From upper depths, the contours indicate isotherms of 28, 24, 22, and 20 °C.

2.3 WWE contributions

2.3.1 WWE contribution to Niño indices

WWE contributions to Niño indices are examined using the monthly SSTA. Figure 2.4 shows the WWE contributions of SSTAs at the Niño3.4 (170 °–120 °W, 5 °S–5 °N) and Niño1+2 (90 °–80 °W, 10 °S–0 °) regions for WWE-160E experiments. In all the experiments, the WWEs commonly warm the regions up to about 0.5 K. Interestingly, the same structure for the WWEs produces a considerable difference in the duration of the coupled response among the experiments.

From Fig. 2.4a, WWE5-160E shows a warming of Niño3.4 SST that persists for more than 5 months with a peak of about 0.5 K in August. Although Niño3.4 SSTA increases up to 0.5 K in the WWE1-160E and WWE7-160E, it decays rapidly. In WWE3-160E, the Niño3.4 warming persists weakly until July in terms of the ensemble mean and is scattered among ensemble members after boreal summer.

The WWE contributions to Niño1+2 SSTA are shown in Fig. 2.4b. In WWE3-160E, the warming in the Niño1+2 region has a significant peak in July and continues for several months. In other experiments, the WWE contributions are scattered.

In summary, WWEs in May are more favorable to increase Niño3.4 SST, whereas those in March are efficient to increase Niño1+2 SST.

2.3.2 WWE contribution to spatio-temporal structures

The difference in the WWE contributions among the experiments is clear not only for the Niño indices but also for the spatial structure of the coupled response. Figure 2.5 summarizes the response in WWE5-160E, in which the Niño3.4 SSTA increased the most. Here, “day 0” in the figure corresponds to the center date of the imposed WWE period (i.e., 15th May for WWE5-160E).

The vertical structure of the ocean temperature along the equator is depicted in Fig.

2.5a. A warm water anomaly is initially formed in the subsurface (100–300 m depth), and its signal propagated eastward as an oceanic Kelvin wave along the thermocline as represented by isotherms of 20–24 °C. The initial peak of the temperature anomaly is located on the eastern side of the WWE region since it is induced by the downwelling balanced with the eastward current anomaly in the surface layer (1–100 m depth) caused by zonal wind stress directly and the westward current anomaly near the thermocline caused by wind stress indirectly (Kessler and Kleeman 2000), rather than that balanced by the Ekman transport (see also McPhaden et al. 1988; Smyth et al. 1996).

The SST rapidly warms in the Niño3.4 region when the Kelvin wave signal reaches the surface by day 60 (Fig. 2.5b). Subsequently, this positive SSTA expands over the equatorial Pacific involving the eastward and equatorward surface wind anomalies and continues for several months, especially in the Northern Hemisphere (hereafter, NH) involved with the stronger wind response. A part of the positive SSTA, accompanied by westerly anomalies, migrates westward and decays gradually. This migration after June may be caused by the seasonal shrink of the warm pool.

Precipitation anomalies associated with the SSTA are shown in Fig. 2.5c. After day 60, positive and negative precipitation anomalies appear at the southern and northern sides of the climatological ITCZ, respectively, indicating the southward shift of the ITCZ. The southward shift of the ITCZ accompanies surface wind anomalies eastward and equatorward in the central equatorial Pacific (Fig. 2.5b), causing the anomalous latent heat flux owing to the weakening of the trade wind. Therefore, the positive SSTA expands westward and persists after day 60, especially in the NH.

The time sequence of the WWE contribution in WWE3-160E is depicted in Fig. 2.6, in a similar manner to Fig. 2.5. Similar to WWE5-160E, a warm water anomaly is formed in the surface and subsurface layers, and a cold water anomaly is also formed in the far western Pacific until day 20. While the positive SSTA accompanied by westerly anomalies shifts westward after day 60, the warm water signal in the subsurface propagates

eastward along the thermocline. However, unlike the result of WWE5-160E, the warm signal reaches around 100 °W. Then, surface warming begins in the Niño1+2 region and persists after day 80 (Fig. 2.6b). In addition, the significant anomalies of precipitation and surface winds are restricted only over the central and western Pacific. That is, the SST response is limited in the far eastern Pacific, and atmospheric response is very weak over the eastern Pacific. This is a discernible difference from the atmosphere-ocean coupled SST response in WWE5-160E.

WWE5-160W and WWE5-180 show responses quite similar to WWE5-160E, and the WWE7 experiments result in WWE contributions similar to WWE5-160E except for the shorter duration of significant signals. Likewise, the three WWE3 experiments share a great similarity in the coupled response. In the WWE1 experiments, although the surface warming occurs initially near the Niño3.4 region similar to WWE5 experiments, it has shorter period and weak wind and precipitation responses in the eastern Pacific.

2.3.3 Role of background seasonality

In the warming process in the eastern equatorial Pacific, background seasonality in the thermocline and precipitation may play a significant role. The signal of the subsurface warm water propagates eastward as a Kelvin wave, along approximately between isotherms of 20 and 24 °C (Figs. 2.5a and 2.6a). Therefore, the steepness of the thermocline tilt and corresponding zonal gradient of the temperature in the eastern Pacific are crucial in determining the initial warming (cf. Harrison and Schopf 1984). The slope of the thermocline is the flattest in May (cf. Fig. 2.5a); after which the WWE-induced warm signal reaches the easternmost equatorial Pacific. The slope becomes steeper after July (cf. Fig. 2.3), corresponding to the strengthening of the equatorial upwelling in the eastern Pacific, resulting in the surface warming near the Niño3.4 region through the vertical advection of the subsurface warm water.

The ITCZ located near 10 °N is active over the equatorial Pacific from June to Septem-

ber (Fig. 2.2c, d). Thus, the positive SSTA in the eastern Pacific can easily interact with the ITCZ, causing a southward shift of the ITCZ. Corresponding to the active ITCZ, the surface wind converges in the ITCZ region, involving the strengthening of the climatological cold tongue in the eastern Pacific (Fig. 2.2a, b). Once the ITCZ shifts southward as a result of the positive SSTA, the cold tongue becomes weak in association with the weakening of the poleward and westward surface wind over the cold tongue in the NH. This reduces poleward heat advection in the surface layer to warm the surface in the eastern Pacific. In addition, the weakening of the trade wind over the southern side of the background ITCZ also contributes to the warming due to the reduction in evaporation over the equatorial Pacific.

The temporal relationship between the southward shift of the ITCZ and equatorward surface wind, causing the anomalous equatorward surface currents, is confirmed in Fig. 2.7a for WWE5-160E. After June, the equatorial precipitation anomaly (orange line) is accompanied by the equatorward wind convergence (blue line). From July to mid-August, the precipitation is activated to the south of the background ITCZ (red line) and the equatorward surface wind anomaly is correspondingly intensified more at the NH (blue line), driving the anomalous equatorward surface current at the NH persisting until November (black line). The meridional advection due to the anomalous current may warm the eastern Pacific in the NH. Such a persisting equatorward current is not observed at the Southern Hemisphere (figure not shown). In contrast, for WWE3-160E, there is no robust peak in the signals of the precipitation and meridional wind, although the precipitation anomaly to the south of the ITCZ is weakly positive during the boreal summer. As shown in Fig. 2.4a, the Niño3.4 warming after August is not statistically significant having the scattered ensemble members, implying that the interaction with the ITCZ after July might occur only in a few members.

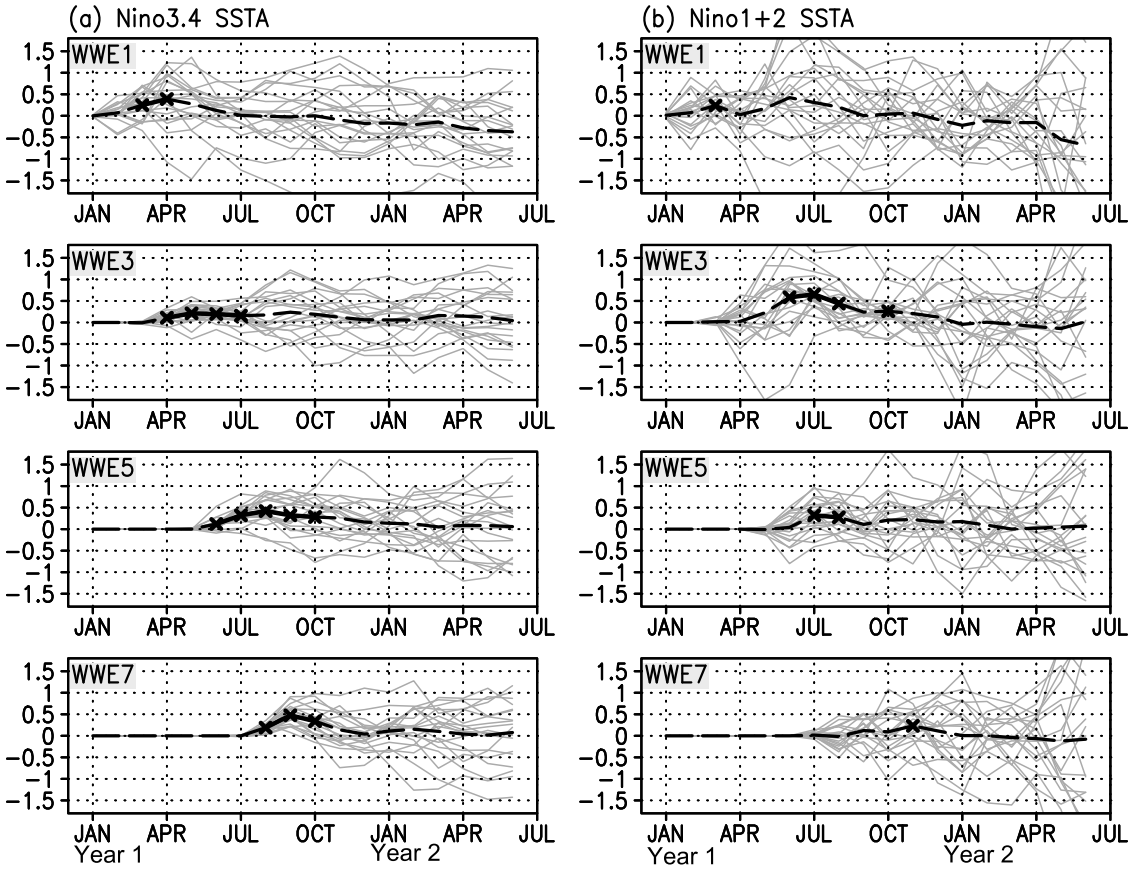

Figure 2.4: WWE contributions of (a) Niño3.4 and (b) Niño1+2 monthly SSTAs [unit: K] for WWE-160E experiments. Thick-dashed lines indicate ensemble means and thin-gray lines indicate each members. From top to bottom, the WWE is imposed in January, March, May, and July. The marks indicate the 95% significant values by t-test.

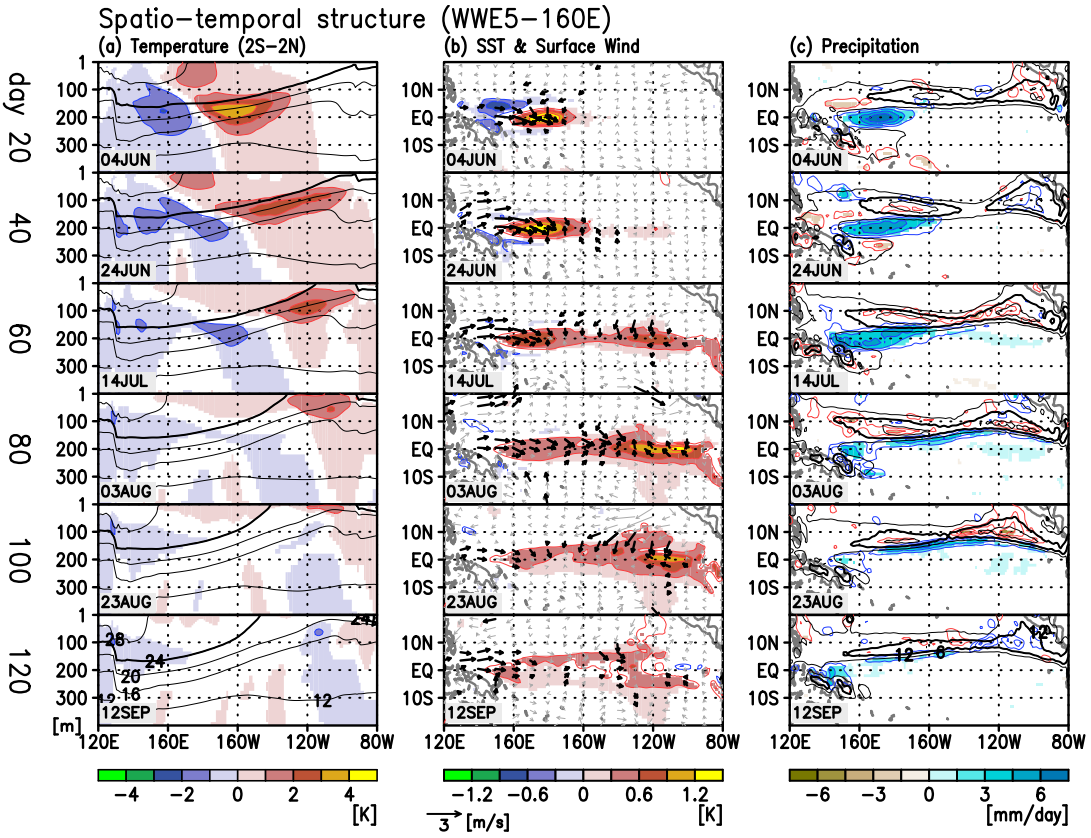

Figure 2.5: Spatio-temporal structures of (a) 2 °S-2 °N averaged ocean temperature anomaly [shade, unit: K] and its climatology [black contour, contour interval: 4 °C] (a thick line corresponds to 24 °C), (b) SSTA [shade, unit: K] and 10 m horizontal wind anomaly [vector], and (c) precipitation anomaly [shade, unit: mm day^{-1}] and its climatology [contour, contour interval: 6 mm day^{-1}] (a thick line corresponds to 12 mm day^{-1}) for WWE5-160E. A 15-day running mean is applied for all values. Time proceeds from top to bottom by 20 days from day 20. Actual date of each figure is shown at the bottom left-hand side of each panel. Shades are depicted only for regions exceeding 95% statistical confidence by t-test, and red (blue) contours with the same interval of shades indicate positive (negative) values except for (c), where red (blue) contours indicate negative (positive) values. Black vectors in (b) indicate the zonal or meridional component exceeds 95% statistical confidence. See the vector scale at the bottom left-hand side of (b) for the wind magnitude.

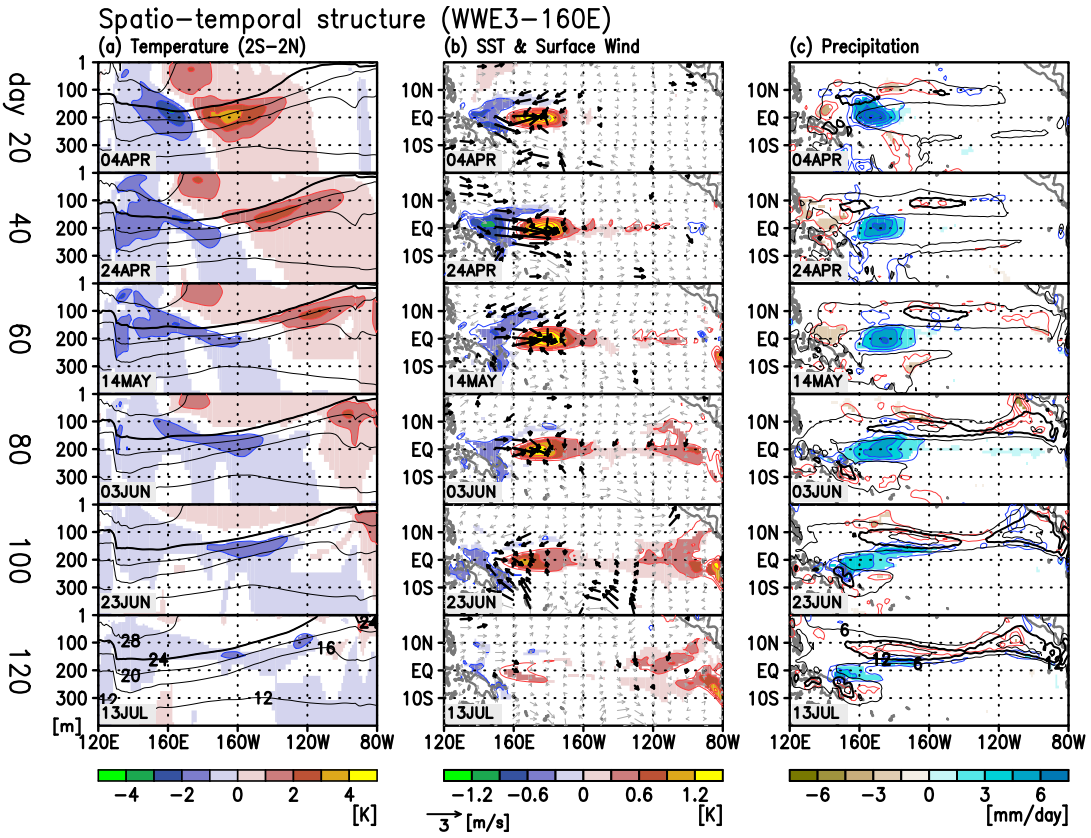

Figure 2.6: As for Fig. 2.5, except for WWE3-160E.

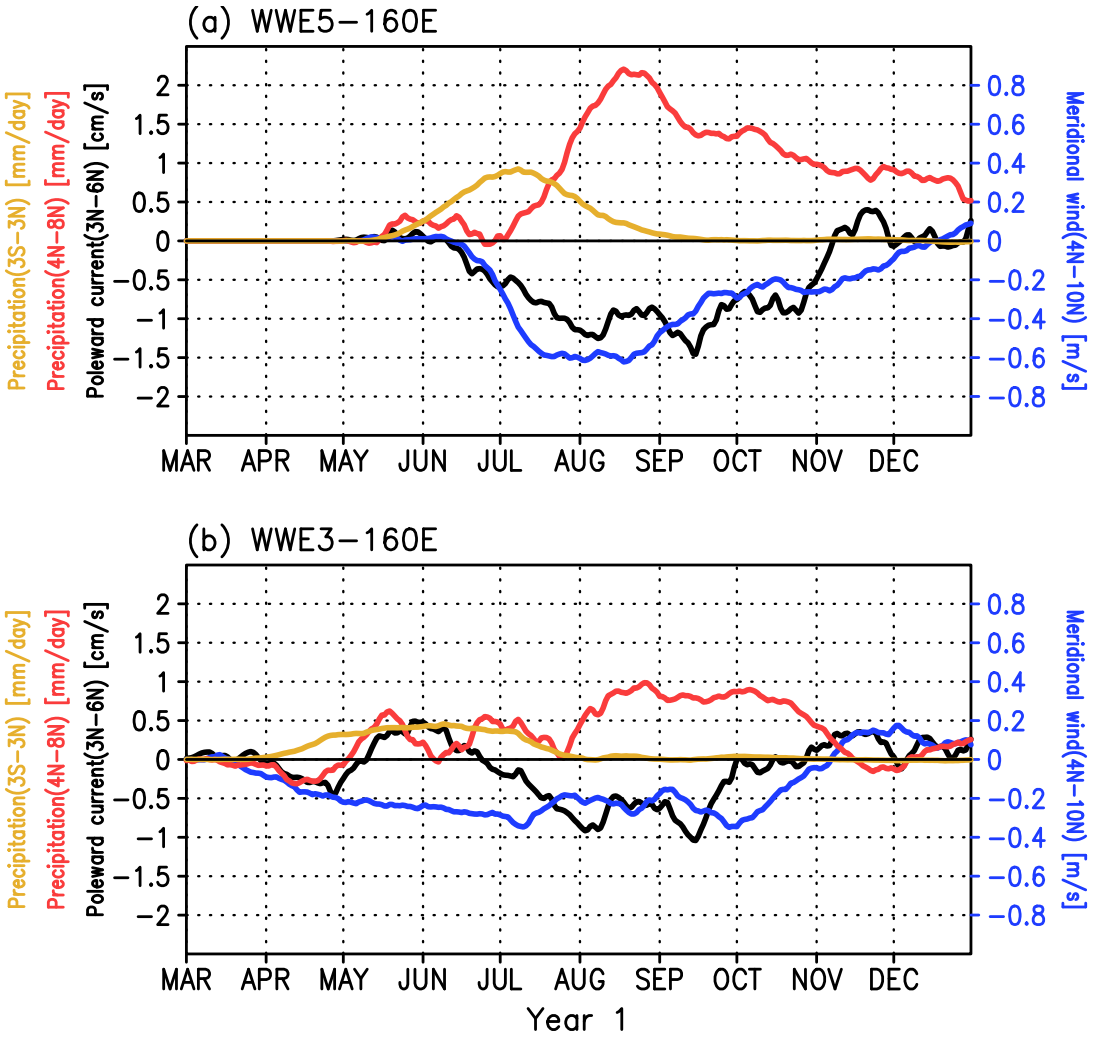

Figure 2.7: Time series of 120 °–170 °W averaged anomalies of the meridional currents averaged over 3 °–6 °N (black solid) in the mixed layer (1–50 m depth), the meridional surface winds averaged over 4 °–10 °N (blue), and the precipitation averaged over 3 °S–3 °N (orange) and 4 °–8 °N (red) for (a) WWE5-160E and (b) WWE3-160E, smoothed by a 31-day running mean.

2.4 Mechanism

2.4.1 Processes responsible for WWE-induced warming

As shown in the previous section, a widespread warming over the equatorial Pacific is induced by an imposed WWE, especially in WWE5-160E. To clarify the mechanism of the warming, we conducted a heat budget analysis for the mixed layer (ML). According to Kang et al. (2001), the mixed layer depth (D) is assumed to be 50 m. Thus, the temperature (T) tendency averaged in the ML is approximately described as the sum of the zonal and meridional advections, vertical advection including the entrainment of cool water into the ML, and surface heat fluxes:

$$\frac{\partial T}{\partial t} = -u\frac{\partial T}{\partial x} - v\frac{\partial T}{\partial y} - \frac{H(w_e)w_e\Delta T}{D} + \frac{Q_{lh} + Q_{sh}}{\rho_0 C_p D} + R, \tag{2.3}$$

where u and v indicate the zonal and meridional ocean currents, respectively, w_e indicates the vertical velocity at the ML base, and ΔT indicates the temperature difference across the ML base. R represents the residual term, including surface radiation. According to Kang et al. (2001), we assume the bulk effect of the entrainment by defining that $H(w_e) = 1$ for $w_e > 0$ and $H(w_e) = 0$ for $w_e \leq 0$. Q_{lh} and Q_{sh} are latent and sensible heat fluxes, respectively. ρ_0 is seawater density and C_p is specific heat, given as 1022.4 kg m^{-3} and 3940 J kg^{-1} °C^{-1}, respectively. By decomposing variables into means and deviations in Eq. (2.3), the tendency equation of the ML temperature anomaly is derived as

$$\begin{aligned}\frac{\partial T'}{\partial t} = & \underbrace{-u'\frac{\partial \overline{T}}{\partial x} - v'\frac{\partial \overline{T}}{\partial y} - \frac{H(w_e)w_e'\overline{\Delta T}}{D}}_{\text{LN1}} \underbrace{-\overline{u}\frac{\partial T'}{\partial x} - \overline{v}\frac{\partial T'}{\partial y} - \frac{H(w_e)\overline{w_e}(\Delta T)'}{D}}_{\text{LN2}} \\ & \underbrace{-u'\frac{\partial T'}{\partial x} - v'\frac{\partial T'}{\partial y} - \frac{H(w_e)w_e'(\Delta T)'}{D}}_{\text{NL}} \underbrace{+\frac{Q'_{lh} + Q'_{sh}}{\rho_0 C_p D}}_{\text{Q}} + R'.\end{aligned} \tag{2.4}$$

The overbars and primes indicate the basic state values including seasonal variation and anomalies, respectively. LN1 is the sum of linear advection terms due to current anomalies, LN2 is the sum of linear advection terms due to basic state current, NL is a combined nonlinear advection term, and Q represents the heat flux anomalies.

Figure 2.8a shows the tendency of T' over the Niño3.4 region for WWE5-160E (gray curve). Two clear peaks are discernible in June and July. These peaks are well reproduced by Eq. (2.4), and are mainly related to the zonal component of LN1 (black curve in the second panel) and the meridional and vertical components of LN2 (red and green curves in the third panel). The meridional component of LN1 (green curve in the second panel) also contributes to warming after July.

The WWE in WWE5-160E induces Niño3.4 warming in the ML by the following processes. First, the linear zonal advection of LN1 warms the region in June, which is responsible for the first peak of the warming tendency, associated with the eastward surface current anomaly of the WWE-forced oceanic Kelvin wave (cf. McPhaden 2002; Harrison and Schopf 1984). Second, the vertical and meridional advection terms in LN2 induce the second peak of warming in July as the thermocline tilt becomes steeper involved with the equatorial upwelling (Fig. 2.3b). Then, the background current in the ML expands the warm water anomaly poleward. In addition, meridional advection in LN1 results in a warming tendency in the Niño3.4 region persistently from July to November mainly in the NH (cf. Fig. 2.7a). As the background SST increases poleward near the cold tongue, this warming tendency is induced by the equatorward anomalous surface current, resulting from the wind anomaly in association with the southward shift of the ITCZ. Correspondingly, easterly trade wind is weakened (Fig. 2.5b), reducing evaporation. This causes the spread of the warm water anomaly toward the central Pacific in the NH (Fig. 2.8b) (Xie and Philander 1994; Xie 1996). Reduction of equatorial upwelling due to the anomalous surface westerly also contributes to warm the SST on the equator (figure not shown), via weakening of the poleward Ekman transport in the eastern Pacific.

The process for WWE3-160E is confirmed based on Fig. 2.9, in a similar manner to Fig. 2.8. The Niño3.4 warming initially occurs only due to the zonal component of LN1 in April. After July, a warming tendency by the meridional component of LN1 is observed (cf. Fig. 2.7b), although the Niño3.4 SSTA is scattered among the ensemble members of WWE3-160E (Fig. 2.4a). This implies that a part of the ensemble members, having southward shift of the ITCZ, might show the warming in boreal summer.

With respect to the Niño3.4 warming, it is found that the seasonality of the ocean and atmosphere plays a crucial role. The subsurface warm water induced by the WWE outcrops in the Niño3.4 region when the slope of the mean thermocline is steeper, and the southward shift of the ITCZ is caused by the interaction between active background precipitation and outcropped warm water. As shown in Figs. 2.2 and 2.3, the background condition is preferable for both the atmospheric and oceanic processes from July to November. As the WWE is imposed in May, the WWE-induced Kelvin wave reaches the eastern Pacific in July-August, resulting in a background condition that is favorable to warming the Niño3.4 region.

2.4.2 Generality

The generality of the mechanism explained above is confirmed by using 12 sets of ensembles. Figure 2.10 collectively plots the central timings and longitudes of the imposed WWEs (crosses), the maxima of the warm water anomaly in the subsurface (open circles), and the SSTA maxima on the eastern/western side of 150 °W (closed circles/triangles) over the background seasonal march of precipitation averaged over 5 °–15 °N, temperature in the ML, and the warm pool edge (defined as 28 °C SST isotherm).

Climatological precipitation associated with the ITCZ (shading) is seasonally active during the boreal summer from June to October. In addition, the area of climatological ML temperature of 20–24 °C (hatched area), where the initial surface warming may appear as indicated in section 2.3.3, expands after June and reaches near 120 °W, cor-

responding to the seasonal strengthening of the equatorial cold tongue or equatorial upwelling in the eastern Pacific. In the western Pacific, the edge of the warm pool expands the most in May.

Subsurface temperature anomalies (open circles) begin with the imposed WWE forcing in each set of experiments (crosses). The warm water anomaly appears in the eastern side of the WWE and its signal propagates eastward as an oceanic Kelvin wave. In the WWE3 experiments, the subsurface warm water outcrops and continues weakly in the easternmost Pacific (near 90 °W), while surface warming continues in the eastern Pacific for several months in the WWE5 experiments (closed circle). The westward propagation of the SSTA maximum after July is possibly associated with the zonal advection due to climatological westward currents. Considering all the ensemble sets, greater and more persistent surface warming occurs where climatological precipitation is active after outcropping of the subsurface warm water near the Niño3.4 region, indicating the importance of both the seasonally steeper slope of the climatological thermocline and the interaction with the ITCZ. An exception is WWE1-160W, where the amplitude of the SSTA maximum is larger at 110 °W for 2 months, due mainly to NL of Eq. (2.4) only for 1 month (not shown).

In the western Pacific, surface warming (triangles) concentrates near the eastern edge of the warm pool, the reason of which can be interpreted as follows. Precipitation is activated near the edge due to the SSTA induced by WWE over the western Pacific. Then, the large-scale motion forced with the precipitation anomaly pushes the edge eastward, although it is shifted back into the west because of the seasonal migration of the warm pool.

2.4.3 WWE impact on the ENSO cycle

The impact of WWEs on the ENSO cycle is investigated in this subsection. We conducted an extra set of numerical experiments, referred to as HIST-WWE5-160E, which is the

same as WWE5-160E except for the ocean and atmosphere initial values. The initial values are given from the historical run on January 1 during the period 1981 to 2005 (cf. section 2.2). A set of experiments without WWE forcing is referred to as HIST-REF. Because of the initial subsurface anomalies, the ocean condition develops into either a warm or a cold phase of the ENSO cycle, or stays neutral without any prescribed WWEs. By prescribing a WWE similar to WWE5-160E, we can estimate the effect of a WWE in May on the subsequent development of ENSO. The number of ensemble members is 25, and by the method described below, we classify the set into four cases: W (moderately warm), E (extremely warm), N (neutral), and C (cold) following the Niño3.4 SSTA in HIST-REF. As the WWE is prescribed in May, the Kevin wave induced by the WWE reaches the eastern Pacific during July and August; therefore, case W/E (C) is defined as an experiment in which Niño3.4 SSTA from July to November is higher (lower) than 0.5/3.0 K (−0.5 K); otherwise, it is classified as case N. The 25 cases are broken down as W 6, E 2, N 7, and C 10. The results described below are not sensitive to the sampling method.

The Niño3.4 indices in each case are depicted in Fig. 2.11. Comparing HIST-WWE5-160E with HIST-REF, the WWE affects cases W and N, with a contribution of 0.5 K to 1 K warming for several months. On the other hand, cases E and C are insensitive to the prescribed WWE. The horizontal structures of the WWE contribution to SST are shown in Fig. 2.12a-d. In case N, the SST warms a wide are of the tropical Pacific, and the ITCZ shifts southward as in WWE5-160E (Fig. 2.12a, e). Similarly, in case W, surface warming expands over the tropical Pacific centered in the Niño3.4 region, involving a southward shift of the ITCZ (Fig. 2.12b, f). Interestingly, two of case W were modulated by the WWE into extreme warm events, accompanied by subsequent westerly anomalies over the western Pacific, as shown by Fedorov et al. (2015). On the other hand, the SST response to a WWE is weak in case E (Fig. 2.12c, g) since Niño3.4 SST almost reaches the temperature determined by the radiative-convective equilibrium

(Jin et al. 2003). However, there are very weak signals in the precipitation field in case C (Fig. 2.12d, h), even though the slope of the thermocline is steeper in the eastern Pacific during cold phases. This may be caused by the northward shift of the ITCZ associated with a cold SSTA over the equatorial Pacific, resulting in weak interaction between the WWE-induced warm water and the ITCZ. While the SSTA induced by a WWE in May can interact with the ITCZ in cases W and N, there is no interaction with the ITCZ in case C. This indicates that the effect of the WWEs is asymmetric to the ENSO phase associated with the difference in atmospheric conditions.

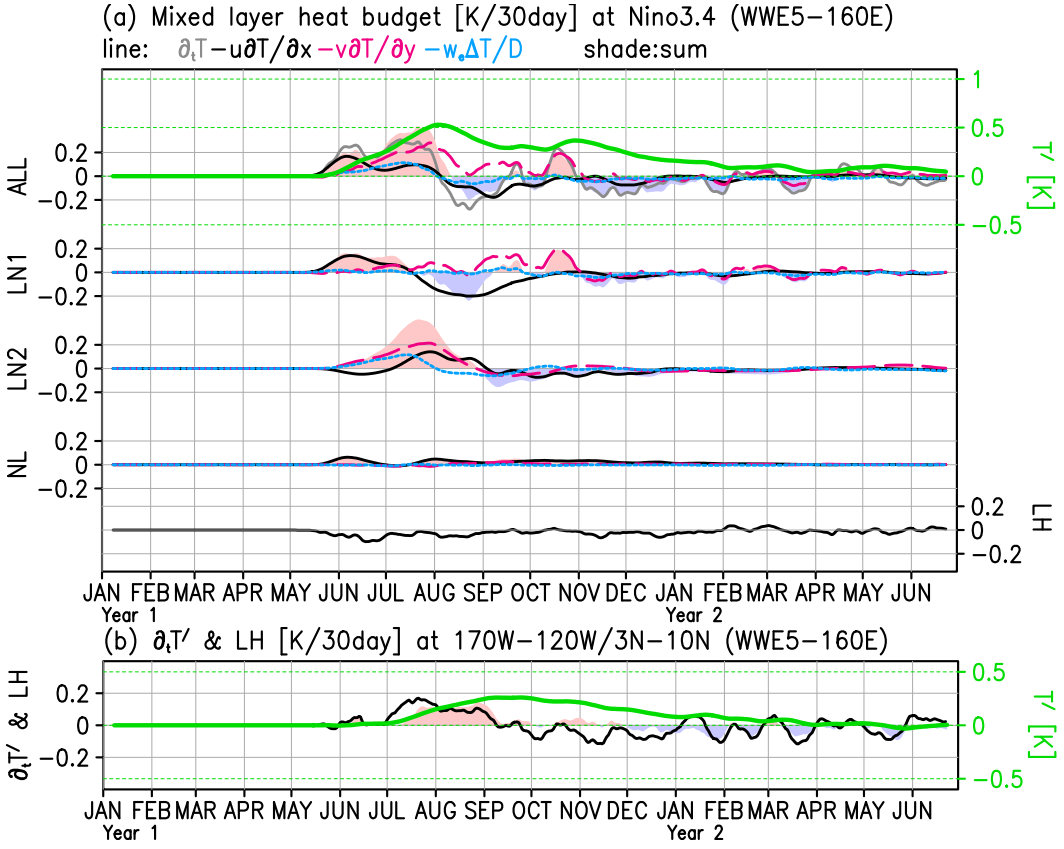

Figure 2.8: (a) Time series of the temperature anomaly [green-solid line, unit: K] in the Niño3.4 region in the mixed layer, and its tendency [gray-solid line in ALL] and the results of the heat budget analysis [unit: K (30 days)$^{-1}$] for WWE5-160E. In ALL, the shade indicates the sum of the advective terms (LN1, LN2, NL) and Q in Eq. (2.4), and black-solid, magenta-dashed, and cyan-dotted lines indicate the zonal, meridional, and vertical components of the advective terms, respectively. Shades in LN1, LN2, and NL indicate the sums of the zonal (black-solid line), meridional (magenta-dashed line), and vertical (cyan-dotted line) components of LN1, LN2, and NL in Eq. (2.4), respectively. Black line in LH indicates the latent heat flux anomaly. (b) Time series of the temperature anomaly green-solid line, unit: K, its tendency [black-solid line, unit: K (30 days)$^{-1}$] and latent heat flux anomaly [shade, unit: K (30 days)$^{-1}$] averaged over 170 °–120 °W and 3 °N–10 °N in the mixed layer. The 15-day running mean is applied for all values.

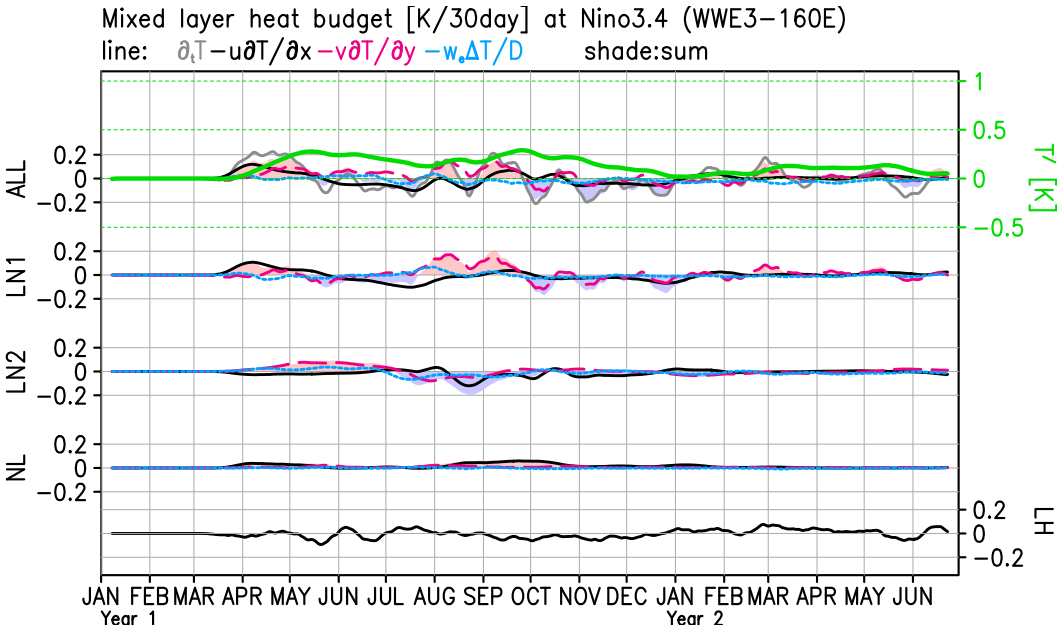

Figure 2.9: As for Fig. 2.8a, except for WWE3-160E.

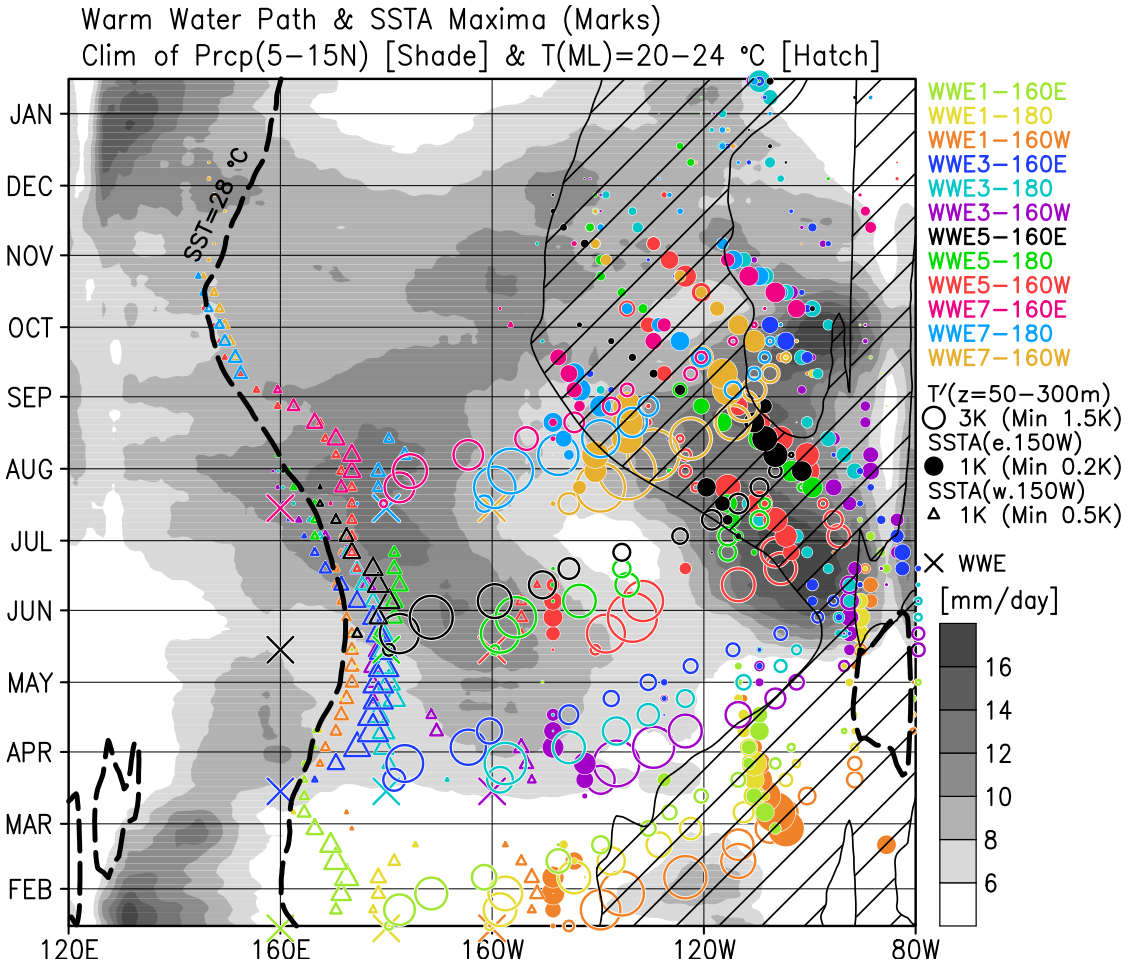

Figure 2.10: Paths of the warm water anomaly on the subsurface (open circles) and maximum points of the SSTA on the eastern side of 150 °W (closed circles) and on the western side of 150 °W (open triangles) for each experiment. The color corresponds to each experiment and the size corresponds to the amplitude of anomalies; see right-hand side. Shade indicates the background precipitation near the ITCZ (5 °–15 °N) [unit: mm day^{-1}]. The solid line and hatching indicate the 22 °C contour and the area between 20 and 24 °C of the background ocean temperature averaged between 2 °S and 2 °N in the mixed layer (from the surface to a depth of 50 m). The dashed line indicates the eastern edge of the warm pool, or 28 °C contour of the background SST.

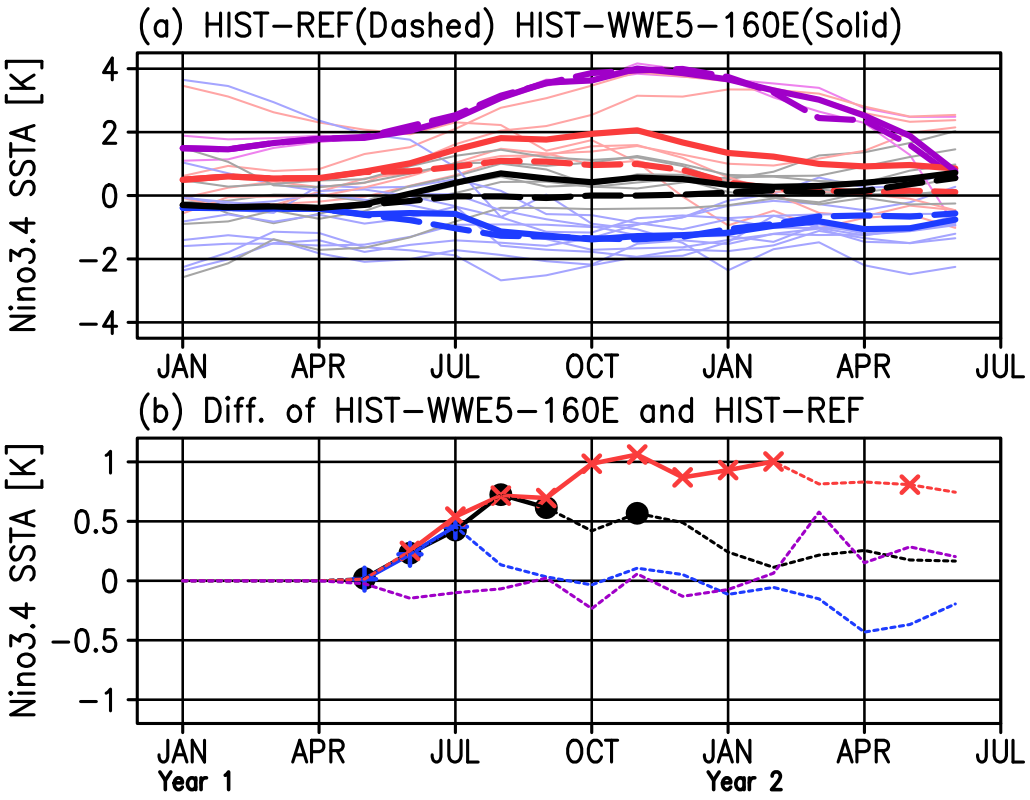

Figure 2.11: (a) Each members of HIST-WWE5-160E (thin lines) and ensemble means of Niño3.4 SSTA in HIST-REF (thick-dashed lines) and HIST-WWE5-160E (thick-solid lines) and (b) the differences between the ensemble means of Niño3.4 SSTA in HIST-WWE5-160E and HIST-REF of cases N (black), W (red), E (purple), and C (blue). The marks in (b) indicate the 95% significant values by t-test for the WWE contributions of Niño3.4 SSTA.

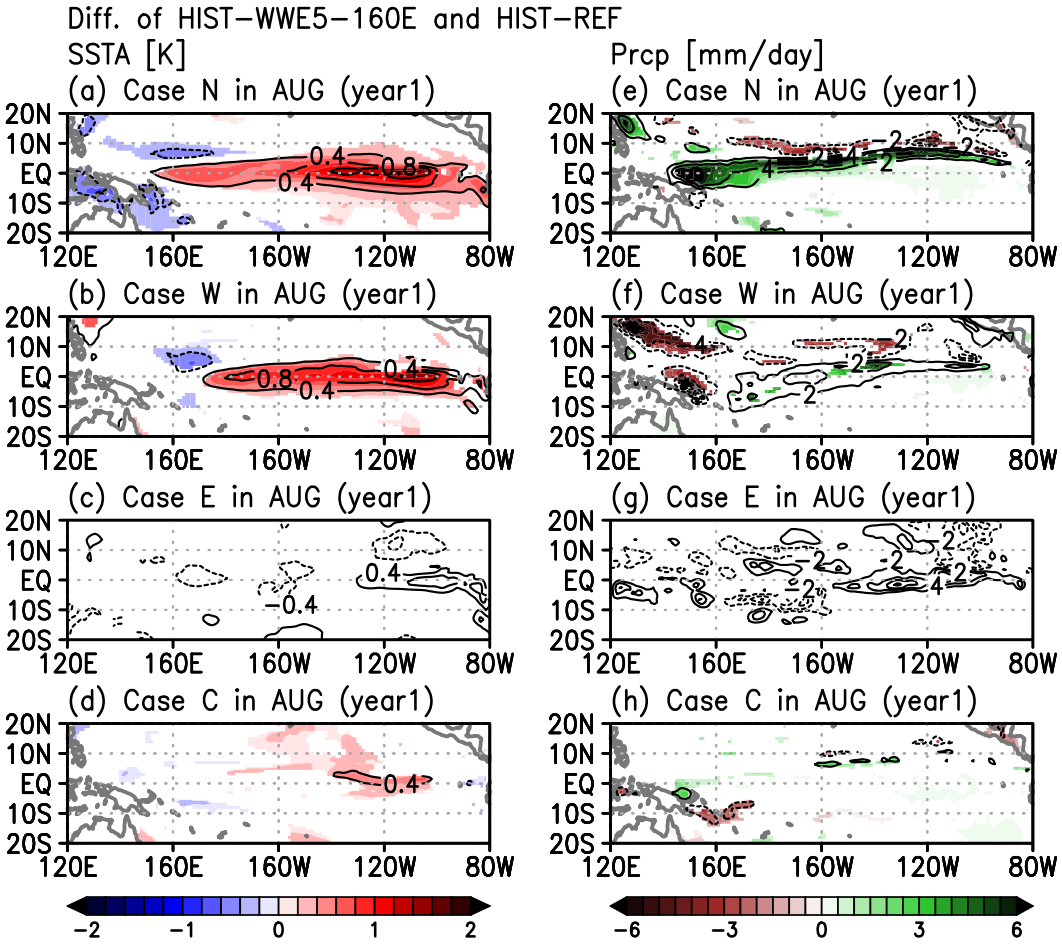

Figure 2.12: Horizontal structures of the differences between HIST-WWE5-160E and HIST-REF of (left column) SSTA [K] and (right column) precipitation [mm day^{-1}] for the ensemble means of cases N, W, E, and C in August of year 1. The 80% significant value by t-test is shaded. The contour intervals of the SSTA and precipitation anomaly are 0.4 K and 2 mm day^{-1}, respectively.

2.5 Discussion

From the series of WWE experiments conducted, it is clear that background seasonality is of importance in a coupled atmosphere-ocean response to the imposed WWE forcing. However, the sensitivity of the response to the mean seasonal march is not guaranteed in nature because of potential model biases in the climatological ITCZ and thermocline. Figure 2.13 shows the mean seasonal variations of the observed precipitation averaged over 5 °–15 °N and ocean ML temperature averaged over 2 °S–2 °N. A comparison with Fig. 2.10 indicates that the model is indeed biased to have too strong an ITCZ and a larger seasonal variation of the 20–24 °C isoline, but they are unlikely to be significant for the mechanism described in section 2.4. Specifically, precipitation over 5 °–15 °N is active and the area with an ML temperature of 20–24 °C reaches 120 °W from June to September, both of which are consistent between the model and the observations. The possible paths of oceanic Kelvin waves (phase speed is assumed as 2.2 m s^{-1}, e.g., McPhaden 2002) indicate that the WWEs inside the thick dotted lines in the figure may efficiently warm the eastern Pacific associated with the interaction with the ITCZ. The probability density function (PDF) of the observed WWE occurrences (cf. top panel of Fig. A1 in appendix A) is higher between 140 °E and 160 °W. Therefore, the rhomboidal area between the thick-dotted lines and red areas in Fig. 2.13 defines the preferable set of combination for timings and longitudes of the WWEs that maximize Niño3.4 warming. WWEs in May are indeed thought favorable to warming the Niño3.4 region, or triggering El Niño in the subsequent winter.

Past studies indicate that the relationship between WWEs and warming in the eastern Pacific is similar to that shown in our results. An example indicating the importance of timing of WWEs is “a curious case of the El Niño predicted for 2014” (McPhaden et al. 2015). Menkes et al. (2014) suggested that the major difference in El Niños in 2014/15 and the El Niño in 1997/98 is the absence of sequential WWEs after April, implying the importance of WWEs in May in triggering El Niño. Two WWEs during the period Jan-

uary to March in 2014 might result in the warming in the Niño1+2 region in June and July 2014. It is interesting that a modulation of the climatological seasonality at the equatorial Pacific in a CGCM resulted in a successful forecast of the Niño3.4 SSTA starting from April 2014 (Masuda et al. 2015), implying the importance of the realistic background seasonality on the response to WWEs. In addition to the case in 2014/15, the evolution of the SSTA in 1974/75 is also curious as McPhaden et al. (2015) pointed out. Despite the frequent occurrence of WWEs during winter 1974/75, the El Niño predicted for 1975 did not happen, but the easternmost Pacific was warmed instead in April 1975. On the other hand, preceding the large El Niños in 1982/83, 1997/98, and 2015, WWEs occurred in May. Another example is the surface warming that occurred in the far eastern Pacific in mid-2012, which had been predicted to develop an El Niño (McPhaden et al. 2015); subsequent WWEs in March and April 2012 might result in warming. Although the results in section 2.3 are derived with near-neutral initial values and therefore independent of ENSO dynamics, we confirmed in section 2.4.3 that WWEs in May similarly warm the Niño3.4 region for cases developing into El Niño.

One limitation of this chapter is that the WWEs have been prescribed. In reality, the timing and location of WWEs are partly controlled by background SST and zonal wind, as shown by Seiki and Takayabu (2007a,b) and many other studies (Lengaigne et al. 2003; Yu et al. 2003; Eisenman et al. 2005; Sooraj et al. 2009; Miyama and Hasegawa 2014; see also, Chapter 3). Generally, WWEs frequently appear over the western Pacific warm pool, and their timing is partly determined by atmospheric intraseasonal phenomena such as the MJO (Chapter 3), although the relationship between the WWEs and MJO is not very significant in previous studies (Seiki and Takayabu 2007a; Chiodi et al. 2014). The eastern edge of the warm pool is usually located to the west of the dateline, while it extends eastward during or just before an El Niño event. Based on the findings of Seiki and Takayabu (2007a), WWEs often occur near the dateline between April and July before El Niño events, consistent with the favorable WWEs that we suggest in this

chapter. Further study is needed to clarify why the timing and location are restricted in the preferable season and longitude prior to El Niño events.

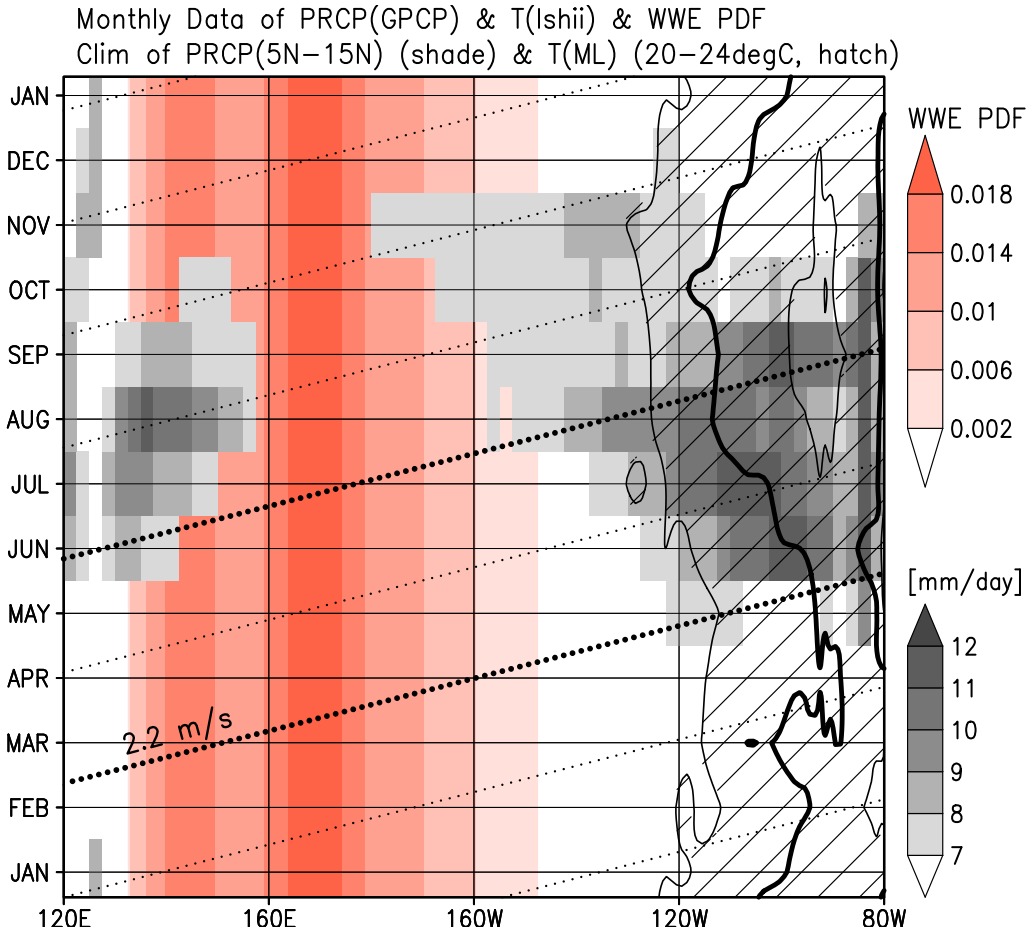

Figure 2.13: Gray color indicates the background precipitation of GPCP data averaged between 5 °N and 15 °N [unit: mm day^{-1}]. The solid line and hatching indicate the 22 °C contour and the area between 20 and 24 °C of the background ocean temperature of Ishii and Kimoto (2009) averaged between 2 °S and 2 °N in the mixed layer (from the surface to a depth of 50 m). Dotted lines indicate eastward propagating paths with a phase speed of 2.2 m s^{-1} assuming those of typical oceanic Kelvin waves in the equatorial Pacific. Red color indicate the probability density function (PDF) of WWE occurrences [longitude^{-1}] shown in Fig. A1 (top) in appendix A. Note the value of the PDF is constant in time, although it is partly overlapped by gray in this figure.

2.6 Conclusions

The response of an atmosphere-ocean coupled system to WWEs was investigated using a CGCM, focusing on the importance of background seasonality. Twelve ensemble sets of experiments initialized with ocean states close to neutral to ENSO indicate that WWEs imposed in May efficiently increase Niño3.4 SSTA, independent of the ENSO dynamics. The following three key processes were found to be responsible for Niño3.4 warming: (i) linear zonal advection resulting from an eastward surface current anomaly associated with an WWE-forced oceanic Kelvin wave; (ii) the outcropping of warm water in the subsurface in Niño3.4 region caused by the steeper background thermocline slope; and (iii) the reduction of poleward surface current at the NH due to the southward shift of the background ITCZ interacted with the positive Niño3.4 SSTA originating from (i) and (ii). The relationship between the timings of WWEs and background states of precipitation and thermocline explained above is schematically shown in Fig. 2.14. As the background seasonal march of the oceanic and atmospheric conditions is essential for (ii) and (iii), the timings of WWEs, rather than their locations, are crucial to the warming the Niño3.4 region. From observation-based data sets, we suggest a preferable set of timings and locations of a WWE that maximizes the role for triggering El Niño in the subsequent winter, indicating the importance of WWEs in May.

The impact of WWEs in May on the ENSO cycle was also investigated using the same method as mentioned above, except that the initial values included ENSO fluctuations. For moderate warm cases like El Niño, the imposed WWE affects the system similar to neutral cases. That is, the contribution to the system is almost additive and the nonlinear interaction between the initial and WWE-induced fluctuations is not dominant. On the other hand, the effect of the WWE is not significant in cold cases such as La Niña. This asymmetry originates from the precipitation activity in the ITCZ, which is more (less) active in warm (cold) cases. Although the ITCZ cannot interact with the warmer SSTA induced by the WWE in cold cases, there is the interaction between them in moderate

warm cases, similar to the neutral cases. Because, in nature, the strength of zonal wind is skewed positively over the western equatorial Pacific (see Chapter 3), the WWE is a candidate for the phenomena that generate the asymmetry of the ENSO.

The coupled atmosphere-ocean response to the WWEs can vary when the interaction with background seasonality is considered. This indicates that tropical atmospheric disturbances such as WWEs contribute to the diversity of ENSO events (Chapter 4; Capotondi et al. 2015). Furthermore, there is a possibility that the bias of atmospheric disturbances in CGCMs results in errors of a modeled ENSO. The relationship between the WWEs and ENSO in CGCMs used for CMIP5 may give us insights into the role of WWEs in the coupled system.

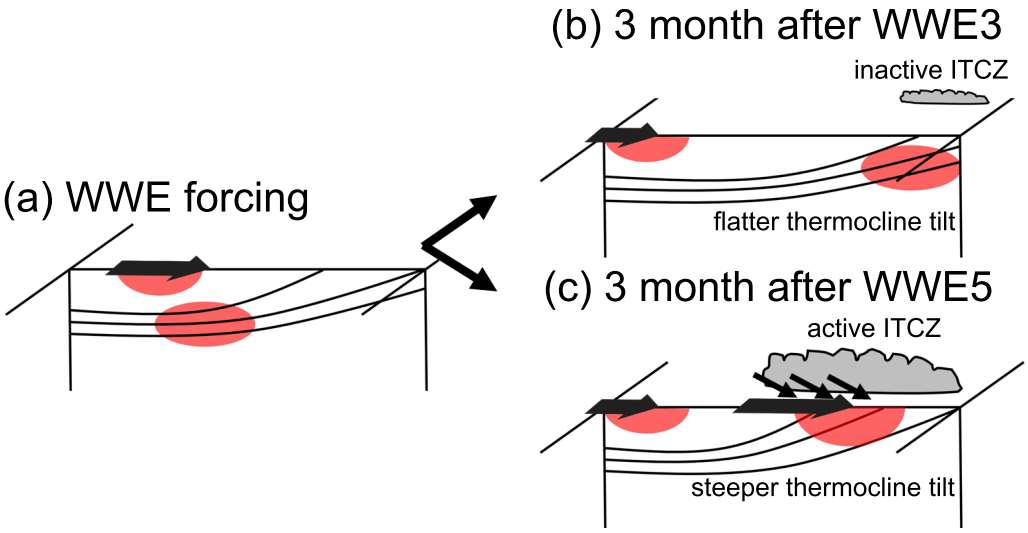

Figure 2.14: Schematic figure of the relationship between the timing of a WWE forcing and background conditions of precipitation and thermocline. Red shadings indicate the anomalous warm water. Black arrows indicate surface wind anomalies. (a) Initial condition and WWE-induced warm water. (b) 3 month after a WWE in March. (c) 3 month after a WWE in May.

Appendix A: Event detection and composited structure of WWEs

WWEs are detected following the method of Seiki and Takayabu (2007a) basically to confirm the typical properties of observed and modeled WWEs. For observed WWEs, we use the daily averaged zonal and meridional momentum fluxes of the Japanese Re-Analysis 55 Years (JRA-55, Kobayashi et al. 2015) from 1 January 1958 to 31 March 2014. The spatial resolution is 1.25° by 1.25° horizontal grids. The background data is derived by applying a 21-day running mean to averaged values for 30 years from 1981 to 2010 twice to ensure smoothness. A daily anomaly is defined as a departure from the background data. For modeled WWEs, a 100-year output of the model with a pre-industrial radiative forcing is used with a similar manner to the observed WWEs. Note that the positive zonal and meridional momentum fluxes correspond to westerly and northerly wind stresses.

Following the method of Seiki and Takayabu (2007a) basically, the conditions for detecting WWE events are as follows: The 7-day running averaged zonal momentum flux anomaly averaged between 3 °S–3 °N is larger than 0.07 N m^{-2} zonally, extending at least 10° in longitude and lasting for at least 2 days. Figure A1 shows histograms of the number of observed and modeled WWE occurrences for every 5° in longitude over the equatorial Pacific and its probability density function (PDF) derived by the kernel method using the Epanechnikov kernel (cf. Kimoto and Ghil 1993). The event number is concentrated over the western and central Pacific and it has two peaks for the observed WWEs (Fig. A1 top), consistent with Fig. 3 of Seiki and Takayabu (2007a). The PDF for the modeled WWEs is concentrated at the western Pacific (Fig. A1 bottom), affected by a model bias in the cold tongue extending too far to the west.

Using the detected WWE events in the longitudinal bins with at least four samples, we derived composite structures of the observed WWEs for each longitudinal bin centered

around the day when the anomaly has its maximum during each event. Then, the composite structures of each bin are constructed, centered in the longitudinal direction, to obtain an averaged structure of WWEs in the equatorial Pacific ignoring the overlap of events, shown in Fig. A2. Note that to confirm the overall structure of WWEs, only data over the ocean are used in compositing, even although the original data exist over the land. The properties in Figs. A1 and A2 are insensitive to the thresholds for our event detection and the averaging method.

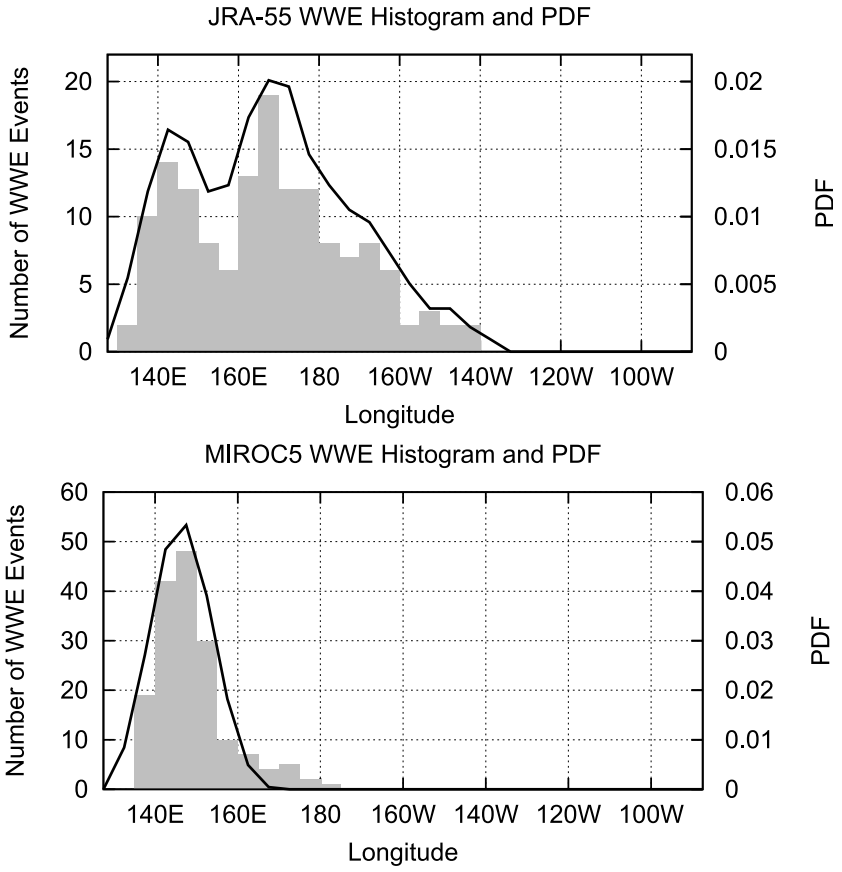

Figure A1: Histogram for the number of WWEs in the (top) observation and (bottom) model at every 5° of longitude over the Pacific (gray bars) and the probability density function (solid line).

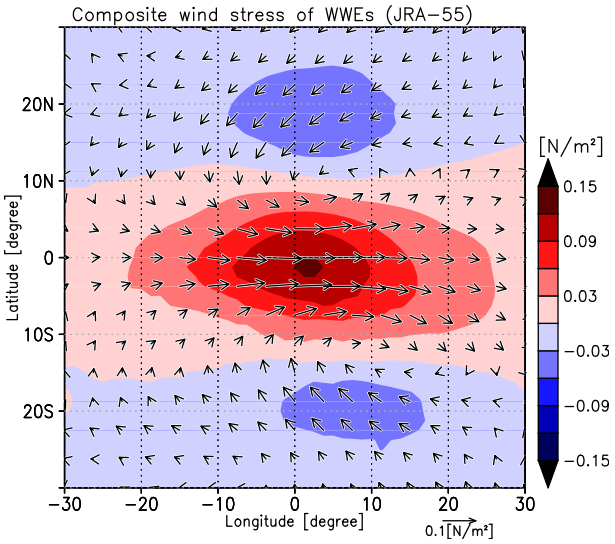

Figure A2: Horizontal structure of composited WWE in the observation. The vector and color indicate the wind stress anomaly and its zonal component, respectively.

Chapter 3

Asymmetry of westerly and easterly wind events: Observational evidence

Abstract

Westerly (WWEs) and easterly (EWEs) wind events, short-lived anomalous surface westerly and easterly winds, are known to occur with unusually large magnitude over the equatorial Pacific. As their relative frequency of occurrence and dependence on background conditions are yet to be fully clarified, we analyzed daily surface winds for 1982–2013 from which WWEs and EWEs are detected. Both types of events appear over the western Pacific warm pool, where sea surface temperature (SST) is sufficiently high for active deep convection, with a similar seasonality, and they favorably occur with increasing Niño4 (160 °E–150 °W, 5 °S–5 °N) SST. The relationship of occurrence of both events with phases of the Madden-Julian oscillation is also identified. However, the frequency of occurrence of EWEs is much less than that of WWEs, resulting in asymmetry in wind amplitude. Local and remote anomalous convections are equally important in exciting these events, but different local development processes cause the asymmetry in the frequency of occurrence. These results can also be seen in wind stress anomalies, albeit obscured

due to nonlinearity therein.

3.1 Introduction

Short-lived anomalous surface westerly wind epochs over the equatorial Pacific, westerly wind events (WWEs) (e.g., Luther et al. 1983; Hartten 1996; Harrison and Vecchi 1997; Seiki and Takayabu 2007a,b), act to warm the eastern equatorial Pacific (Chapter 2; Vecchi and Harrison 2000; Lengaigne et al. 2002; Chiodi et al. 2014) and sometimes trigger El Niños (McPhaden 1999; Lengaigne et al. 2004). Eisenman et al. (2005) showed that WWE occurrence is dependent on sea surface temperature (SST) variability in the western Pacific warm pool associated with the El Niño-Southern Oscillation (ENSO) phenomenon (see also, Lengaigne et al. 2003; Vecchi et al. 2006). In contrast, anomalous easterly counterparts, easterly wind events (EWEs), induce a cold SST anomaly in the eastern Pacific and may suppress El Niño growth (Takayabu et al. 1999; Lengaigne et al. 2004, 2006; Chiodi and Harrison 2015; Min et al. 2015). Takayabu et al. (1999) showed that an abrupt intensification of the easterly trade winds in May 1998 caused the rapid termination of the 1997 El Niño. Lengaigne et al. (2004, 2006) indicated that episodic reinforcement of trade winds limits the central and eastern Pacific warming and initiates La Niña. However, very few studies have compared the statistical properties of these events and their relationship with interannual variability.

Presence of EWEs has been uncovered in two recent studies (Chiodi and Harrison 2015; Puy et al. 2015). Despite a similarity between WWEs and EWEs in terms of the spatio-temporal structure and the impact on the underlying ocean, their relationship with the interannual variability is still under debate. Chiodi and Harrison (2015) showed frequent occurrence of EWEs during the cold phase of ENSO, whereas Puy et al. (2015) argued that the above state dependence of EWEs relies on the definition and found no robust relationship between EWE occurrence and the warm pool displacement in the west-

ern Pacific once the interannual anomalies of wind stress are excluded. While Chiodi and Harrison (2015) did not make a direct comparison of the frequency of occurrence of WWEs and EWEs, Puy et al. (2015) showed that EWEs occurred as frequently as WWEs with given thresholds for the event detection. However, the use of wind stress anomaly results in an exaggeration of EWEs over the central and eastern Pacific due to nonlinearity of the wind stresses (see appendix B and Chiodi and Harrison 2015). This causes ambiguity in the relative occurrence frequency between WWEs and EWEs and their dependence on the background conditions, although these may influence the ENSO cycle. In this chapter, statistical properties of WWEs and EWEs are investigated using surface wind data, with focuses on the asymmetry of their occurrence frequencies and the relationship with the interannual SST variability.

The rest of this chapter is structured as follows. Section 3.2 shows data sets of atmosphere and ocean and methods of analysis. In section 3.3, the characteristics of WWEs and EWEs is described. The development process of WWEs and EWEs is examined in section 3.4. Section 3.5 provides conclusions and discussion.

3.2 Data and Method

3.2.1 Observational data

We use daily-averaged data derived from the following atmospheric and oceanic reanalysis products interpolated on a 1° by 1° grid from 1 January 1982 to 31 December 2013: the Japanese Re-Analysis 55 Years (JRA-55) data (Kobayashi et al. 2015) for atmospheric variables including the horizontal wind at 10 m height (surface wind), NOAA High Resolution SST (Reynolds et al. 2007), and interpolated outgoing longwave radiation (OLR) data provided by the NOAA/OAR/ESRL PSD (Liebmann and Smith 1996). We define anomaly as a deviation from the climatology, which is calculated as the long-term daily average for 1982–2013 with an 11-day running mean. The high-frequency (HF) com-

ponent of the anomaly is then defined by subtracting the interannual component, i.e., a 91-day running mean of the anomaly, and then applying a 3-day running mean to remove daily-scale noise. The sum of the climatology and the interannual component is regarded as the background state for the HF anomalies.

To analyze the relationship between WWE/EWE and the Madden-Julain oscillation (MJO) (e.g., Madden and Julian 1971, 1972, 1994; Zhang 2005), we use an MJO index of Wheeler and Hendon (2004) (provided by H. Hendon), defined by the principal component time series of a pair of empirical orthogonal function of the combined fields of near-equatorially averaged 850-hPa zonal wind, 200-hPa zonal wind, and OLR data.

3.2.2 Event detection

Several criteria have been used to detect WWEs in surface wind datasets (Hartten 1996; Harrison and Vecchi 1997; Seiki and Takayabu 2007a; Chiodi et al. 2014). Following the previous investigations into WWEs, we extract WWEs and EWEs based on the method in Seiki and Takayabu (2007a) using the HF surface wind anomaly averaged between 2.5 °S and 2.5 °N. The thresholds of the magnitude, duration, and zonal extent are 5 m s^{-1}, 2 days, and 10° in longitude, respectively. An event is required to satisfy the three thresholds at each grid over the equatorial Pacific (120 °E–80 °W). Note that results are qualitatively similar with different thresholds for wind magnitude (Table B1 and Fig. B1a in appendix B). The central day and longitude of each event are determined by the date and location of the maximum magnitude of the event. An event is considered to be consecutive when its center is less than 10° in longitude distant from its position in the previous day.

3.2.3 Analysis Method

In the composite analysis, the central longitude of each event is set to be 0° in relative longitude (hereafter, RL). In the lag composite analysis, "day 0" indicates the central day of the event and "day $-N$ ($+N$)" indicates the Nth day lagging (leading) it. For calculating

the statistical significance level, a two-tailed Student's t-test is conducted assuming that individual events are independent.

In the eddy kinetic energy (EKE) tendency analysis, the HF anomaly of zonal wind at 850 hPa is decomposed into the eddy (u', higher than about 20 days) and intraseasonal (u'', lower than about 20 days) components. Since barotropic energy accumulation due to the low-level zonal winds is a dominant contributor to the EKE generation along the equator for both WWEs and EWEs (appendix C), the difference in developing processes between WWEs and EWEs is demonstrated by

$$\frac{\partial K'}{\partial t} = -\overline{u'u'\frac{\partial U_0}{\partial x}} - \overline{u'u'\frac{\partial u''}{\partial x}} + R, \tag{3.1}$$

where $K' \equiv \overline{u'^2 + v'^2}/2$ is the EKE, v' is the eddy component of the meridional wind at 850 hPa, the overbar indicates an 11-day running mean, U_0 is the background of the zonal wind, and R indicates the other terms.

A linear baroclinic model (LBM) (Watanabe and Kimoto 2000, 2001) is used to examine the linear response of atmospheric circulation to anomalous deep convection associated with WWEs and EWEs. The LBM consists of the primitive equation system linearized about a basic state and has a spatial resolution of T42 with 20 σ levels in the vertical. The three-dimensional composite backgrounds of WWEs and EWEs are used for the model basic state of the horizontal wind, temperature, and sea level pressure to simulate the WWE and EWE, respectively (e.g., vectors in Figs. 3.10c and 3.10d). The horizontal structure of the prescribed heating is determined based on the composite structures of the HF OLR anomaly associated with the WWE and EWE (cf. Fig. 3.7), and the vertical structure $S(z)$ is provided as

$$S = m_0(1 + \nu^2)\{1 + \exp(\pi\nu)\}\exp(m_0\nu z)\sin(m_0 z), \tag{3.2}$$

where ν is a dimensionless parameter, $m_0 = \pi/h$, and h is the top of the tropopause (15

km) (Fuchs et al. 2012). For the peak to occur at upper levels (about 400–300 hPa), $\nu = 0.5$ is used. For translation into σ levels, the equivalent depth is assumed to be 8.3 km. The forcing is standardized to have a maximum magnitude of 5 K day^{-1}. Note that the magnitude itself has no meaning owing to the linearity. The steady response to the forcing is obtained by time integration for 80 days.

3.3 Results

3.3.1 Statistics of WWEs and EWEs

We detected 101 and 23 WWEs and EWEs for 32 years, respectively (Fig. 3.1a). The number of events varies with slightly different detection thresholds, but the frequency of occurrence of EWEs is less than that of WWEs regardless of the threshold (Table B1 in appendix B). This robust asymmetry in the frequency of occurrence may result in WWEs to have stronger magnitude and longer duration than EWEs probabilistically (Fig. 3.2).

On the other hand, both events favorably occur in a similar season and location (Fig. 3.3); they occur rarely in the boreal summer but frequently in the boreal winter, and preferentially appear over the Eastern Hemisphere (a few WWEs are also observed over the Western Hemisphere). This indicates the similar dependence of the occurrences of both WWEs and EWEs on background state with its seasonal march.

3.3.2 Dependence on background state

The relationship between event occurrence and interannual SST variability is shown in Fig. 3.1. A comparison of the number of events with the time series of the monthly Niño4 SST anomaly (160 °E–150 °W, 5 °S–5 °N) shows that WWEs and EWEs are both observed frequently during the positive Niño4 SST anomaly. Indeed, the histogram of the event occurrence and the probability density function (PDF) calculated by the Epanechnikov kernel (Kimoto and Ghil 1993) indicate that both WWEs and EWEs have a very

similar shape skewed toward the positive Niño4 SST anomaly. The interannual variations associated with WWEs and EWEs are seen in the composite structures of the interannual anomalies of SST, OLR and horizontal wind at the peak date of these events (Fig. 3.4). Both WWEs and EWEs occur to the west of the broadly positive SST anomaly accompanied by anomalous active deep convections and low-level westerly, consistent with the dependence on the Niño4 SST anomaly. Since the Niño4 SST anomaly is related to the warm pool expansion having important roles in El Niño onset and growth (Picaut et al. 1996; Lengaigne et al. 2004) and is a measure of the central Pacific El Niño and La Niña (Takahashi et al. 2011; Cai et al. 2015), the above relationship implies that not only WWEs but also EWEs are probabilistically state dependent as suggested by Jin et al. (2007). Note that the dependence of WWEs and EWEs on the Niño3.4 (120 °–170 °W, 5 °S–5 °N) SST anomaly vanishes when the interannual wind anomaly is removed (Fig. B1a, b in appendix B).

The dependence of the HF zonal wind including the WWE/EWE events on the background SST and OLR is presented in Fig. 3.5. The HF wind anomaly greater than 5 m s^{-1} or less than −5 m s^{-1}, thresholds for the WWE and EWE, preferentially occurs when the background SST is greater than 28.5 °C (Fig. 3.5a) and the background OLR is less than 230 W m^{-2} (Fig. 3.5b). This indicates that the warm pool, where the SST is sufficiently high for active deep convection, is favorable not only for WWEs but also for EWEs, consistent with the fact that the eastward expansion of the warm pool or the positive Niño4 SST anomaly is accompanied by the frequent occurrences of WWEs and EWEs (Fig. 3.1).

Any difference in occurrence frequency of WWEs and EWEs is unclear when using the HF zonal wind stress anomaly. The nonlinearity of the wind stress anomaly with respect to the background winds (e.g., Trenberth et al. 1989) makes the anomaly skewed negatively (Fig. B2) and exaggerates the EWE occurrences over the central and eastern Pacific (Fig. B3), as suggested by Chiodi and Harrison (2015). This exaggeration

of EWEs obscures the asymmetry in the frequency of occurrence except for extremely strong events (Table B1), consistent with Puy et al. (2015), and their dependence on the background (Fig. B1). See appendix B for further discussion.

3.3.3 Relationship with the phases of the MJO

The relationship of occurrence of WWEs and EWEs with the MJO is examined using a MJO index (Wheeler and Hendon 2004). Figure 3.6 shows the histograms of occurrences of WWEs and EWEs for eight phases of the MJO. WWEs favor to occur during phase 7, where active (suppressed) deep convection and low-level westerly (easterly) over the western Pacific (Indian) Ocean (see Fig. 8 of Wheeler and Hendon (2004)). In contrast, EWEs frequently occur during phase 3, where suppressed (active) deep convection and low-level easterly (westerly) over the western Pacific (Indian) Ocean. This relationship is still robust when the events are detected using different thresholds (figure not shown). Although some previous studies showed the statistically insignificant relationship of WWEs identified using surface wind anomalies relative to seasonal cycle with the MJO (Seiki and Takayabu 2007a; Chiodi et al. 2014), this result implies that both the occurrences of WWEs and EWEs are supported by the MJO.

3.3.4 Spatio-temporal structures

The structure of the WWE and EWE is examined using the composite analysis. Horizontal patterns of HF winds and OLR anomalies at the peak date are similar to each other except with the sign reversed (Fig. 3.7). The WWE (EWE) is shown to couple with in situ active (suppressed) convections, which accompany anomalous convections having the opposite sign and extending in the upstream region from -90° to -30° in RL. Such horizontal structures are also seen in Fig. 4 of Puy et al. (2015), but only the in situ anomalies were focused. The local and remote OLR patterns are consistent with the vertical profiles of HF upward motions (Fig. 3.8). Since the horizontal extent of the remote OLR

anomalies is about twice area of the local anomalies, atmospheric circulation induced by the remote anomalies can be comparable to that induced by the local anomalies in a linear sense. A dynamical analysis demonstrates that local and remote convective activities are equally important for intensifying the zonal wind anomaly associated with the WWE and EWE (see the next section). From the vertical structures of equatorial zonal wind of the WWE and EWE (Fig. 3.8), it is found that the westerly anomaly of the WWE at the central longitude is deeper than the easterly anomaly of the EWE.

The temporal evolutions of the WWE and EWE along the equator are shown in Fig. 3.9. The remote suppressed (active) convective anomaly of the WWE (EWE) propagates eastward from -90° to 0° in RL with a phase speed of about 5 m s^{-1}. The cyclonic and convective signal of the WWE propagates eastward slowly from -50° to 0° in RL prior to the peak date, but the propagation is not robustly seen. The cyclonic vorticity associated with the WWE propagates westward after the peak date. The EWE is accompanied by a westward-propagating disturbance with anticyclonic vorticity prior to the peak date from -30° to 0° in RL. The growth rate of the WWE is greatly larger than that of the EWE near the peak date at the central longitude, indicating the importance of local development processes for WWEs.

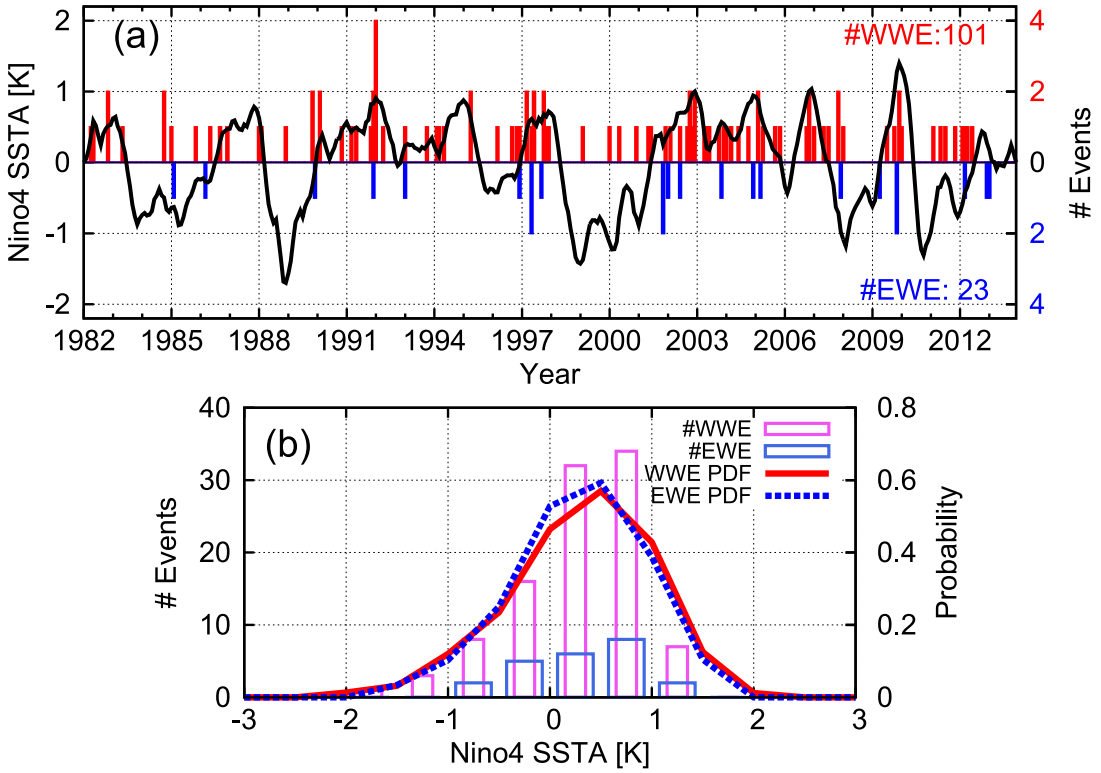

Figure 3.1: (a) Time series of the Niño4 SST anomaly [K] (solid line) and the number of occurrences of WWEs (red bars) and EWEs (blue bars) in every month. The total numbers of the event occurrence are shown in the panel. (b) Histogram for the occurrences of WWEs (pink boxes) and EWEs (light blue boxes) and probability density function of WWEs (red solid) and EWEs (blue dotted) with respect to the Niño4 SST anomaly [K].

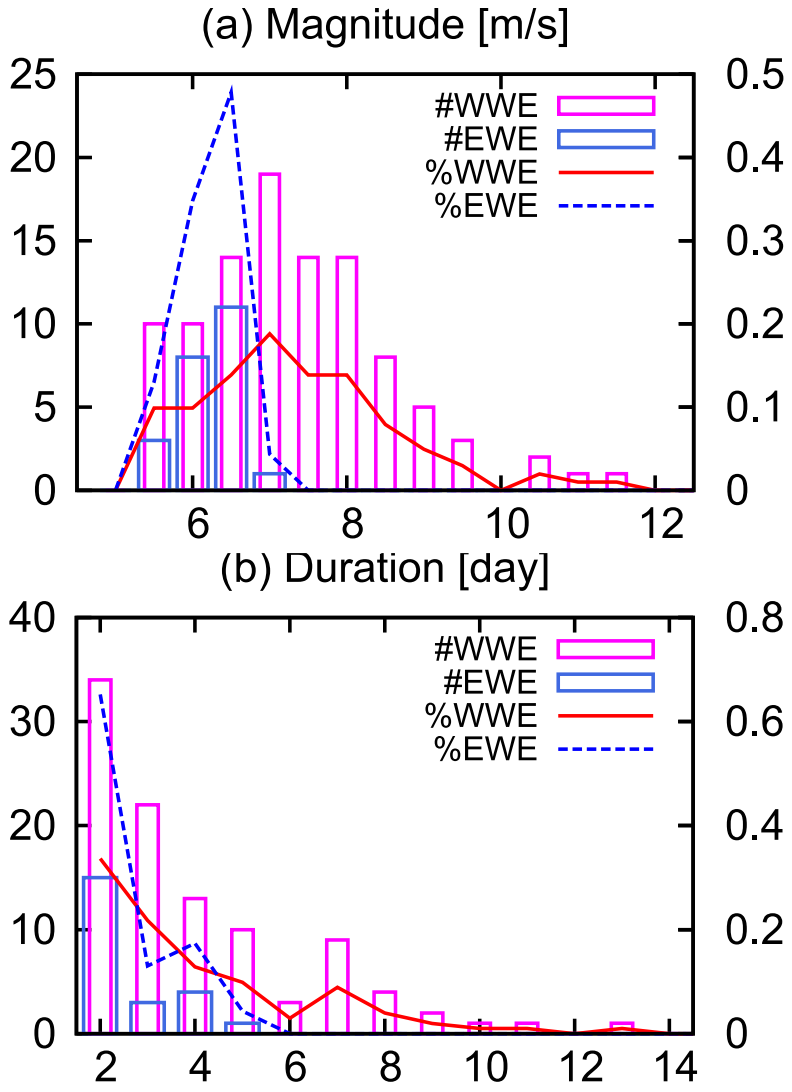

Figure 3.2: Histograms for occurrences of WWEs and EWEs (left vertical axis) and their ratio to the total number (right vertical axis): (a) magnitude [m s^{-1}] and (b) duration [day].

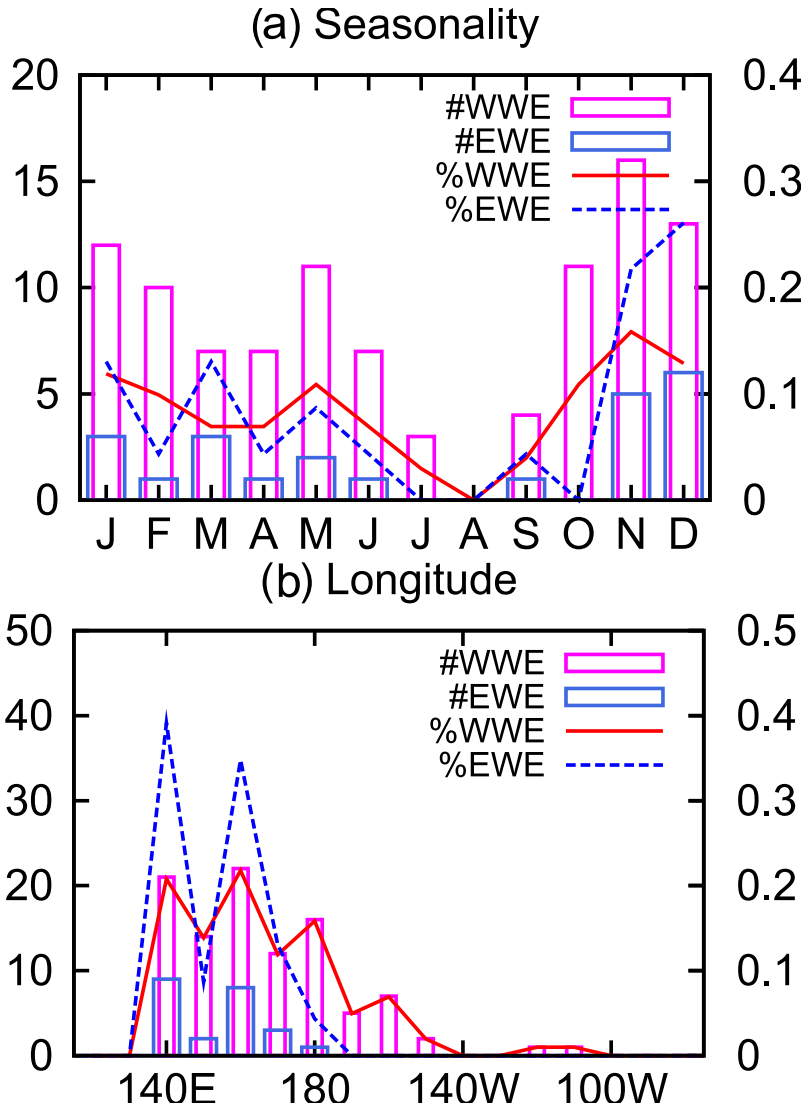

Figure 3.3: Histograms for occurrences of WWEs and EWEs (left vertical axis) and their ratio to the total number (right vertical axis): (a) seasonality from January to December and (b) location [degree in longitude].

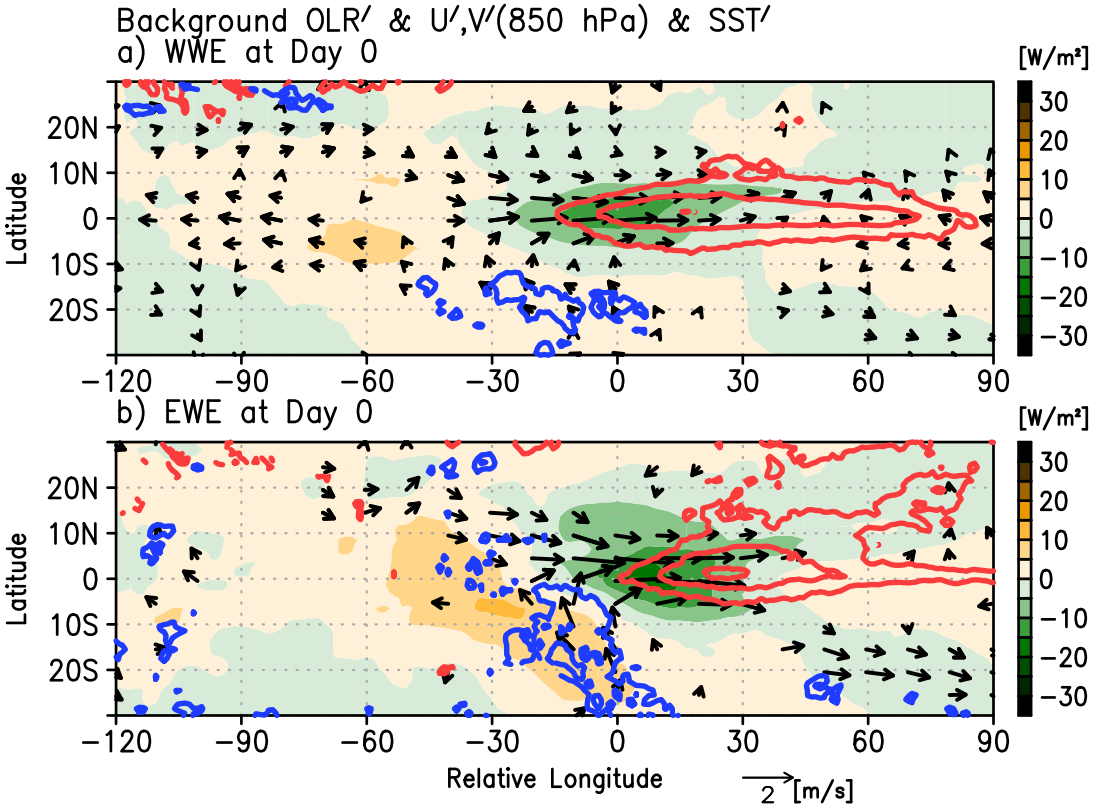

Figure 3.4: Composite horizontal structures of the interannual anomalies of (a) WWEs and (b) EWEs. Vector indicates the wind anomaly at 850 hPa [see legend for magnitude] where both the zonal and meridional components exceed 95% statistical confidence. Shade indicates the OLR anomaly [W m^{-2}]. Red and blue contours indicate the positive and negative SST anomaly [contour interval: 0.2 K].

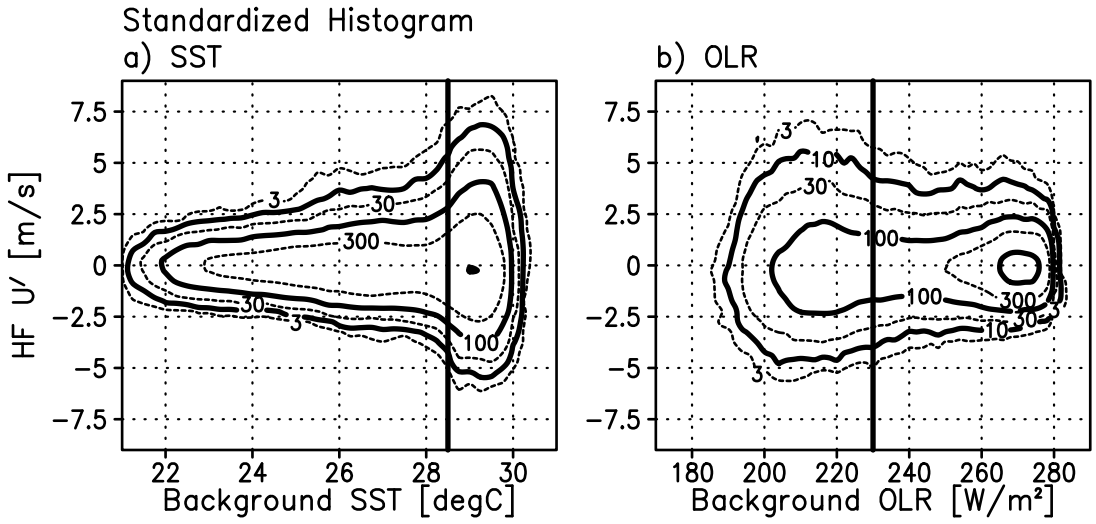

Figure 3.5: Histograms standardized by the total number of occurrence for the HF zonal surface wind anomaly [m s^{-1}] averaged between 2.5 °S and 2.5 °N over the equatorial Pacific (120 °E–80 °W) with respect to background (black contour, $\times 10^{-5}$) of (a) SST [°C] and (b) OLR [W m^{-2}]. Vertical solid lines in (a) and (b) indicate 28.5 °C and 230 W m^{-2}, respectively.

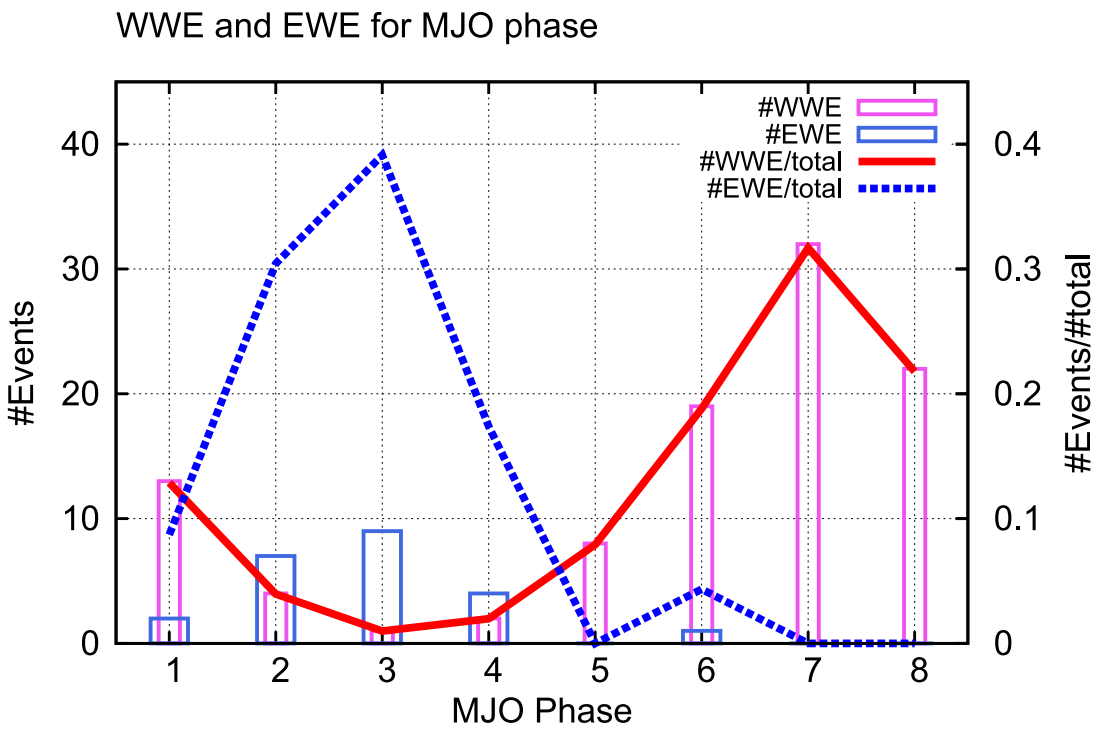

Figure 3.6: Histograms of the number of occurrence of (red boxes) WWEs and (blue boxes) EWEs for phases of the MJO (left vertical axis). MJO index produced by Wheeler and Hendon (2004) is used. Red and blue lines indicate the ratio to the total number of occurrence (right vertical axis).

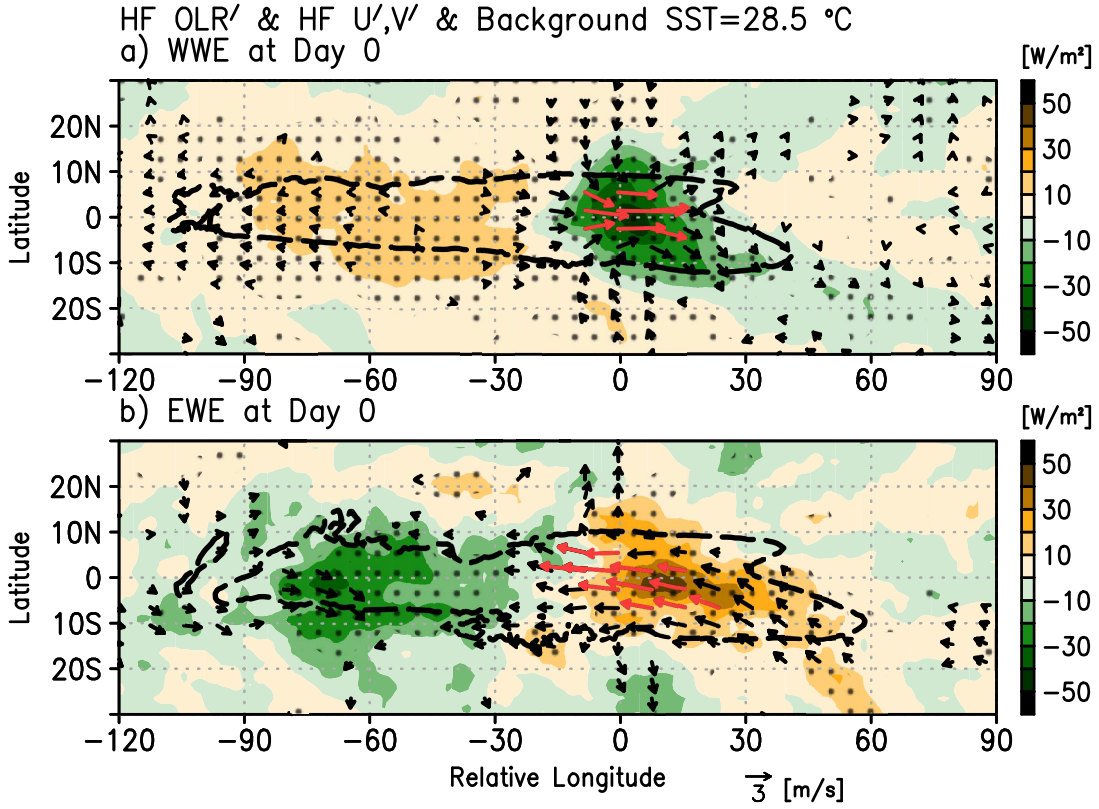

Figure 3.7: Horizontal structures of the composite of (a) WWEs and (b) EWEs at the peak day. Vector indicates the HF surface wind anomaly [see legend for magnitude] where both the zonal and meridional components exceed 95% statistical confidence. Red vectors indicate the zonal component is larger than 3 m s^{-1}. Shade indicates the HF OLR anomaly [W m^{-2}] and dots indicate the value exceeds 95% statistical confidence. Thick dashed line indicates the background SST is 28.5 °C.

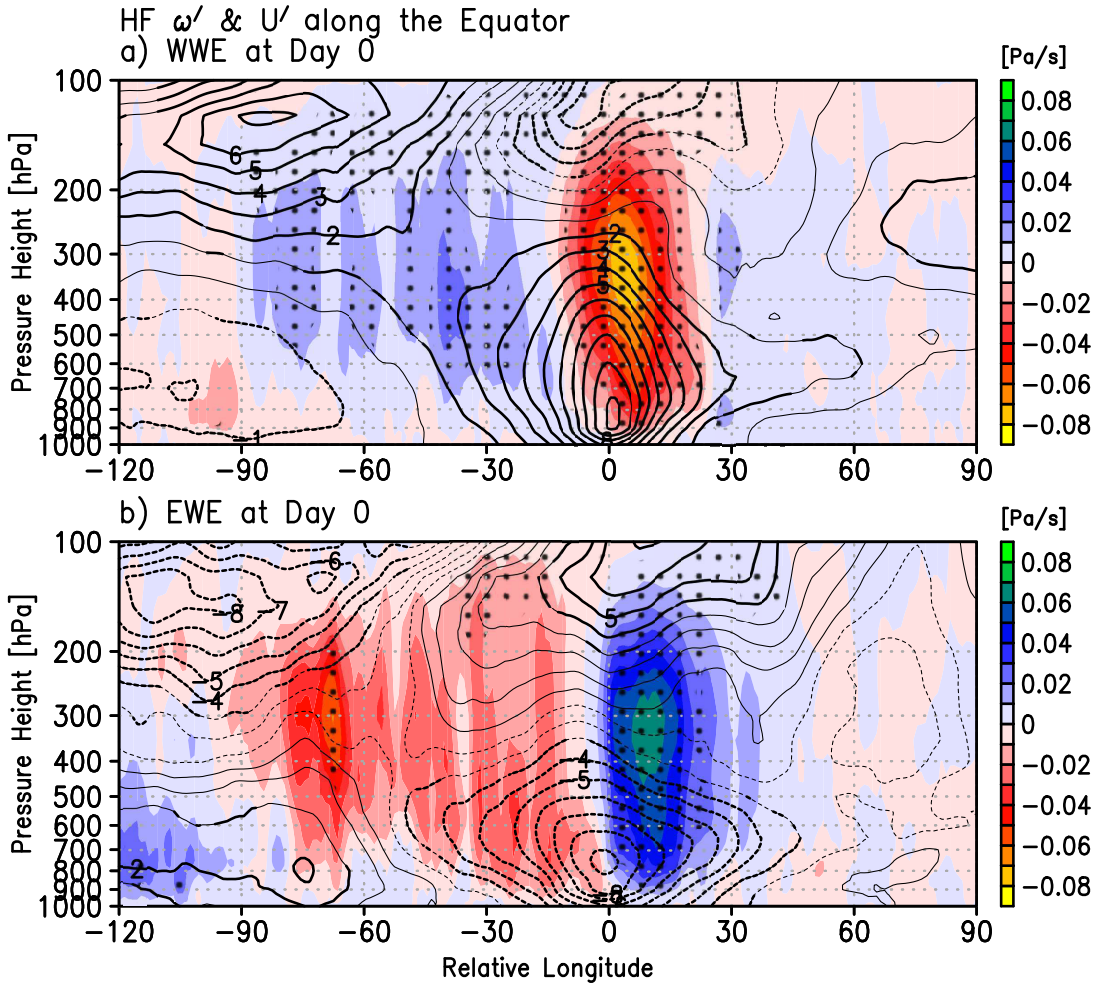

Figure 3.8: Composite vertical structures of the HF anomaly of (a) WWEs and (b) EWEs along the equator. Contour and shade indicate the zonal wind [contour interval: 1 m s^{-1}] and pressure velocity [Pa s^{-1}], respectively, and thick line and dot indicate values exceed 95% statistical confidence.

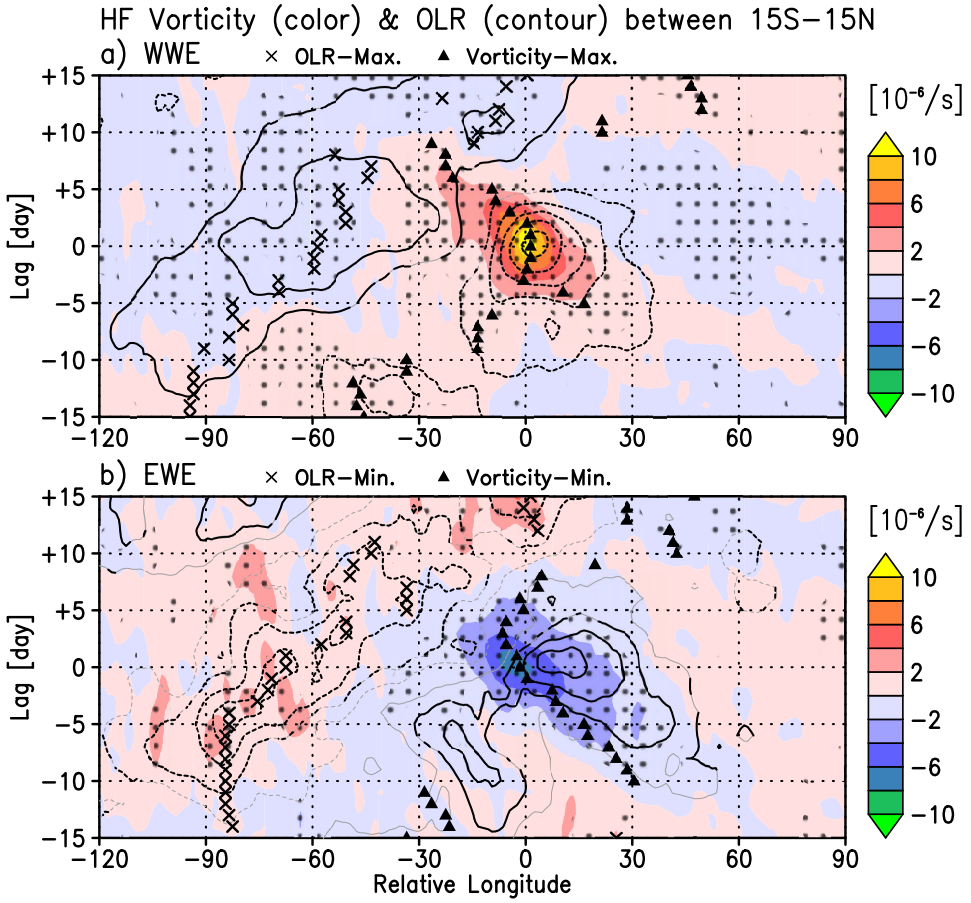

Figure 3.9: Lag composite structure of (a) WWEs and (b) EWEs for the HF components of the equatorial-symmetric vorticity at 850 hPa (shade) and OLR (contour) averaged between 15 °S and 15 °N from day −15 to day +15. Contour interval is 5 W m^{-2}, and negative contours are dashed. Triangles denote the negatively (positively) maximum points of the vorticity for the WWE (EWE) between −50° and 50° in RL. Crosses denote the positively (negatively) maximum points of the OLR for the WWE (EWE) between −120° and 90° in RL. Dots and thick lines indicate values of the vorticity and OLR, respectively, exceed 95% statistical confidence

3.4 Development processes

3.4.1 Local process

An analysis on the EKE at the peak date demonstrates the difference in development processes near the central longitude between the WWE and EWE (see subsection 3.2.3). The EKE of the WWE is larger than that of the EWE along the equator (Fig. 3.10a, b). The EKE is similarly generated due to barotropic energy accumulation by U_0 (background) for both the WWE and EWE (Fig. 3.10c, d). On the other hand, the EKE tendencies associated with u'' (intraseasonal) have asymmetric structures between the WWE and EWE since u'' is westerly for the WWE but easterly for the EWE at lower levels (Fig. 3.10e, f). Since the peaks of both terms for the WWE share their locations, the EKE is effectively generated, resulting in the deep westerly along the equator as seen in Fig. 3.8a, consistent with Seiki and Takayabu (2007b). This process causes the rapid growth of the WWE shown in Fig. 3.9a. In contrast, the structure of u'' associated with the EWE is unfavorable to generate the EKE near the central longitude where U_0 contributes to the EKE generation, causing the EKE of EWEs smaller than that of WWEs.

This result indicates that the anomalous surface easterly is not detectable frequently as an epoch of EWEs, resulting in less frequent occurrence of EWEs. Therefore, the asymmetry in the intraseasonal zonal wind embedded in WWEs and EWEs contributes nonlinearly to the asymmetry in the frequency of occurrence. In other words, the local development process that is crucial for WWEs (Seiki and Takayabu 2007b) is not efficient to produce EWEs. This implies the importance of other processes to enhance the surface easterly (see the next subsection).

3.4.2 Remote process

In the composite structures (Figs. 3.7 and 3.9), the WWE and EWE are involved with the suppressed and active convective region extending in the upstream region, respec-

tively. However, it is unclear whether such remote anomalous convection induces the in-situ zonal wind with considerable magnitude. To estimate the relative importance of the remote convective anomaly, a dynamical analysis was conducted using the LBM (see subsection 3.2.3). To separate the contributions of heating and cooling to the response, we conducted three kinds of experiments for each event: "CTL" experiment with both the heating and cooling (Fig. 3.11a, e), "Cooling" experiment with the cooling only (Fig. 3.11b, f), and "Heating" experiment with the heating only (Fig. 3.11c, g). The responses to the remote (i.e., around -60° in RL) convective anomalies of the WWE and EWE are corresponding to WWE Cooling (Fig. 3.11b) and EWE Heating (Fig. 3.11g) experiments, respectively, and those to the local (i.e., around 0° in RL) convective anomalies of the WWE and EWE are corresponding to WWE Heating (Fig. 3.11c) and EWE Cooling (Fig. 3.11f) experiments, respectively.

The steady responses of the atmospheric circulation to the prescribed heating scenarios are shown in Fig. 3.11. In CTL experiments, the structures of the horizontal flow are similar to the composite WWE and EWE. The responses in Heating and Cooling experiments shown in Fig. 3.11 (b, c, f, g) indicate that both the local and remote convective anomalies induce the zonal winds with the same sign at lower levels. Figure 3.11d (3.11h) shows that the response to the remote cooling (heating) has magnitude comparable to that to the local heating (cooling) for the WWE (EWE). The responses to both the remote and local convective anomalies have their peak near 0° in RL since the background structure prescribed in the model is favorable to amplify the response there (cf. Fig. 3.10c, d). The above results indicate that the westerly (easterly) wind is intensified not only by the local active (suppressed) convection but also by the remote suppressed (active) convection in terms of the linear response to the prescribed heating scenarios. Therefore, both the local and remote anomalous convections are crucial to excite WWEs and EWEs.

3.4.3 Implications for development of WWEs and EWEs

The temporal evolution of WWEs and EWEs was examined in subsection 3.3.4 based on the composite analysis (Fig. 3.9). To further discuss the development of these events, the preceding structures of the atmospheric circulation and specific humidity at day −9 are shown in Figs. 3.12 and 3.13. The vertical structures of the zonal-vertical flow and the equatorial-symmetric part of the meridional velocity in Fig. 3.12 indicate that the remote convective anomalies of both the WWE and EWE near −90° in RL are accompanied by disturbances having baroclinic structures, which propagates eastward from −90° to 0° in RL with a phase speed of about 5 m s^{-1} (Fig. 3.9). The eastward-propagating disturbance is involved with the drier (wetter) humidity at lower levels for the WWE (EWE) (Figs. 3.12 and 3.13). Such remote suppressed (active) convective anomaly of the WWE (EWE) may be associated with the MJO because of their slow eastward propagation (Fig. 3.9) and a baroclinic structure (Fig. 3.12). The cyclonic and convective signal prior to the WWE also seems to propagate eastward slowly from −50° to 0° in RL (Fig. 3.9a) accompanied by a baroclinic structure near 20° in RL at day −9 (Fig. 3.12a), although the eastward propagation is not robustly seen in Fig. 3.9a as mentioned in previous studies (Seiki and Takayabu 2007a; Chiodi et al. 2014). This implies the importance of local development processes for WWEs. Nevertheless, the MJO, accompanied by large-scale circulation from the Indian to western Pacific Oceans, robustly influences the occurrences of both WWEs and EWEs (Fig. 3.6).

The westward propagation of cyclonic vorticity lagging the WWE from day 0 to +5 near the central longitude (Fig. 3.9a) is probably related to a single cyclone or a series of cyclones in one or both hemisphere (Hartten 1996; Harrison and Vecchi 1997). A westward-propagating disturbance with anticyclonic vorticity, leading the EWE from day −10 to 0 (Fig. 3.9b), has the equivalent barotropic structure near 20° in RL at day −9 (Fig. 3.12b). Its anticyclonic structure is confirmed not only at the lower level (Fig. 3.9b) but also at the upper level near 30° in RL prior to the EWE (Fig. 3.13b). This

westward-propagating disturbance associated with the EWE could be convectively coupled equatorial Rossby waves (Kiladis and Wheeler 1995; Yang et al. 2007; Puy et al. 2015). This accompanies a negative specific humidity anomaly in the mid-troposphere and subsidence through the troposphere near 30° in RL (Figs. 3.12b and 3.13b), contributing to suppress the convection associated with the EWE. The suppressed convection can enhance the surface easterly (cf. Fig. 3.11f), generating detectable epochs as EWEs.

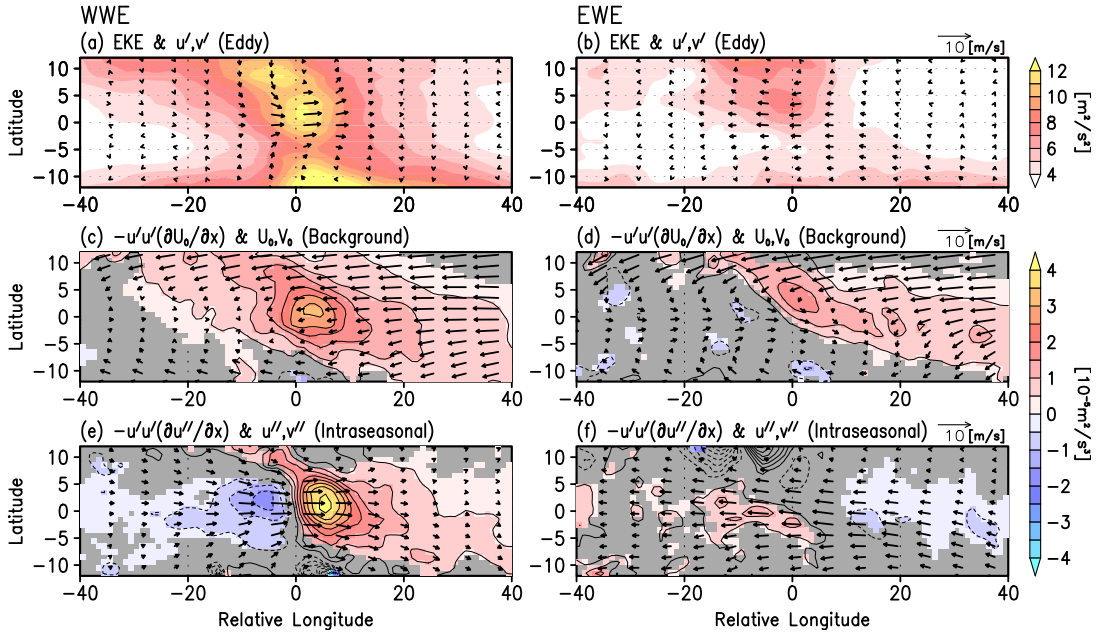

Figure 3.10: Composite structures of (a, b) the EKE with colors [m^2 s^{-2}] and (c-f) its tendencies due to the zonal gradients of the background and intraseasonal zonal winds at 850 hPa with colors and contours [10^{-5} m^2 s^{-3}] for (left) WWEs and (right) EWEs at the peak day. Vectors indicate the 3-day running means of the (a, b) eddy, (c, d) background, and (e, f) intraseasonal components of the horizontal winds at 850 hPa [m s^{-1}]. Gray shade in (c-f) indicates the value does not exceed 95% statistical confidence.

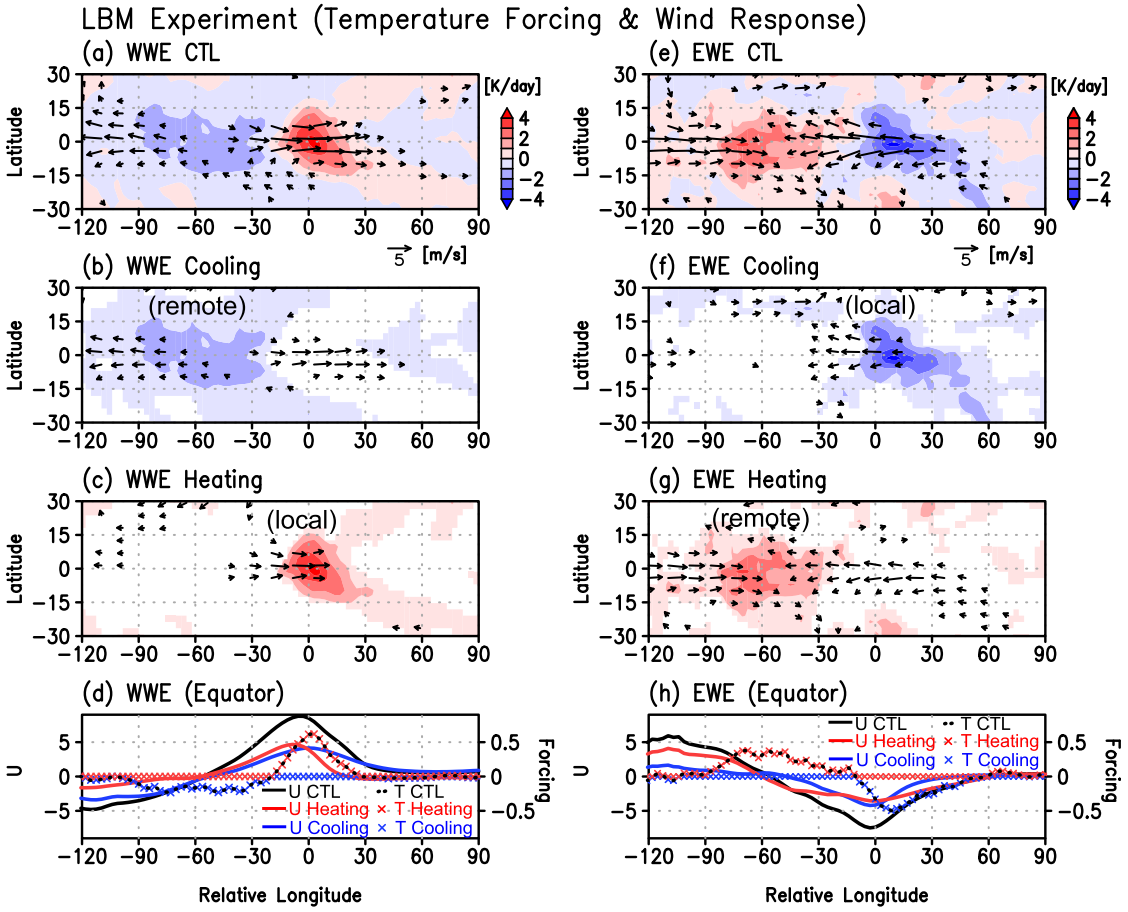

Figure 3.11: Results of the LBM experiments for WWE (left column) and EWE (right column). (a-c and e-g) Horizontal structures of horizontal wind response [m s^{-1}] at 850 hPa larger than the magnitude of 2 m s^{-1} (vector) and prescribed heating [K day^{-1}] at 400 hPa (shade) for CTL, Heating, and Cooling experiments. (d and h) Longitudinal structures of the prescribed heating [K day^{-1}] at 400 hPa (dotted line and red/blue marks indicate CTL and Heating/Cooling experiments, respectively) and the corresponding zonal wind response [m s^{-1}] at 850 hPa (solid black, red, and blue lines, respectively) averaged between 5 °S and 5 °N.

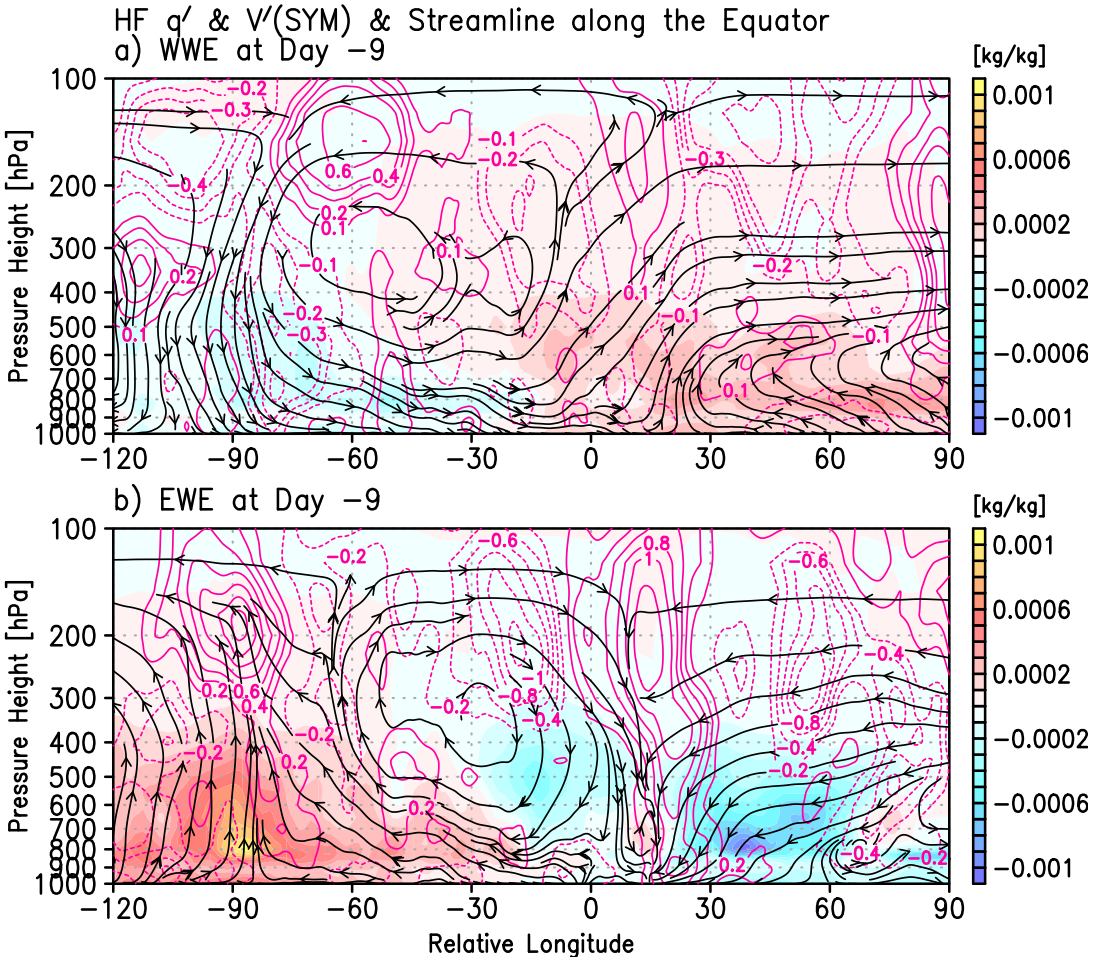

Figure 3.12: Composite vertical structures of the HF anomaly of (a) WWEs and (b) EWEs at day −9. Contour indicates the equatorial-symmetric part of meridional velocity averaged between 15 °S and 15 °N [m s^{-1}]. Shade and streamline indicate the specific humidity [kg kg^{-1}] and zonal-vertical flow averaged between 5 °S and 5 °N.

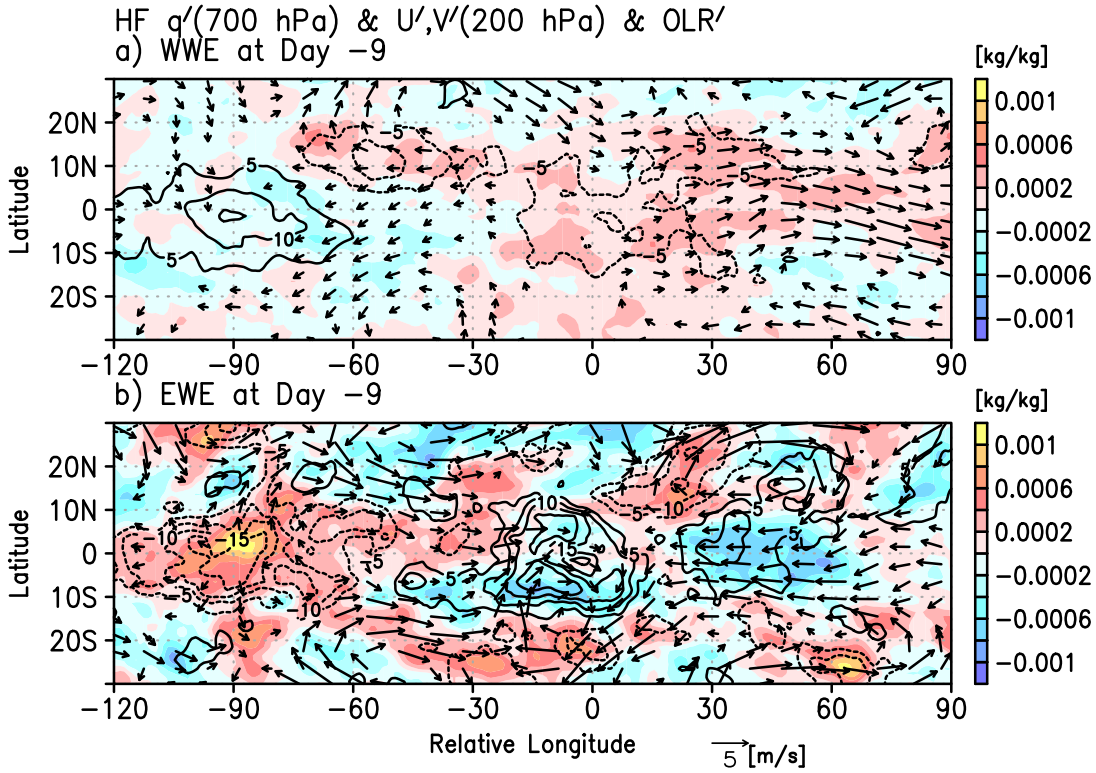

Figure 3.13: Composite horizontal structures of the HF anomaly of (a) WWEs and (b) EWEs at day −9. Contour and shade indicate the OLR [W m^{-2}] and specific humidity at 700 hPa [kg kg^{-1}], respectively. Vector indicates the horizontal flow at 200 hPa greater than 1 m s^{-1}.

3.5 Concluding discussion

Here, we have shown observational structures of WWEs and EWEs and their relationship with the interannual SST variability and background states in the equatorial Pacific based on reanalysis data. The analysis of HF surface wind anomalies indicates that (i) the frequency of occurrence of EWEs is less than that of WWEs regardless of the threshold for wind magnitude to detect events, (ii) background states of SST greater than 28.5 °C and OLR less than 230 W m^{-2}, geographically corresponding to the Pacific warm pool, are favorable for development of both WWEs and EWEs, and thereby they occur more frequently with increasing Niño4 SST, (iii) the occurrence of both WWEs and EWEs is highly related with the phase of the MJO, and (vi) the composite structure of WWEs (EWEs) is accompanied not only by the active (suppressed) convection locally but also by the broadly suppressed (active) convection at the far western side of the events. The asymmetry in the frequency of occurrence of detectable WWEs and EWEs is caused by the asymmetry in the local EKE generation associated with intraseasonal disturbances embedded in them.

The asymmetry in the frequency of occurrence might also originate from other reasons. The PDF of convective activity is nonlinear as the suppression of deep convection is bounded by clear skies (Zhang 1993). The easterly associated with suppressed convection might be weaker than the westerly associated with the active deep convection. However, well-suppressed convective anomalies are rarely related to the detectable EWEs in our analysis; therefore, it is insufficient to explain the asymmetry only by the nonlinearity in deep convection. There is also a possibility that interaction with the ocean brings asymmetry between WWEs and EWEs (Lengaigne et al. 2003; Eisenman et al. 2005; Vecchi et al. 2006). While EWEs may act to shrink the warm pool and result in unfavorable condition for subsequent EWEs, WWEs tend to result in subsequent WWEs by expanding the warm pool (e.g., Lengaigne et al. 2002, 2003, 2004; Miyama and Hasegawa 2014) since both events preferentially occur over the warm pool and the positive Niño4 SST anomaly.

Further study is needed to estimate the impact of this coupled process on the asymmetry.

The difference in the frequency of occurrence and the similarity in the dependence on background states are important aspects of WWEs and EWEs. For instance, more frequent occurrence of WWEs than EWEs with the similar state dependence may contribute to net warming at the equatorial Pacific probabilistically. The impact of state-dependent stochastic forcing on ENSO asymmetry was shown in a conceptual model (Jin et al. 2007); therefore, our observational analysis indicating probabilistic state dependence of both WWEs and EWEs suggests that the relationship between WWEs/EWEs and interannual SST variability in the central equatorial Pacific can be partly responsible for the irregular behavior of ENSO (cf. Chapter 4; Chen et al. 2015).

Appendix B: Using surface winds or wind stresses

Many previous studies have used the surface zonal wind to examine the observational characteristics of WWEs (Hartten 1996; Harrison and Vecchi 1997; Vecchi and Harrison 2000; Seiki and Takayabu 2007a; Chiodi et al. 2014). However, some recent studies have used the zonal wind stress to examine WWEs and EWEs with a focus on their possible impacts on the ocean (Chiodi and Harrison 2015; Puy et al. 2015).

The zonal wind stress anomaly, τ', nonlinearly depends on the surface wind. According to Trenberth et al. (1989),

$$\tau' = \rho_0 C_D \{|u'|(\overline{u} + u') + |\overline{u}|u'\}, \tag{B1}$$

where $\overline{u}$ and u' are the background and HF components of the surface zonal wind, respectively, ρ_0 (= 1.2 kg m^{-3}) is the reference density, and C_D (= 1.2×10^{-3}) is the drag coefficient. Here, no meridional wind is assumed. Figure B2 (left) shows the value of τ' in Eq. (B1) with respect to $\overline{u}$ and u', superposed on the observational value (see the caption of Fig. B2). As suggested by Chiodi and Harrison (2015), the magnitude of the negative τ' increases sharply when the climatological easterly wind is intensified (Fig. B2 left); for instance, τ' associated with u' of -4 m s^{-1} monotonically declines from about -0.01 to -0.1 N m^{-2} as $\overline{u}$ changes from 2 to -6 m s^{-1}. Accordingly, u' with a Gaussian probability density function (PDF) is transformed into τ' having negatively skewed PDFs for the easterly backgrounds (Fig. B2 right). This leads to the drastic increase in the occurrence of strong easterly wind stresses outside of the Pacific warm pool, i.e., over the central and eastern Pacific (Fig. B3): the frequency of occurrence of EWEs is exaggerated owing to the use of wind stress anomalies. On the other hand, the positive τ' does not strongly depend on $\overline{u}$ (Fig. B2 left). Therefore, the use of wind stress anomalies makes the asymmetry in the frequency of occurrence between EWEs and WWEs obscure except for extremely strong events (Table B1 and Puy et al. 2015).

The observational characteristics of the EWEs exaggerated by the use of wind stress anomalies is influenced by the background trade winds. For instance, when using the wind stress, the number of EWEs is less in boreal spring and early summer (Chiodi and Harrison 2015; Puy et al. 2015), corresponding to the season of the weakest trade winds. In addition, the EWEs mainly appear over the central and eastern Pacific, where the easterly trade winds are strengthened (Chiodi and Harrison 2015; Puy et al. 2015). When using the surface winds, however, the seasons and locations favorable for EWEs are very similar to those for WWEs (Fig. 3.3). Furthermore, when using the wind stress, the dependence of the EWE occurrences on the Niño4 SST anomaly is obscured (Fig. B1); instead, the EWEs slightly prefer the negative Niño3.4 SST anomaly, reflecting the intensified trade winds during La Niña. As suggested by Puy et al. (2015), the features of both events are considerably modified by using the anomaly of wind stresses or surface winds relative to seasonal cycle (Fig. B1 and Table B1).

The use of the surface wind or wind stress should be determined carefully to investigate WWEs and EWEs. In this chapter, we analyzed surface wind anomalies from which WWEs and EWEs are detected; in this case, the frequency of occurrence of EWEs is less than that of WWEs, and they appear over the Pacific warm pool and favorably occur with increasing Niño4 SST. These can also be seen in wind stress anomalies, albeit obscured because of the nonlinearity therein.

Table B1: Numbers of event occurrences by the same method in the paper but using different magnitude thresholds for the event detection or differently filtered data of surface wind [m s^{-1}] or wind stress [N m^{-2}]. From left to right, data, filtering, threshold, the occurrence numbers of WWEs and EWEs, and ratio of the number of WWEs to that of EWEs. In the table, "Intraseasonal" indicates a 3-day running averaged deviation of anomalies from a 91-day running mean, and "Relative to seasonal cycle" indicates 3-day running averaged anomalies.

Data	Filtering (anomaly)	Threshold	WWE	EWE	WWE/EWE
Surface wind	Intraseasonal	5.0 m s^{-1}	101	23	4.4
		4.0 m s^{-1}	228	87	2.6
		2.5 m s^{-1}	680	493	1.4
Surface wind	Relative to seasonal cycle	5.0 m s^{-1}	208	49	4.3
Wind stress	Intraseasonal	0.06 N m^{-2}	60	29	2.1
		0.05 N m^{-2}	103	108	1.0
		0.04 N m^{-2}	229	297	0.8
Wind stress	Relative to seasonal cycle	0.05 N m^{-2}	196	252	0.8

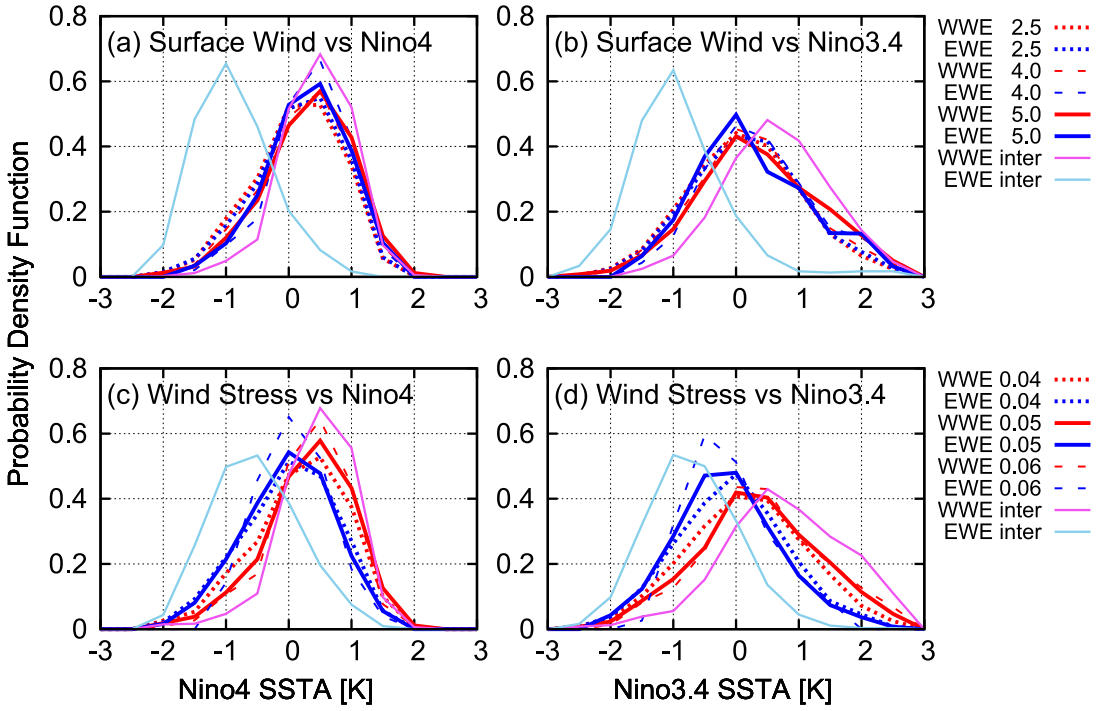

Figure B1: Probability density function of the events with respect to the Niño4 (left) and Niño3.4 (right) SST anomalies [K]. (a, b) WWEs (red) and EWEs (blue) are detected from intraseasonally filtered surface wind anomaly with thresholds of 2.5 (dotted), 4.0 (dashed), and 5.0 (solid) m s^{-1} and from the anomaly relative to seasonal cycle with the threshold of 5.0 m s^{-1} (thin magenta for WWEs and thin cyan for EWEs). (c, d) WWEs (red) and EWEs (blue) are detected from intraseasonally filtered wind stress anomaly with thresholds of 0.04 (dotted), 0.05 (solid), and 0.06 (dashed) N m^{-2} and from the anomaly relative to seasonal cycle with the threshold of 0.05 N m^{-2} (thin magenta for WWEs and thin cyan for EWEs).

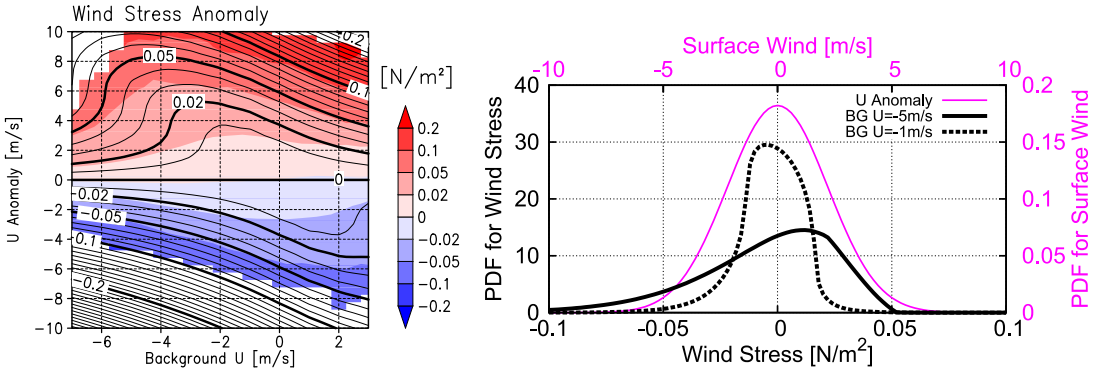

Figure B2: (Left) Dependence of τ' in Eq. (B1) (contour) and τ'_{OBS} (shade) on $\overline{u}$ and u'. The horizontal and vertical axes indicate $\overline{u}$ and u', respectively. τ'_{OBS} is the mean of HF τ' (averaged over 2.5 °S–2.5 °N) at grids where $\overline{u}$ and u' correspond to each 0.5 m s^{-1} bin over 120 °E–80 °W for 1982–2013, derived from JRA-55 (Kobayashi et al. 2015). Note that the assumptions of constant C_D, climatological wind stress, and no meridional wind may cause the difference between τ' in Eq. (B1) and τ'_{OBS}. (Right) Probability density functions of τ' for $\overline{u} = -5$ m s^{-1} (black solid) and $\overline{u} = -1$ m s^{-1} (black dotted) associated with the Gaussian u' with the standard deviation of 2 m s^{-1} (magenta), derived from 2×10^6 random samples using Eq. (B1).

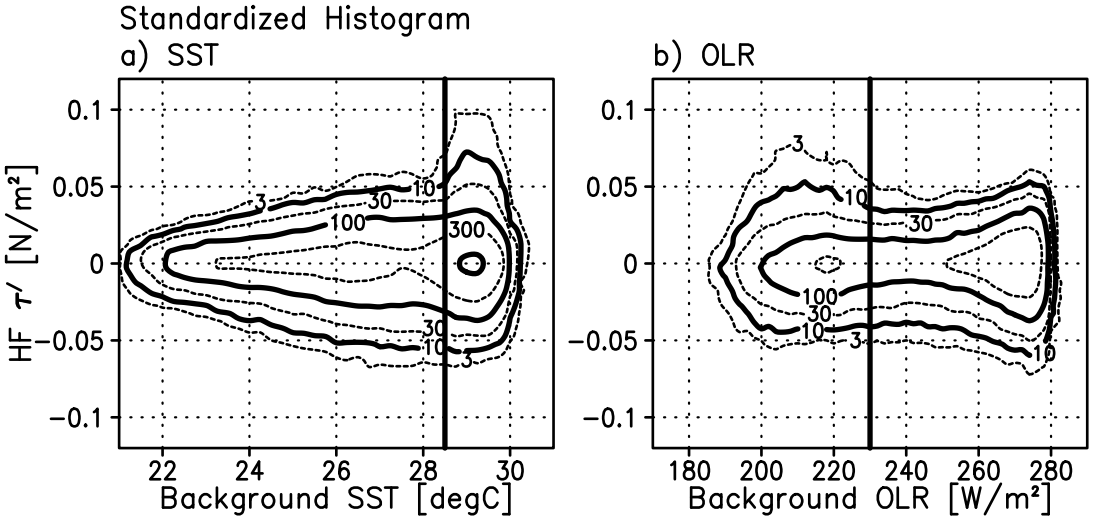

Figure B3: Same as Fig. 3.5, but for the HF zonal wind stress anomaly in the vertical axis.

Appendix C: EKE budget analysis

The EKE tendency terms are calculated by

$$\frac{\partial K'}{\partial t} = \underbrace{-\overline{\mathbf{V}'_h(\mathbf{V}'_3 \cdot \nabla)\overline{\mathbf{V}}_h}}_{\text{KmKe}} \underbrace{-\overline{\mathbf{V}}_3 \cdot \nabla\overline{K'}}_{\text{AmKe}} \underbrace{-\overline{\mathbf{V}'_3 \cdot \nabla K'}}_{\text{AeKe}} \underbrace{-\frac{R}{p}\overline{\omega' T'}}_{\text{PeKe}} \underbrace{-\nabla \cdot (\overline{\mathbf{V}'_3 \Phi'})}_{\text{GKe}} + D, \qquad \text{(C1)}$$

where the prime indicates the eddy component, the overbar indicates an 11-day running mean (intraseasonal plus background components), $K' = \overline{u'^2 + v'^2}/2$ is the EKE, $\mathbf{V}_3 = (u, v, \omega)$ is the three-dimensional velocity vector, $\mathbf{V}_h = (u, v)$ is the horizontal velocity vector, R is the gas constant for dry air, T is the temperature, Φ is the geopotential height, and D indicates dissipation or subgrid-scale effects (Seiki and Takayabu 2007b). Following Seiki and Takayabu (2007b), the first, second, third, fourth, and fifth terms on the right-hand side in (C1) are represented by KmKe, AmKe, AeKe, PeKe, and GKe, respectively.

Figure C1 shows the composite vertical profiles of the EKE tendency terms averaged around the central locations of WWEs and EWEs along the equator. The KmKe term mainly generates the EKE for both the WWE and EWE at lower levels although its magnitude is greater for the WWE. The overall result for the WWE is consistent with Seiki and Takayabu (2007b). The main contributor in the KmKe term is the barotropic EKE accumulation due to the zonal convergence of the environmental low-level westerly (i.e., $-\overline{u'u'\partial\overline{u}/\partial x}$). This indicates that the difference in the environmental low-level westerly, $\overline{u}$ ($\overline{u} = u'' + U_0$ in section 3.2), may explain the asymmetry in the magnitude of the EKE generation between the WWE and EWE.

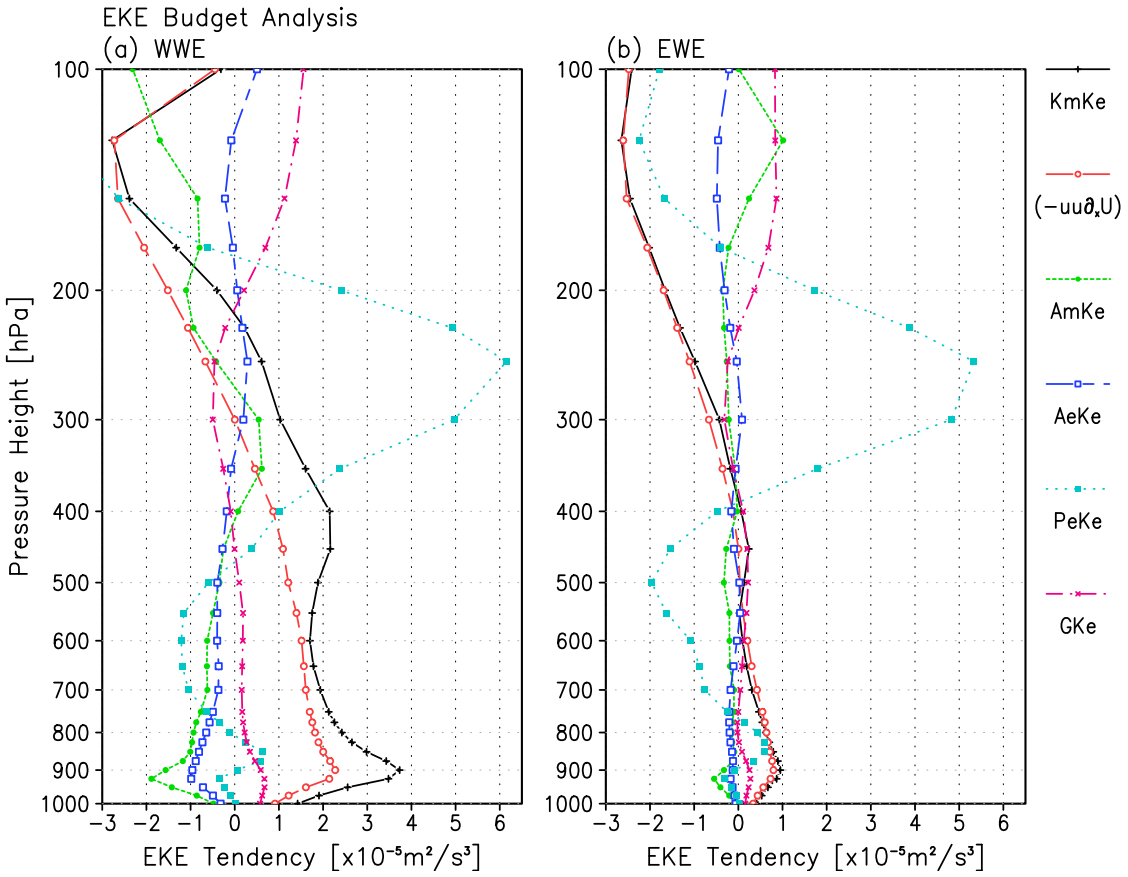

Figure C1: Composite vertical profiles of the EKE tendency [10^{-5} m^2 s^{-3}] for (a) WWEs and (b) EWEs averaged between 5 °S and 5 °N, −10 ° and +10 ° in RL at the central date. Lines indicate KmKe (black), AmKe (green), AeKe (dark blue), PeKe (light blue), and GKe (magenta). Red lines indicate the EKE accumulation due to the zonal convergence of the environmental low-level westerly, $-\overline{u'u'\partial\overline{u}/\partial x}$, in KmKe.

Chapter 4

Coupling between westerly wind events and ENSO

Abstract

A coupled dynamics between westerly wind events (WWEs) and El Niño-Southern Oscillation (ENSO) is examined using an atmosphere-ocean coupled model with intermediate complexity. WWEs are short-lived surface westerly wind anomalies over the western-central equatorial Pacific and observed frequently at the eastern edge of the warm pool when the sea surface temperature (SST) anomaly at the Niño4 region (160 °E–150 °W, 5 °S–5 °N) is positively large. These features of WWEs are parameterized as a state-dependent stochastic noise to wind stresses in the model. Without the noise (experiment NO), the model produces a periodic ENSO-like oscillation with a period of 6 years and its variance increases with respect to a parameter that controls efficiency of the positive thermocline feedback, γ. When additive (purely stochastic) noise is given to the model over the western Pacific (experiment AD), oscillations become irregular with the dominant period of about 5 years and the increase of its variance relative to NO depends on γ. When the state-dependent noise is adopted (experiment SD), the oscillatory solution is

also irregular besides its variance and asymmetry increase irrespective the value of γ.

Both the additive and state-dependent noises help to produce two types of oscillation, corresponding to the eastern-Pacific (EP) and central-Pacific (CP) El Niños, although there is no such diversity in NO. EP El Niño is magnified in SD due to the eastward shift of the noise location caused by the warm pool expansion. CP El Niño is even favored by the state-dependent stochastic noise, which enhances the zonal advection to warm the central Pacific, and in turn the warmer Niño4 SST increases the probability of occurrence of the noise. This positive feedback ensures the existence of CP El Niño regardless of γ in SD, while the number of CP El Niño declines with larger γ in AD. The above results thereby suggest that the state dependence of WWEs may play a crucial role on the asymmetry and diversity of ENSO in nature.

4.1 Introduction

The El Niño-Southern Oscillation (ENSO) phenomenon is the interannual variability intrinsic to the atmosphere-ocean coupled system in the equatorial Pacific (Schopf and Suarez 1988; Battisti and Hirst 1989; Jin 1997a,b). The oscillatory behavior arises from a delayed feedback in the slow coupled process per se, but a possible interaction of ENSO with high-frequency atmospheric disturbances has been investigated in recent decades. Westerly wind events (WWEs) or westerly bursts are sporadic surface wind anomalies that persist for a few days to weeks with large magnitude over the western and central Pacific (Luther et al. 1983; Hartten 1996; Harrison and Vecchi 1997; Seiki and Takayabu 2007a; Puy et al. 2015; Chapter 3). The eastward wind stress anomaly associated with WWEs increases the sea surface temperature (SST) in the eastern equatorial Pacific through the thermocline deepening and zonal advection (Vecchi and Harrison 2000; Lengaigne et al. 2002; Belamari et al. 2003; Karnauskas 2013; Chiodi et al. 2014; Chapter 2), while the occurrence of WWEs is more frequent with the SST anomaly associated with El Niño and

corresponding eastward expansion of the western Pacific warm pool (Vecchi and Harrison 2000; Eisenman et al. 2005; Seiki and Takayabu 2007a; Hendon et al. 2007; Tziperman and Yu 2007; Gushchina and Dewitte 2012; Chapter 3). This indicates that WWEs are not purely stochastic (additive) but multiplicative (state dependent). Despite a short duration of each WWE episode, frequent WWEs induce anomalous oceanic variations and cause discernible warming in the eastern Pacific during the developing phases of extremely large El Niños in the boreal winter of 1982, 1997, and 2015 (Wyrtki 1985; McPhaden 1999; Jin et al. 2003; Lengaigne et al. 2004).

The modulation of ENSO by additive/state-dependent atmospheric noise that mimics WWEs has been examined using various atmosphere-ocean couped models (Eisenman et al. 2005; Zavala-Garay et al. 2005; Perez et al. 2005; Gebbie et al. 2007; Jin et al. 2007; Levine and Jin 2010; Kapur and Zhang 2012; Lopez et al. 2013). Overall, state dependence of noise robustly increases the ENSO instability, and transfers a damped system to be oscillatory in intermediate coupled models (Eisenman et al. 2005; Perez et al. 2005), an ocean general circulation model (OGCM) coupled with a statistical atmosphere model (Gebbie et al. 2007), coupled general circulation models (CGCMs) (Lopez et al. 2013), and a simple recharge oscillator model (Jin et al. 2007; Levine and Jin 2010). It has also been shown that the low-frequency tail (i.e., envelop) of the state-dependent noise or WWEs plays a crucial role in the ENSO modification (Eisenman et al. 2005; Zavala-Garay et al. 2005; Gebbie et al. 2007; Levine and Jin 2010; Kapur and Zhang 2012; Lopez et al. 2013). Some studies also demonstrated that the state dependence increased the positive skewness of the SST anomaly (Perez et al. 2005; Gebbie et al. 2007; Jin et al. 2007; Levine and Jin 2010) or reduced a negative bias of the ENSO skewness in a CGCM (Lopez et al. 2013).

However, contribution of additive/state-dependent noise may depend on inherent ENSO stability and imposed state dependence. For instance, additive noise worked to reduce the variance of ENSO in Lopez et al. (2013), but amplified in Perez et al. (2005) and Geb-

bie et al. (2007) or did not influence in Eisenman et al. (2005), Jin et al. (2007), and Levine and Jin (2010). Kapur and Zhang (2012) noted that the ENSO modulation by the noise can be different between stable and unstable regimes. Different state dependence parameterizing WWEs may cause the different conclusions on the noise-induced ENSO asymmetry. While noise variance synchronized with the developing phase of El Niño may increase the El Niño amplitude (Perez et al. 2005; Jin et al. 2007; Gebbie et al. 2007; Levine and Jin 2010; Lopez et al. 2013), Gebbie et al. (2007) implied that the eastward shift of WWEs may also contribute to amplifying El Niño through the zonal advection at the edge of the warm pool, as indicated by Lengaigne et al. (2004). The irregularity of ENSO can be introduced by noise, but the modulation of periodicity due to noise has not been investigated quantitatively.

Recently, two types of El Niño have been distinguished based on their structural difference in the SST anomaly, called the El Niño flavor or diversity (e.g., Yeh et al. 2014; Capotondi et al. 2015). One has the maximum of SST anomaly in the eastern Pacific similar to the convectional El Niño (EP El Niño), and another has the peak in the central Pacific, which is named dateline El Niño (Larkin and Harrison 2005), El Niño Modoki (Ashok et al. 2007), warm-pool El Niño (Kug et al. 2009), or central-Pacific (CP) El Niño (Kao and Yu 2009). The thermocline feedback is dominant in the development of EP El Niño, while CP El Niño is mainly driven by the zonal advection of mean SST by anomalous zonal currents (Kug et al. 2009; Kao and Yu 2009; Yeh et al. 2014). The impact of WWEs on the El Niño flavor was investigated using CGCMs. Lopez and Kirtman (2013) showed the contribution of state-dependent WWEs to EP and CP El Niños in long-term integrations of two CGCMs with a WWE parameterization by Gebbie and Tziperman (2009). While WWEs affected both types of El Niño in one CGCM, they modified only EP El Niño in another model. The different results in the two CGCMs indicate that the influence of WWEs depends on the inherent ENSO stability of CGCMs. Fedorov et al. (2015) and Hu et al. (2014) imposed a WWE in a CGCM, and indicated that whether

the WWE induces EP or CP El Niño is controlled by the initial state of the ocean. The El Niño flavor was also examined by Lian et al. (2014) and Chen et al. (2015) using a modified version of Zebiak-Cane (ZC) model (Zebiak and Cane 1987) with a parameterization of WWEs. They suggested that CP El Niño and extremely strong EP El Niño can be produced by the state-dependent WWEs. However, the contribution of the state dependence to CP El Niño is still unclear since they did not conduct experiments with additive WWEs. Using a linearized ZC model, Bejarano and Jin (2008) suggested that EP and CP El Niños resemble "quasi-quadrennial (QQ)" and "quasi-biennial (QB)" modes, respectively, which were their theoretical solutions. Although both modes exist inherently in their model, the coexistence is sensitive to a small change in the basic state and model parameter. Thus, the ENSO flavor in ZC model with state-dependent WWEs is possibly dependent on the model's stability.

In this chapter, an intermediate coupled model is constructed to examine a coupling between WWEs and ENSO. We coupled the ocean component of ZC model and a linearized steady atmospheric global model, which can present a realistic atmospheric response to SST anomalies. The annual cycles of both atmosphere and ocean are prescribed in the model given its importance on the ENSO cycle (Chapter 2). The WWEs are parameterized based on an observational analysis for the relationship between WWEs and SST (Chapter 3). By perturbing a parameter controlling the model's ENSO stability, we qualify the ENSO modulation due to additive and state-dependent WWEs in stable and unstable regimes.

The rest of this chapter is structured as follows. An intermediate atmosphere-ocean coupled model and WWE parameterization are explained in section 4.2. In section 4.3, the overview of ENSO in the model is described. The statistics of the model's ENSO is examined in section 4.4, and the impact of WWEs on the El Niño flavor is focused in Section 4.5. Summary and discussion are given in section 4.6.

4.2 Method

4.2.1 Model

An intermediate atmosphere-ocean coupled model is used in this chapter. The atmospheric component consists of a moist linear baroclinic model (mLBM), which is based on primitive equations linearized about a basic state (Watanabe and Jin 2003). The model variables consist of the perturbations of vorticity, divergence, temperature, logarithm of surface pressure, and specific humidity. The mLBM calculates the atmospheric steady response to SST anomaly under the seasonally varying basic state. A steady linear response in the mLBM is symbolically written as

$$\mathbf{X} = \mathbf{L}^{-1}\mathbf{F}, \tag{4.1}$$

where $\mathbf{X}$ is a state vector containing atmospheric variables, $\mathbf{L}$ is a linear dynamical operator associated with the basic state, and $\mathbf{F}$ is a forcing vector containing the SST anomaly. The mLBM has been used to examine the linear dynamical response of the atmospheric general circulation to observed or idealized SST anomalies. Here, we use a low resolution version of T21 and vertical 11 levels, and climatology derived from the National Centers for Environmental Prediction-National Center for Atmospheric Research (NCEP-NCAR) reanalysis as a basic state that varies monthly (Kalnay et al. 1996).

The ocean component is a prognostic anomaly model for the equatorial Pacific (124 °E–80 °W, 29 °S–29 °N), comprised of a shallow-water equation and a thermodynamic model for the temperature of the surface layer. This model was adopted from the ZC coupled atmosphere-ocean model (Zebiak and Cane 1987). The zonal and meridional resolutions are 5.625° and 2°, respectively, and the time step is 10 days. The basic states, including monthly varying SST and currents, are prescribed from observations. In the

thermodynamic equation, the SST anomaly (T) is formulated as follows.

$$\frac{\partial T}{\partial t} = -\mathbf{u}_h \cdot \nabla_h(\overline{T}+T) - \overline{\mathbf{u}}_h \cdot \nabla_h T - \{M(\overline{w}+w) - M(\overline{w})\}\frac{\partial \overline{T}}{\partial z} - M(\overline{w}+w)\frac{\partial T}{\partial z} - \alpha T + Q, \quad (4.2)$$

where $\mathbf{u}_h$ and w are the anomalies of the horizontal surface currents and upwelling, respectively, overbars indicate the basic states, α (= $1/125$ day^{-1}) is the coefficient for linear damping, Q is the surface heat flux calculated in the mLBM, and

$$M(x) = \begin{cases} 0 & \text{for} \quad x \le 0 \\ x & \text{for} \quad x > 0 \end{cases} \quad (4.3)$$

so that the SST is affected by vertical advection only in the presence of upwelling.

The anomalous vertical temperature gradient is defined by

$$\frac{\partial T}{\partial z} = \frac{T - T_e}{H_1}, \quad (4.4)$$

where H_1 is the surface layer depth (50 m), and T_e is the temperature anomaly entrained into the surface layer having the form

$$T_e = \gamma T_{sub} + (1-\gamma)T. \quad (4.5)$$

The ratio between the subsurface temperature anomaly (T_{sub}) and T in T_e is defined by γ, and T_{sub} is prescribed as a function of h:

$$T_{sub} = \begin{cases} T_1\{\tanh[b_1(\overline{h}+h)] - \tanh(b_1\overline{h})\} & \text{for} \quad h > 0 \\ T_2\{\tanh[b_2(\overline{h}-h)] - \tanh(b_2\overline{h})\} & \text{for} \quad h < 0, \end{cases} \quad (4.6)$$

where h and $\overline{h}$ are the anomaly and prescribed mean of the thermocline depth, respectively. Parameter values, (T_1, T_2, b_1, b_2) = (28 °C, −40 °C, 0.0125 m^{-1}, 0.0303 m^{-1}) as the same with values in Zebiak and Cane (1987), were estimated from observations. The

ocean model can reproduce observed interannual SST anomalies in the equatorial Pacific when forced by observational wind stress anomalies (e.g., Kang and Kug 2000), and has been used to predict El Niño events (e.g., Chen et al. 1995) and to examine the ENSO dynamics (e.g., Zebiak and Cane 1987).

The atmospheric response to the SST anomaly is calculated at each time step. The ocean component model is forced by the wind stress anomalies using a linearized standard bulk formula,

$$\tau = \rho_a C_d(|\overline{\mathbf{u}}_a|\mathbf{u}_a + |\mathbf{u}_a|\overline{\mathbf{u}}_a), \tag{4.7}$$

where τ is wind stress anomaly, ρ_a is the air density, C_d is a bulk transfer coefficient, and $\mathbf{u}_a$ and $\overline{\mathbf{u}}_a$ are anomalous and climatological surface winds, respectively. The magnitude of τ is reduced to 70% assuming larger damping effect in the planetary boundary layer of the mLBM, by referring to previous studies for stabilizing a coupled model (e.g., Perez et al. 2005; Eisenman et al. 2005; Kapur et al. 2012).

4.2.2 Observational data

The long-term SST data (COBE-SST, Ishii et al. 2005) for 1850–2014 is used. The monthly SST anomaly is defined as deviations from the 1981–2010 average.

We also use daily-averaged surface wind data derived from the Japanese Re-Analysis 55 Years (JRA-55) project (Kobayashi et al. 2015) from 1 January 1982 to 31 December 2013. WWEs are extracted following Seiki and Takayabu (2007a) by using the surface wind anomaly averaged between 2.5 °S and 2.5 °N after subtracting its interannual component. The thresholds of the magnitude, duration, and zonal extent are 5 m s^{-1}, 2 days, and 10° in longitude. An event is required to satisfy the three thresholds at each grid over the equatorial Pacific (120 °E–80 °W). See Chapter 3 for the detail and the statistics of WWEs.

4.2.3 WWE parameterization

In Chapter 3, we have shown that the occurrence of WWEs depends on the Niño4 SST anomaly. There are other conditions that affect the occurrence of WWEs: edge of the warm pool (Eisenman et al. 2005), low-level background westerly (Seiki and Takayabu 2007b; Sooraj et al. 2009), and zonal SST gradient in the western Pacific (Lengaigne et al. 2003; Miyama and Hasegawa 2014). Note that the Niño4 SST anomaly is highly correlated with the other three indicators for occurrence of WWEs.

The parameterization of WWE in this chapter is as follows. We fix the spatial pattern of zonal wind stress anomalies (τ_x^{WWE}).

$$\begin{aligned} \tau_x^{WWE} &= \tau_0 \exp\left\{-\frac{(x-x_0)^2}{L_x^2} - \frac{y^2}{L_y^2}\right\} \\ &\quad \text{for} \quad -1.5L_x \le x \le 1.5L_x \quad \text{and} \quad -1.5L_y \le y \le 1.5L_y, \end{aligned} \tag{4.8}$$

where x and y indicate longitude and latitude, respectively, $\tau_0 = 0.15$ [N m^{-2}] is the amplitude of the WWEs, x_0 is the central longitude of the WWEs, and L_x and L_y are 20° and 6°, respectively. In some experiments described below, we set $x_0 = x_{pool} - 10°$, where x_{pool} is the longitude of the eastern edge of the western Pacific warm pool defined by the longitude of 28.5 °C SST isotherm along the equator. The above τ_x^{WWE} is imposed to the model with the probability at each time step (P),

$$P = P_0 \cdot (1 + GT_4), \tag{4.9}$$

where P_0 (= 0.2 [1/10 day^{-1}]) is the basic probability of WWE occurrence, T_4 [K] is the Niño4 SST anomaly, and G [K^{-1}] is a constant to assume the state dependence of WWE occurrence. That is, the probability of WWE occurrence becomes higher (lower) for positively (negatively) larger T_4. A WWE occurs centered at x_0 when a random number from 0 to 1, generated at each time step, is less than P, and persists for 20 days. The

minimum recurrence interval between WWEs is 30 days.

4.2.4 Numerical experiments

A reference case (referred to as NO) is conducted without external forcing, i.e., $P = 0$, which produces ENSO-like interannual oscillations (see section 4.3). In the purely additive or stochastic case (referred to as AD), we set $G = 0$ and $x_0 = 168.75$ °E so that the WWEs are added at the western Pacific independently of T_4. In the state-dependent or multiplicative case (referred to as SD), we set $G = 1.5$ and $x_0 = x_{pool} - 10°$. In addition to AD and SD, the T_4-dependent and x_{pool}-dependent cases are considered (referred to as N4 and WP, respectively). In N4, $G = 1.5$ is used but the WWEs occur centered at $x_0 = 168.75$ °E. In WP, the WWEs occur centered at $x_0 = x_{pool} - 10°$ but $G = 0$. Assuming the association of WWEs with deep cumulus convection, the WWEs appear only when the SST at x_0 along the equator is greater than 28.5 °C in SD, N4, and WP.

The parameterization produces WWEs at the timings and locations similar to the observations. Figure 4.1 shows examples of parameterized WWEs calculated with the observed SST anomaly from 1996 to 2005. The timings and locations of WWEs are comparable to those in the observations. For instance, WWEs frequently occur prior to 1997 El Niño and migrate eastward associated with the warm pool expansion, while they are less frequent during La Niña from the mid-1998 to late-2000. In addition, frequent occurrence of WWEs for 2002–2005 is modeled well. The probability density function (PDF) of the occurrence of WWEs has its peak at the positive T_4, similar to the observations (Fig. 4.2, see also, Fig. 3.1b in Chapter 3).

The coupled model, ZC-mLBM, is initially kicked by the westerly wind stress patch along the equator (Zebiak and Cane 1987). The WWE parameterization is switched on after 10-year integrations. To calculate T_4 in Eq. (4.9), we removed the climatology defined by 10-daily average for 30 years before each time step. We analyze the model output after the 51st year in model integrations, where the climatology during the data

period (300 years in NO, and 1000 years in the others) is removed. Therefore, anomalies indicate the departure from the climatology of each variable. Hereafter, "year *N*" indicates the *N*th year of the model integration.

Table 4.1: List of the names of experiments, experimental designs, and values of the dependence on the Niño4 SST anomaly (G), and central longitude of WWEs (x_0). The eastern edge of the western Pacific warm pool is indicated by x_{pool}.

Exp.	Design	G	x_0
NO	No WWE		
AD	Additive	0.0	168.75°E
SD	State-dependent	1.5	$x_{pool} - 10°$
N4	T_4-dependent	1.5	168.75°E
WP	x_{pool}-dependent	0.0	$x_{pool} - 10°$

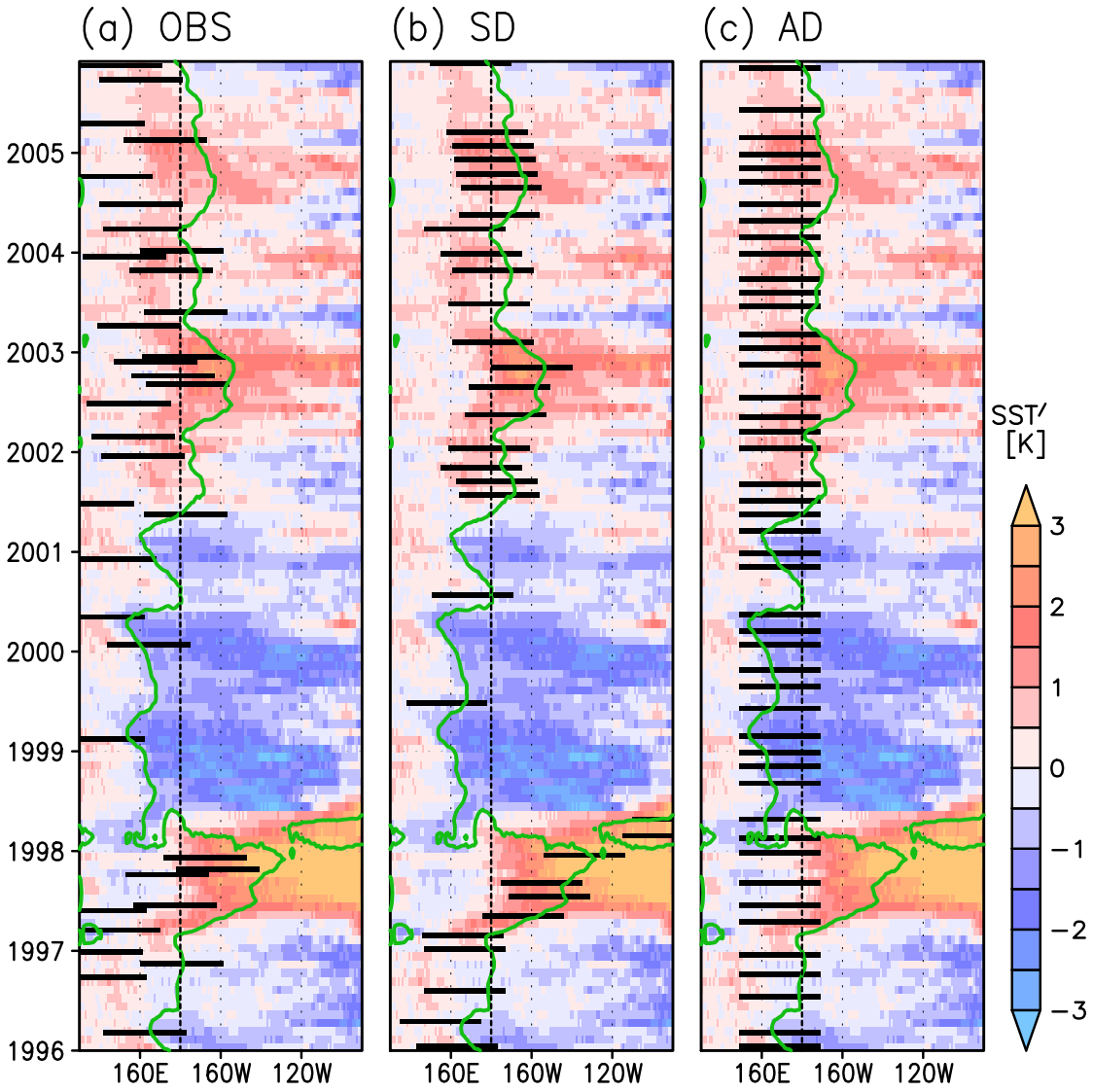

Figure 4.1: Examples of the WWE parameterization applied on the observed SST anomaly in (a) the observation, (a) SD, and (c) AD with $G = 1.0$ and $P_0 = 0.2$. Black bars indicate the timing and location of WWEs. Shade and green contour indicate the monthly SST anomaly and 3-month running mean of the 28.5 °C SST isotherm, respectively, averaged between 2 °S and 2 °N. The dateline is represented by black dashed line.

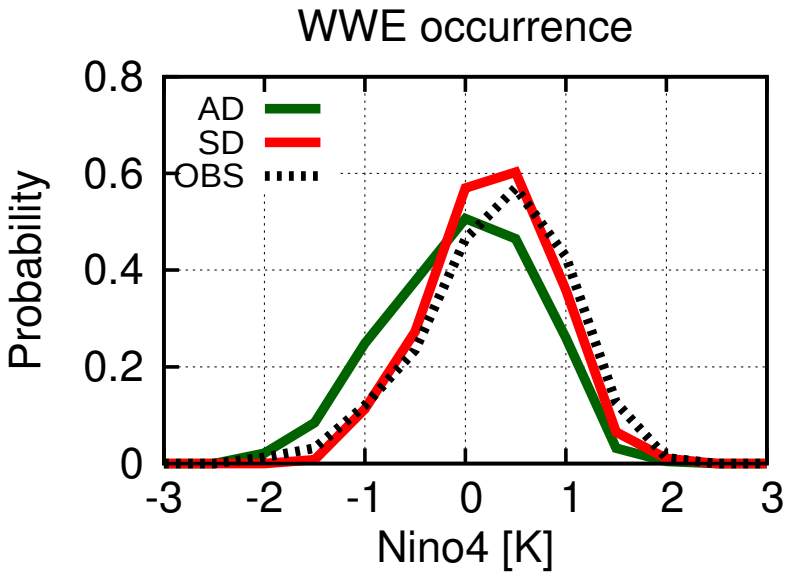

Figure 4.2: Probability density function of the occurrence of WWEs with respect to the Niño4 SST anomaly [K] in AD (green solid), SD (red solid), and the observation (black dotted) (see Fig. 3.1b in Chapter 3), calculated using Epanechnikov kernel (Kimoto and Ghil 1993).

4.3 ENSO-like oscillations in NO and SD

Mechanism of the oscillatory solutions in NO and SD are examined in this section. Figures 4.3a and 4.3b show the anomalies in SST, zonal wind stress, thermocline depth, and zonal surface current along the equator in NO with $\gamma = 0.45$. The edge of the warm pool as determined by the 28.5 °C SST isotherm is imposed in Fig. 4.3a. The ENSO-like oscillation has a period of 6 years, having peaks of the SST anomaly in the eastern Pacific. The anomalies of westerly (easterly) wind stress and eastward (westward) current have their peaks to the west of the positive (negative) SST anomaly. The thermocline depth anomaly is out of phase with the wind stress anomaly and slightly leads the SST anomaly.

The SST tendency is determined by zonal, meridional, and vertical advective terms in the surface layer and a damping term including heat flux from the ocean to the atmosphere in Eq. (4.2). Time evolution of these budget terms in the eastern equatorial Pacific are shown in Fig. 4.4. All advective terms contribute to the growth of the ENSO-like oscillation (e.g., from year 4 to 5). Prior to El Niño, the deepened thermocline induces the positive subsurface temperature anomaly, which is entrained into the surface by the mean upwelling. Associated with the wind response to the SST anomaly, the thermocline is deepened further (thermocline feedback) and the eastward surface current anomaly advects the warm water to the east (zonal advective feedback). The equatorial upwelling is reduced by the weakening of the easterly trade winds, causing the eastern Pacific to warm. The anomalous equatorial downwelling is mainly balanced with the equatorward surface current anomaly, contributing to the equatorial warming through the meridional advection. During El Niño, the zonal mean of the thermocline depth is shoaling associated with the poleward mass transport in the subsurface, leading to the termination of El Niño. The development process of La Niña is vice versa. This is a typical ENSO cycle described by classical theories (e.g., Jin 1997a), except that El Niño has a slightly larger magnitude than La Niña (Fig. 4.3a). The asymmetry of ENSO in NO can be caused in the subsurface temperature equation (4.6) determined by the thermocline depth anomaly

and the nonlinear advection (Jin et al. 2003; An and Jin 2004; Duan et al. 2008).

State-dependent WWEs modify the ENSO-like oscillation of the model dramatically. Figure 4.5 shows the anomalies in SST, zonal wind stress, thermocline depth, and zonal surface current along the equator during a 10-year period in SD with $\gamma = 0.45$. The zonal wind stress anomalies are separated into the slow component as calculated with Eq. (4.7) (denoted as τ_x^{ENSO}) and the parameterized component using Eqs. (4.8) and (4.9). Unlike the solution in NO, the SST anomaly evolves irregularly in time and has various structures, and the magnitude of El Niño is much larger than that of La Niña. El Niño events, having its peak greater than 2 K in the eastern Pacific, emerge for years 187–188 and 191–192, while the positive anomalous SST appears near the dateline from year 183 to 184 (Fig. 4.5a). As expected, WWEs occur frequently (rarely) for the positive (negative) Niño4 SST anomaly (Fig. 4.5c). They excite the oceanic Kelvin waves as indicated by the eastward-propagating signals of the deepened thermocline and eastward surface current (Fig. 4.5d, e). The central longitude of WWEs shifts eastward when the warm pool expands to the east during El Niño. The development process of the SST variability in SD will be quantitatively discussed in section 4.5.

The comparison between NO and SD indicates that the state-dependent WWEs induce the structural diversity of the model's ENSO and enhance its asymmetry and irregularity. The statistics and diversity of the model's ENSO will be further discussed in sections 4.4 and 4.5, including their dependence on γ.

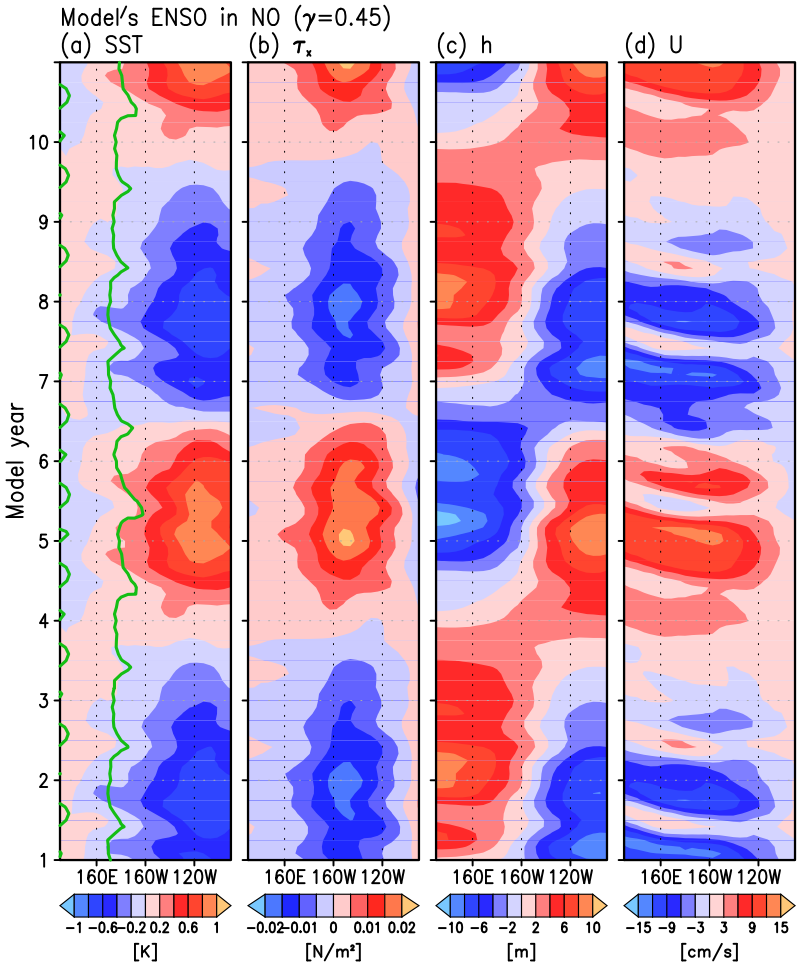

Figure 4.3: Time-longitudinal plots averaged between 1 °S and 1 °N for 10 years in NO with $\gamma = 0.45$. (a) 3-month running averaged SST anomaly [K], (b) zonal wind stress anomaly associated with ENSO [N m^{-2}, shade], (c) thermocline depth anomaly [m], and (d) zonal surface current anomaly [cm s^{-1}]. Green contour in (a) indicates 3-month running mean of 28.5 °C SST isotherm.

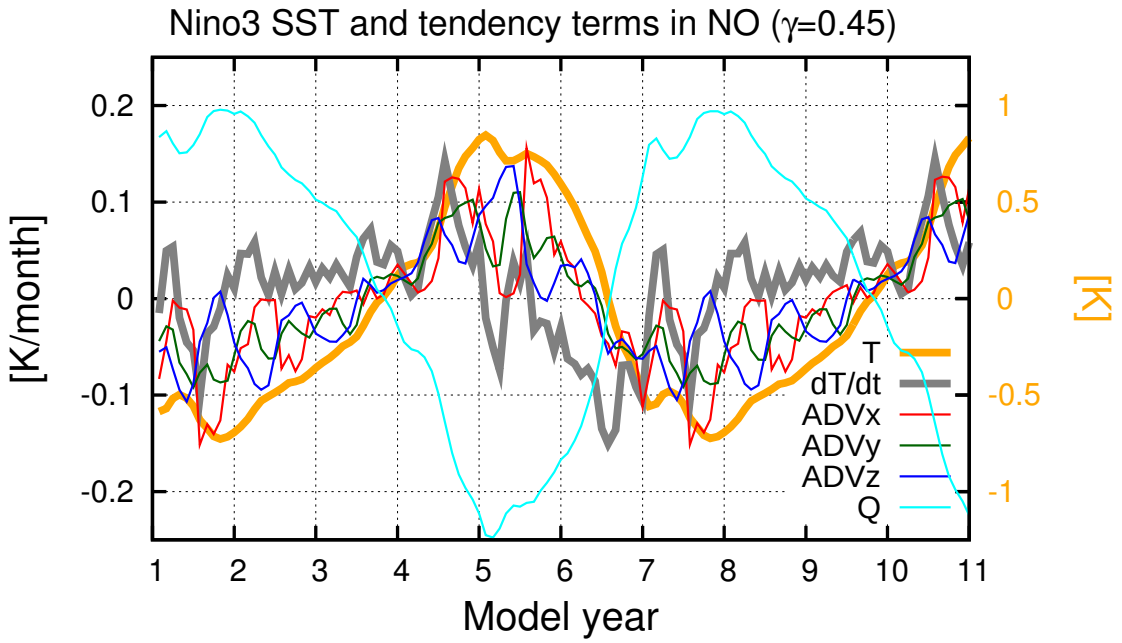

Figure 4.4: Temporal evolutions of the SST anomaly [orange thick, K] and its tendency [gray thick, K month^{-1}] in NO with $\gamma = 0.45$. The values are averaged at the Niño3 region but 1 °S–1 °N. Thin red, green, blue, and cyan lines show the zonal, meridional, and vertical adective terms and a damping term including the surface heat flux, respectively, in Eq. (4.2). The left and right vertical axes indicate the SST anomaly and its tendency terms, respectively.

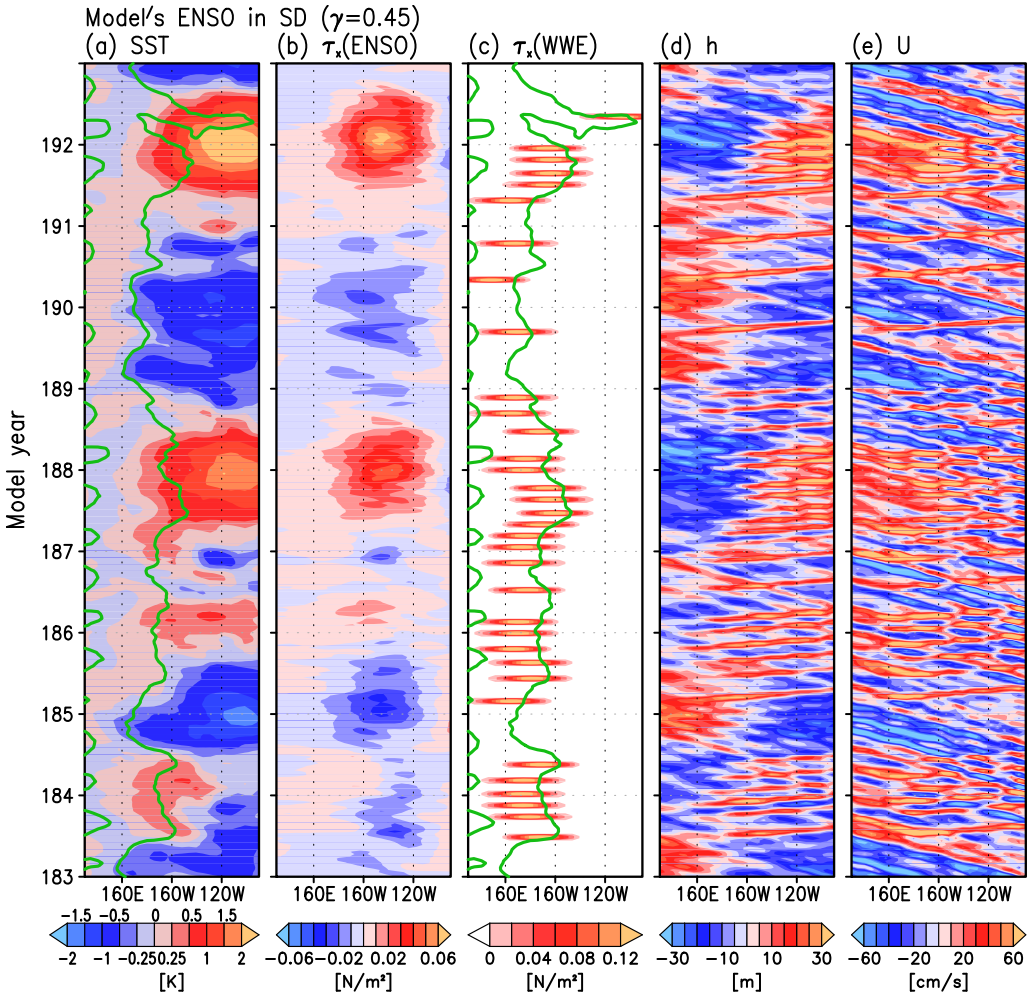

Figure 4.5: Same as Fig. 4.3, except for in SD and a panel (c) of the zonal wind stress associated with WWEs [N m^{-2}] and 28.5 °C isotherm. Scales in shadings are different from Fig. 4.3.

4.4 El Niño indices

The statistics of El Niño indices is examined in this section. Figure 4.6 shows the time series of the monthly SST anomalies in the Niño3 region (150 °–90 °W, 5 °S–5 °N) derived from the COBE SST data for 1850–2014 (Fig. 4.6a) and the model experiments with $\gamma = 0.45$ for 300 years (NO, AD, SD, N4, and WP, Fig. 4.6b–f). The observed ENSO is irregular and positively skewed, and extremely strong El Niño events appeared in 1982/83 and 1997/98. The model's ENSO in NO is periodic with small amplitude. In AD, WWEs make ENSO-like oscillation irregular but the variance is similar to or smaller than that in NO. The model's ENSO in SD is also irregular, and has a large variance due to extreme El Niños during some epochs. Larger variance is also observed in N4. In WP, stronger El Niño events, reaching 2 K, appear more frequently than in AD.

4.4.1 Variance

The PDFs of the Niño3 SST anomalies are compared between the observation and the model experiments with $\gamma = 0.45$ (Fig. 4.7a). Their standard deviations (σ_3) are shown in Table 4.2. The PDF in NO is bimodal, as was shown by Perez et al. (2005), while the PDFs are close to the Gaussian shape in the other experiments and observation. In SD and N4, σ_3 is larger than the others, indicating that the dependence of occurrence of WWEs on T_4 increases the variance of ENSO in the model. The standard deviations of the Niño4 SST anomalies (σ_4) are increased in SD, N4 and WP (Table 4.2), although they are much smaller than the observed value due to limitation in the ocean model (Kang and Kug 2000).

Values of σ_3 and σ_4 depend on γ (Fig. 4.8a and 4.8b). By dividing each 1000-year run into ten 100-year segments, the means of σ_3 and σ_4 and their standard deviation (uncertainty) are obtained in AD and SD. Because of the regularity, only the means are plotted for the 300-year NO run. In all experiments, σ_3 and σ_4 increase with γ except for

σ_4 for $\gamma \geq 0.45$ in AD. Comparing between NO and AD, the additive WWEs are found to increase σ_3 and σ_4 for $\gamma < 0.45$, while suppress for $\gamma \geq 0.45$. This indicates that the additive WWEs damp the model's ENSO cycle for unstable oscillatory regime (Fedorov 2002; Lopez et al. 2013), but magnify it for stable system (Perez et al. 2005; Gebbie et al. 2007) and weakly oscillatory system. In stable and weakly oscillatory systems, WWEs may trigger El Niño and increase the model's ENSO variance. It is also seen that σ_3 and σ_4 in SD are greater than those in NO and AD for the entire range of γ, although the difference of σ_3 between SD and NO is not significant for $\gamma \geq 0.55$. That is, the state-dependent WWEs act to destabilize ENSO independent of the inherent model's stability.

4.4.2 Asymmetry

Figure 4.7b shows the positive and negative tails of the PDF in Fig. 4.7a. The Niño3 SST anomaly greater than 2 K is more frequent in SD and WP than in AD and N4, and it is not observed in NO. The numbers of occurrence during 1000 years are 0 in AD, 29 in SD, 1 in N4, and 12 in WP. This indicates that the occurrence of WWEs at the warm pool edge favors to trigger stronger El Niño events. On the other hand, the probability of values less than -2 K is almost zero in all the model experiments, although it slightly increases in SD.

Dependency of the ENSO asymmetry on γ is shown in Fig. 4.8c and 4.8d in the same manner as Fig. 4.8a and 4.8b. Here, we define an asymmetricity parameter, b, which is the variance-weighted skewness suggested by An et al. (2005):

$$b = \frac{m_3}{(m_2)^{1/2}}, \tag{4.10}$$

where m_k is the kth moment, $m_k = \sum_{i=1}^{N}(x_i - \overline{X})^k/N$ (x_i is the ith data, $\overline{X}$ is the mean, and N is the number of data). The asymmetricity is used instead of skewness (the normalized third statistical moment, $m_3/(m_2)^{3/2}$) to avoid causing the larger skewness associated with

the small standard deviation. Values of b for the Niño3 and Niño4 SST anomalies (b_3 and b_4, respectively) are shown in Table 4.2 for the experiments with $\gamma = 0.45$ and observation. In the observation for 1850–2014, $b_3 = 0.44$ and $b_4 = -0.01$, although these values largely change interdecadally and have larger magnitude in the post 1980's ($b_3 = 0.78$ and $b_4 = -0.20$ for 1981–2014, cf. An 2005). In NO, b_3 increases and b_4 decreases with γ. For any value of γ, b_3 in AD is smaller than NO. This may be caused by the climatology of the themocline depth induced by the WWE forcing, which is positive in the eastern Pacific, so that nonlinearity in Eq. (4.6) is reduced. Comparison between AD and SD shows that b_3 in SD is larger for $\gamma < 0.55$, consistent with previous studies using several models (Perez et al. 2005; Gebbie et al. 2007; Jin et al. 2007; Levine and Jin 2010; Lopez et al. 2013). This indicates that the state dependence of WWEs, especially the dependence on the warm pool expansion (Fig. 4.7b), is responsible for the ENSO asymmetry in the model. Values of b_4 in AD and SD also decrease but are largely negative than NO, and b_4 in SD is negatively larger than AD. Thus, state dependence also enhance the negative asymmetricity in the western-central Pacific. The above results suggest that the state-dependent WWEs help to produce the asymmetry in SST as in observations (cf. An and Jin 2004).

4.4.3 Periodicity

Figure 4.9 shows the power spectrum of the monthly Niño3 SST anomalies in the experiments with $\gamma = 0.45$ and observation. Owing to the regular oscillation in NO, the power is concentrated in the period of 6 years and there is a secondary peak in the period of 3 years. In the other experiments forced, the spectra are widened and have broad peaks in the period of 4–5 years. The powers in SD and N4 are larger than that in AD in all periods (cf. Table 4.2). The difference between WP and AD is not clear. On the other hand, the power in the dominant period is magnified in SD relative to N4, although the difference of SD from N4 is only the dependence on x_{pool}. This indicates that the dependences of

WWEs on T_4 and x_{pool} are nonlinearly related in the parameterization, and both of them play the crucial role to modulate the model's ENSO cycle.

Dependence of the model's ENSO periodicity on γ is shown in Fig. 4.10a–c for NO, AD, and SD. The result in Fig. 4.9 is robust for a wide range of γ. In NO, the power has dominant and weak peaks in the periods of 6 and 3 years, respectively. These two peaks may correspond to two inherent modes, QQ and QB modes, in the linearized ZC model (see the introduction), although the two frequencies in ZC-mLBM are slightly lower than those in Bejarano and Jin (2008). The dominant peaks in AD and SD shift toward higher frequency than that in NO regardless of γ. The difference of the powers between SD and AD is largely positive in the period of 3–5 years (Fig. 4.10d), indicating that the state dependence of WWEs enriches the power in the higher frequency. This frequency shift is also observed in CGCMs with additive WWEs (Lopez et al. 2013).

The dominant period of ENSO-like oscillations shifts from 6 years in NO to 4–5 years in the other experiments (Fig. 4.9). From the composites of El Niño and La Niña events using the 3-month running averaged Niño3 SST anomaly (Fig. 4.11), the rapid termination of La Niña in AD and SD is mainly responsible for the frequency shift. If the system were linear, additive WWEs would shorten La Niña and lengthen El Niño, and the dominant period would not change. The asymmetrical influence of WWEs on the solutions can be caused by nonlinearity in the subsurface temperature Eq. (4.6). The thermocline depth anomaly induced by WWEs further increases the subsurface temperature during La Niña (Fig. 4.12), and mean upwelling entrains the subsurface warm water into the surface efficiently. Therefore, WWEs work to terminate La Niña rapidly but not to lengthen El Niño. This can be interpreted that the shallower (deeper) thermocline associated with ENSO is more (less) sensitive to the thermocline deepening by WWEs in terms of the subsurface temperature anomaly. Enrichment of the power in higher frequency due to the state dependence in SD may be related with the modulation in the model's ENSO flavor, described in the next section.

Table 4.2: Standard deviations of the Niño3 and Niño4 SST anomalies (σ_3 and σ_4, respectively) and asymmetricities (4.10) of the Niño3 and Niño4 SST anomalies (b_3 and b_4, respectively) in the experiments with $\gamma = 0.45$ and observations for 1850–2014 (denoted as OBS) and 1981–2014 (denoted as OBS81).

	NO	AD	SD	N4	WP	OBS	OBS81
σ_3 [K]	0.45	0.41	0.63	0.56	0.47	0.79	0.91
σ_4 [K]	0.16	0.17	0.25	0.23	0.20	0.58	0.67
b_3 [K^2]	0.05	0.01	0.13	0.02	0.07	0.44	0.78
b_4 [K^2]	0.00	-0.02	-0.03	-0.04	-0.02	-0.01	-0.20

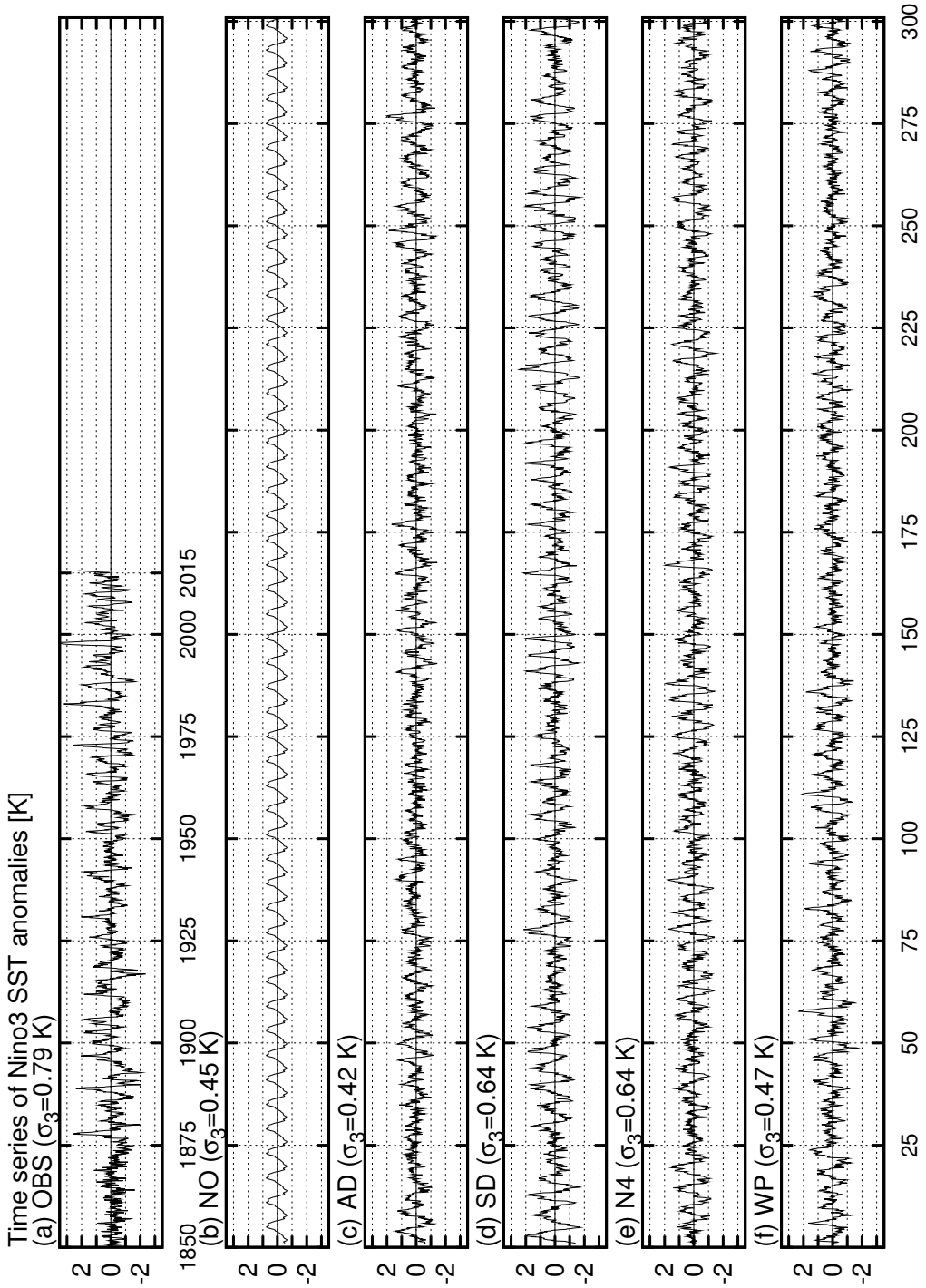

Figure 4.6: Time series of the monthly Niño3 SST anomalies [K] in (a) the observation from 1850 to 2014, (b) NO, (c) AD, (d) SD, (e) N4, and (f) WP from year 1 to 300.

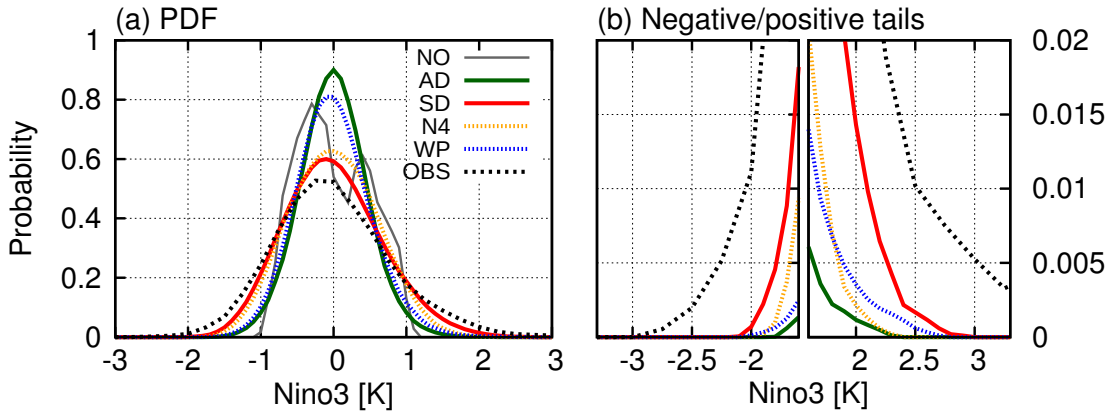

Figure 4.7: (a) PDFs of the Niño3 SST anomalies [K] in NO (dark-gray solid), AD (green solid), SD (red solid), N4 (orange dotted), WP (blue dotted), and the observation (black dotted). (b) The negative and positive tails of the PDFs. The PDFs are calculated using Epanechnikov kernel (Kimoto and Ghil 1993).

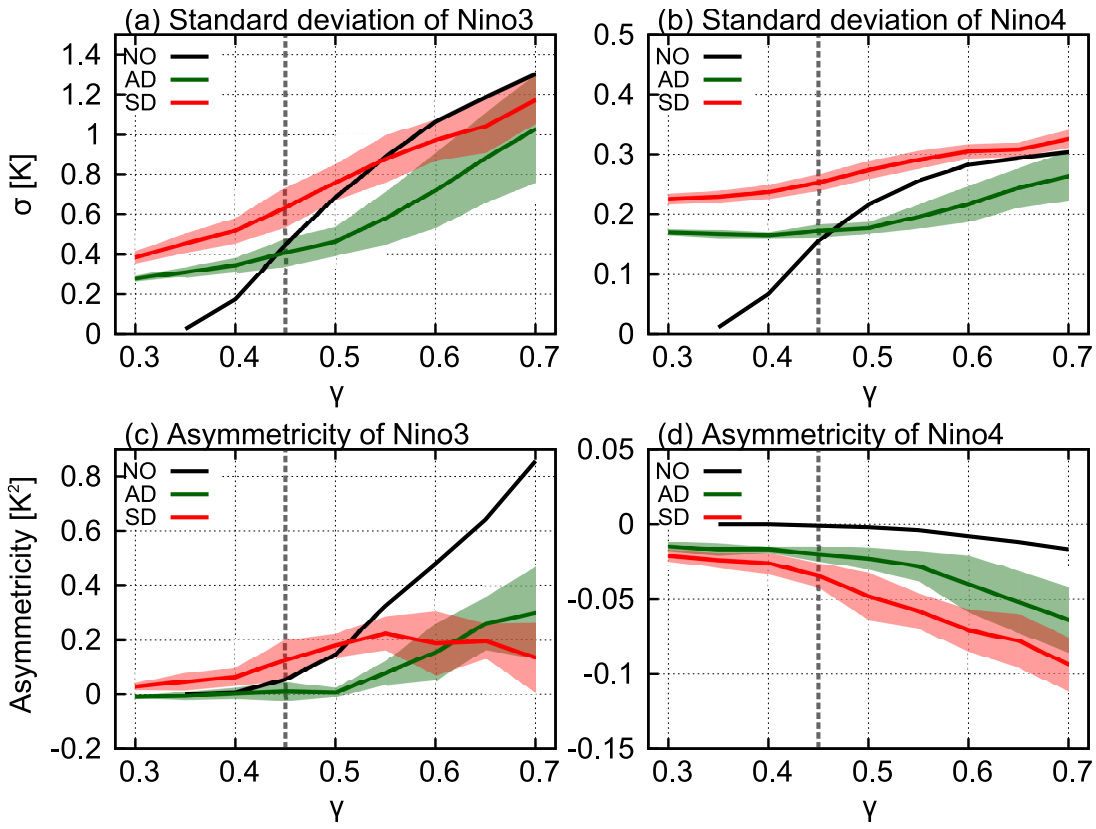

Figure 4.8: Dependence of standard deviations [K] and asymmetricities [K^2] of the Niño3 and Niño4 SST anomalies on γ in NO (black), AD (green), and SD (red). Solid line and shade indicate the mean and uncertainty, respectively, where the uncertainty is defined as the standard deviation of ten-time series separated from a single 1000-year time series. The uncertainty in NO is not depicted due to its rigid periodicity. The value for $\gamma = 0.3$ is not depicted in NO since ENSO-like oscillations are damped. Vertical dashed lines denote $\gamma = 0.45$.

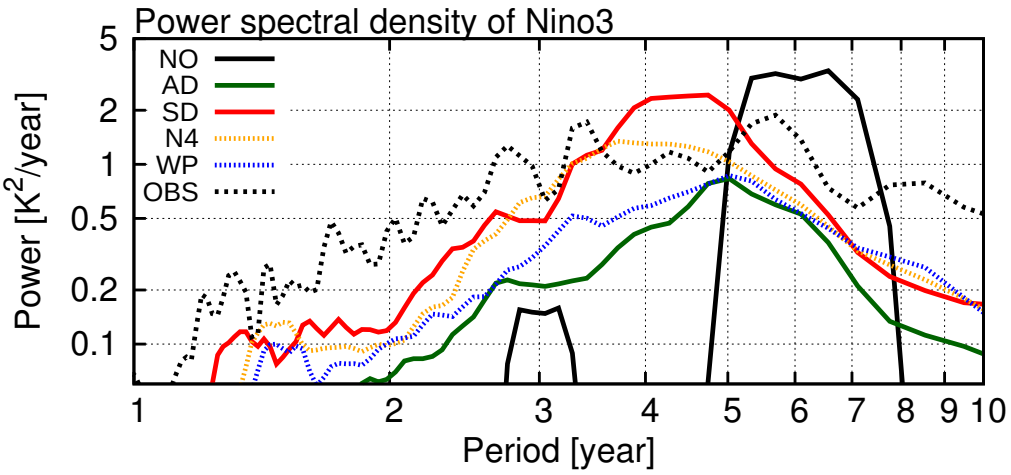

Figure 4.9: Power spectral densities [K^2 $year^{-1}$] of the Niño3 SST anomalies in NO (black solid), AD (green solid), SD (red solid), N4 (orange dotted), WP (blue dotted), and the observation (black dotted), calculated by Welch's overlapped segment averaging with 50-year windows using Hamming taper and zero padding.

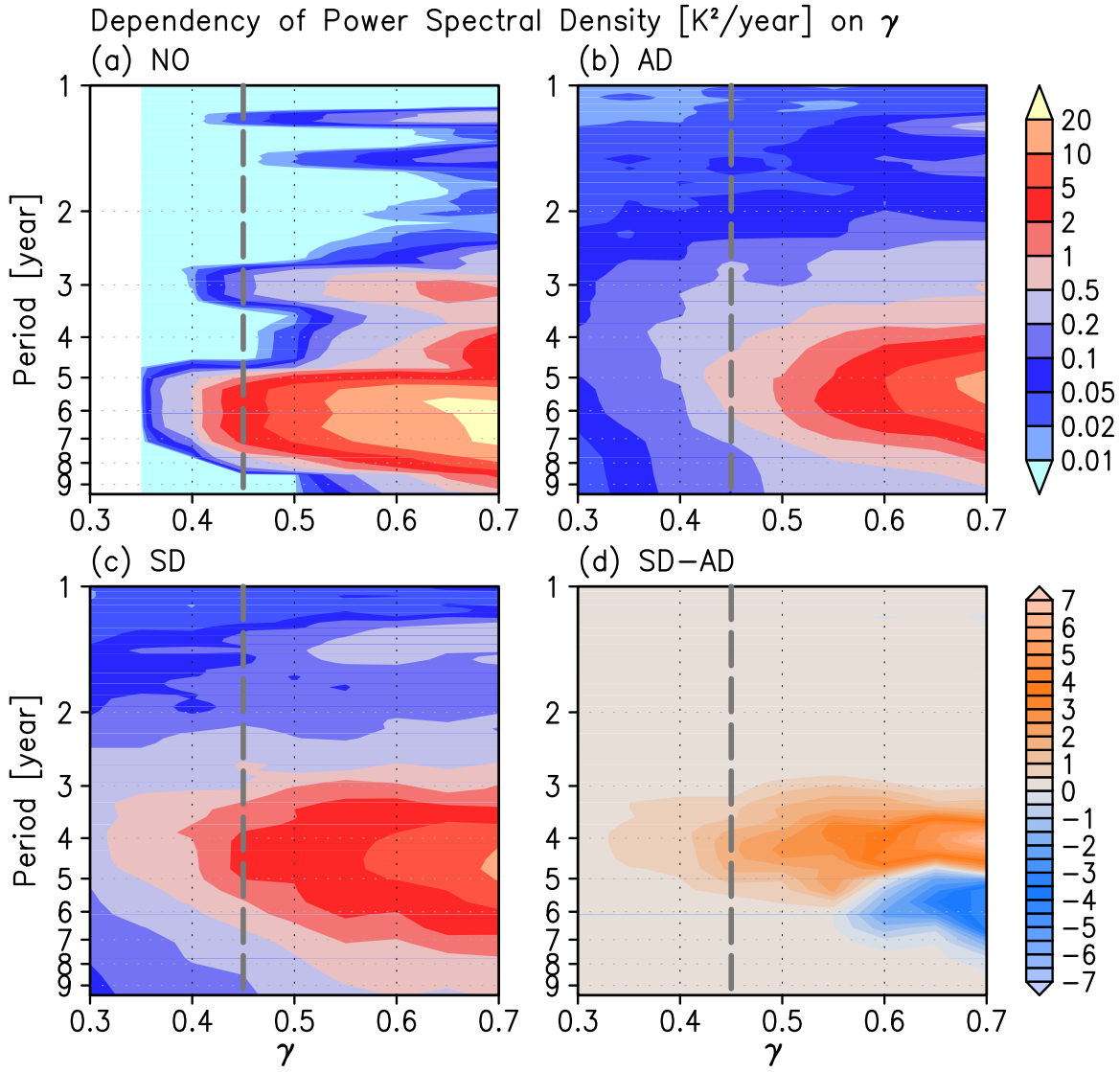

Figure 4.10: Dependency of the power spectral density on γ in (a) NO, (b) AD, and (c) SD, and (d) difference of SD from AD. In (a), the value for $\gamma = 0.3$ is not depicted since the model's ENSO cycle is damped in NO. Vertical dashed lines denote $\gamma = 0.45$.

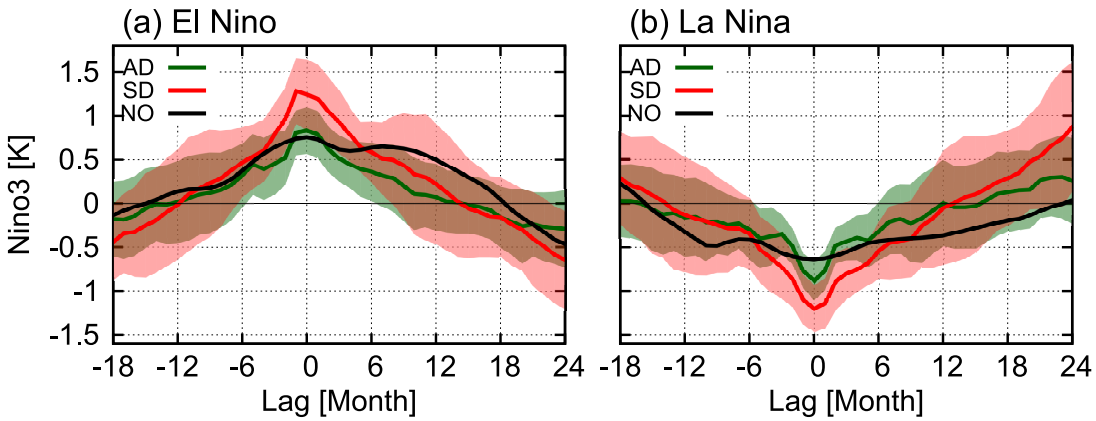

Figure 4.11: Composite of the Niño3 SST anomalies for (a) El Niño and (b) La Niña in AD (green), SD (red), and NO (black). Solid line and shade indicate the mean and standard deviation, respectively. Each El Niño (La Niña) event is detected when the Niño3 SST anomaly is greater (less) than its standard deviation (minus its standard deviation) for, at least, consecutive 3 months.

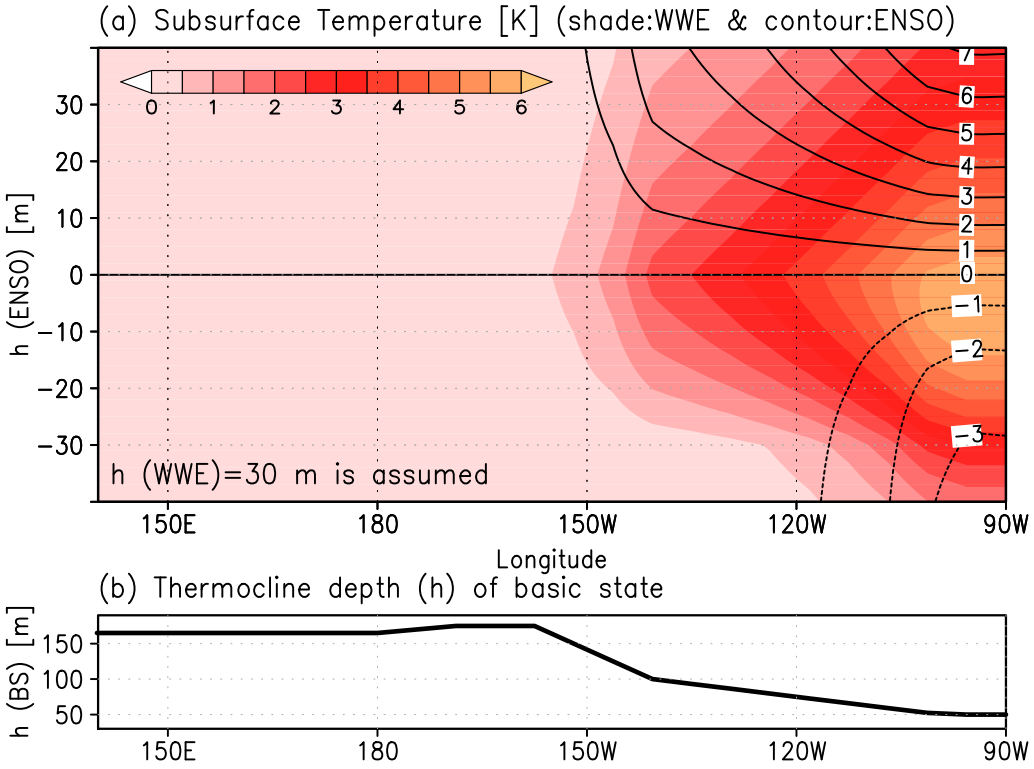

Figure 4.12: (a) Theoretical relationship between the thermocline depth anomaly (h) [m] associated with ENSO, $h(ENSO)$, and subsurface temperature (T_{sub}) [K] induced by a WWE. Here, the thermocline deepening due to the WWE, $h(WWE)$, is assumed to be 30 m. The vertical axis indicate a typical range of $h(ENSO)$ and the horizontal axis indicate the longitude. In (a), T_{sub} due to $h(ENSO)$ [contour] is calculated providing $h = h(ENSO)$, and that due to $h(WWE)$ [shade] is the difference of T_{sub} calculated from $h = h(ENSO) + h(WWE)$ and $h = h(ENSO)$ in Eq. (4.6). (b) Longitudinal profile of the thermocline depth [m] in the basic state, which is deeper in the western Pacific and shallower in the eastern Pacific.

4.5 Roles of state-dependent noise in the El Niño flavor

The El Niño flavor, i.e., coexistence of EP and CP El Niños, is examined in the model. According to Kug et al. (2009), the two types of El Niño events can be separated based on the relationship between magnitudes of the standardized Niño3 and Niño4 SST anomalies (T_3^* and T_4^*) averaged for the boreal winter (December–January–February). To clearly divide these two types, EP (CP) El Niño is detected when two conditions are satisfied: $T_3^*(T_4^*) \geq 1.0$ and $T_3^*(T_4^*) > T_4^*(T_3^*) + 0.5$. Using these criteria, 10 EP and 14 CP El Niño events are detected in the COBE SST data for 165 years (red and blue circles in Fig. 4.13a); they include typical EP El Niños in 1972/73, 1982/83, and 1997/98 and CP El Niños in 1994/95, 2002/03, 2004/05, and 2009/10. The composite horizontal structures of the winter SST anomalies are shown in Fig. 4.14a and 4.14b for EP and CP El Niños. The SST maximum of the EP (CP) El Niño is located in the eastern (central) Pacific, consistent with Kug et al. (2009).

Figure 4.13b–d shows the scatter diagram of T_3^* and T_4^* in NO, AD, and SD with $\gamma = 0.45$. Whereas T_3^* and T_4^* are highly correlated and quasi-periodic in NO (plots for 300 years are overlapped in Fig. 4.13b), their relationship is scattered in AD and SD and indicates that the El Niño flavor appears in these experiments. The numbers of EP and CP El Niños for 1000 years are 92 and 49 in AD, and 76 and 26 in SD, respectively. The composite winter SST anomalies of EP and CP El Niños in AD and SD show similar patterns to the observations (Fig. 4.14c–f), albeit the magnitudes of CP El Niños are considerably smaller.

Temporal evolutions of EP and CP El Niños are obtained from the lagged composites of SST and other anomaly fields in AD and SD. In AD, EP El Niño develops after boreal summer and matures in winter, accompanied by the atmospheric response (τ_x^{ENSO}) to the SST anomaly (Fig. 4.15a). Although the occurrence of WWEs is independent of SST in AD due to the formulation (4.9), the composite of τ_x^{WWE} indicates that EP El Niño tends to be triggered by WWEs in early summer through the oceanic response. CP El Niño in AD

is accompanied by several peaks of WWEs, which induce the eastward surface current, while τ_x^{ENSO} is weak (Fig. 4.15b). That is, WWEs stochastically push the warm water eastward and increase the SST in the central Pacific, generating CP El Niño. The zonal advection due to τ_x^{ENSO} may also contribute to persisting CP El Niño.

In SD, WWEs frequently occur during the developing phase of EP El Niño (during Jul(-1) and Jan(0)) and migrate eastward associated with the warm pool expansion (Fig. 4.16a). Correspondingly, the thermocline is deepened and the eastward surface current is enhanced, causing El Niño to amplify compared with AD. During CP El Niño in SD (Fig. 4.16b), successive WWEs in τ_x^{WWE} facilitate the eastward current persisting in the central Pacific. The Niño4 warming due to τ_x^{WWE} increases the probability of occurrence of WWEs, resulting in further warming. This positive feedback between the SST anomaly and τ_x^{WWE} acts to generate CP El Niño in SD. The relationship between WWEs and SST during EP and CP El Niños in SD is similar to typical events in 1997/98 and 2002/03 (Fig. 4.1, see also, Figs. 1.3 and 1.4), and it ensures reality of simulated events in SD.

The development process of El Niños is quantitatively discussed based on the budget analysis of the SST tendency. The tendency terms were directly dumped from the model following Eq. (4.2). Similar to the prototype oscillation in NO (Fig. 4.4), all the advective terms act to increase the Niño3 SST for EP El Niño in AD and SD (Fig. 4.17a, c). While the zonal advective term has only a weak peak at Jun(-1) in AD, it greatly contributes to the warming after the boreal spring in SD, corresponding to the occurrences of WWEs. The vertical and meridional advective terms are also enhanced in SD as compared with AD. Since the state-dependent WWEs force the eastward currents at the warm pool edge, the zonal advection of warm water further strengthens EP El Niño. This is consistent with the increase of the standard deviation and asymmetricity of Niño3 SST in SD (Fig. 4.8a and 4.8c). In the development of CP El Niño (Fig. 4.17b, d), the zonal advective term dominates in AD and SD, but it is larger and persists for a longer period in SD. This indicates that the frequent occurrence of WWEs for $T_4 > 0$ enhances the zonal advective

warming and induces CP El Niño with larger magnitude.

Interestingly, both EP and CP El Niño tend to have their peaks in boreal winter, even though CP El Niño is generated by stochastic additive WWEs in AD. WWEs in winter tend to warm the Niño4 region due to seasonally large zonal SST gradient in the basic state, while WWEs in late-spring to fall are favorable to trigger and intensify EP El Niño, consistent with Chapter 2, owing to the annual cycle of the atmosphere-ocean coupled system.

The flavor of El Niño depends on γ. The number of occurrence of EP El Niño is almost the same between AD and SD, and increases with γ (Fig. 4.18a and 4.18b). Therefore, the occurrence frequency of EP El Niño is independent of the state dependence of WWEs. On the other hand, when γ increases, CP El Niño becomes less frequent in AD but more frequent in SD (Fig. 4.18a and 4.18b). Consequently, the ratio of CP to EP El Niños declines with γ in AD (Fig. 4.18c), whereas it is roughly independent of γ in SD and is about 0.4 (Fig. 4.18d). In other words, the state dependence of WWEs ensures the existence of CP El Niño, or the El Niño flavor in the model. Since the period of CP El Niño is shorter than that of EP El Niño, the ensured existence of CP El Niño can enrich the model's ENSO power in higher frequency in SD (Figs. 4.9 and 4.10).

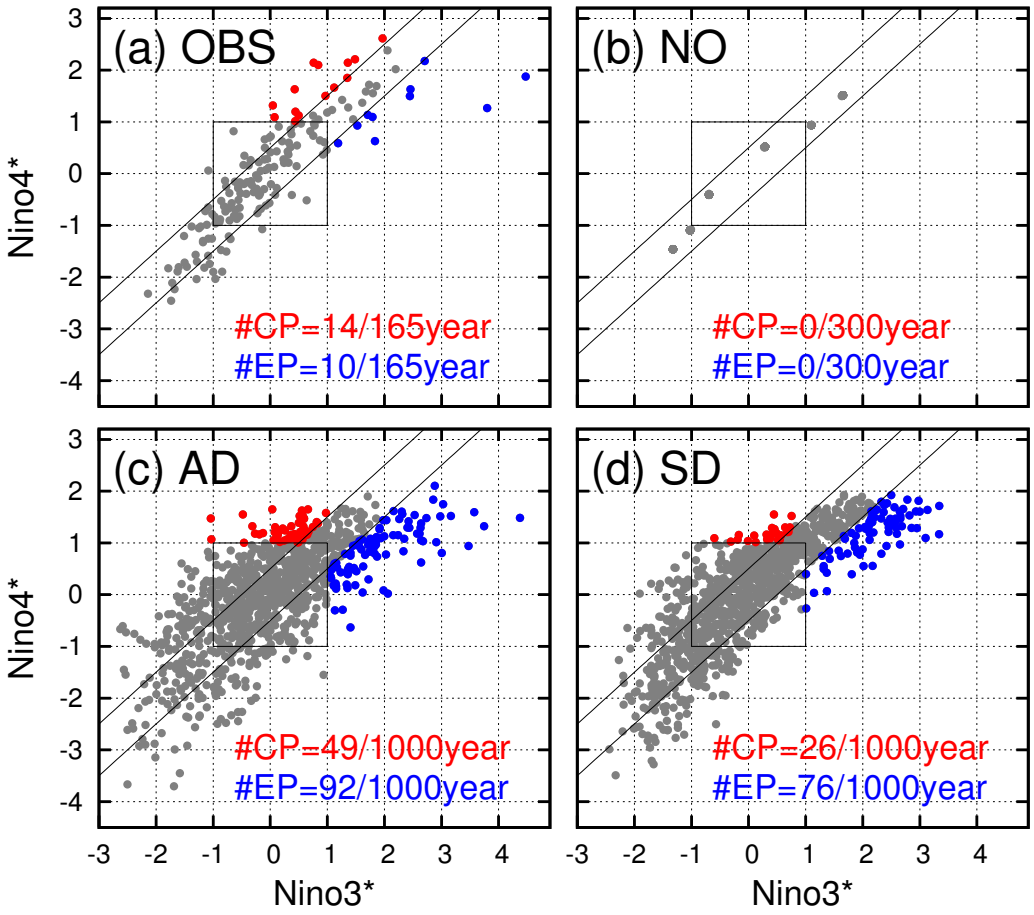

Figure 4.13: Scatter plot (gray dots) of the December-January-February (DJF) averaged Niño3 and Niño4 SST anomalies standardize by their standard deviations in (a) the observation, (b) NO, (c) AD, and (d) SD with $\gamma = 0.45$. Note that the plots for 300 years are overlapped in NO. Red and blue dots correspond to CP and EP El Niños, respectively. Thin lines in each panel are related to the conditions to determine CP and EP El Niños. The numbers of CP and EP El Niños for the period of each time series are shown at the bottom of each panels.

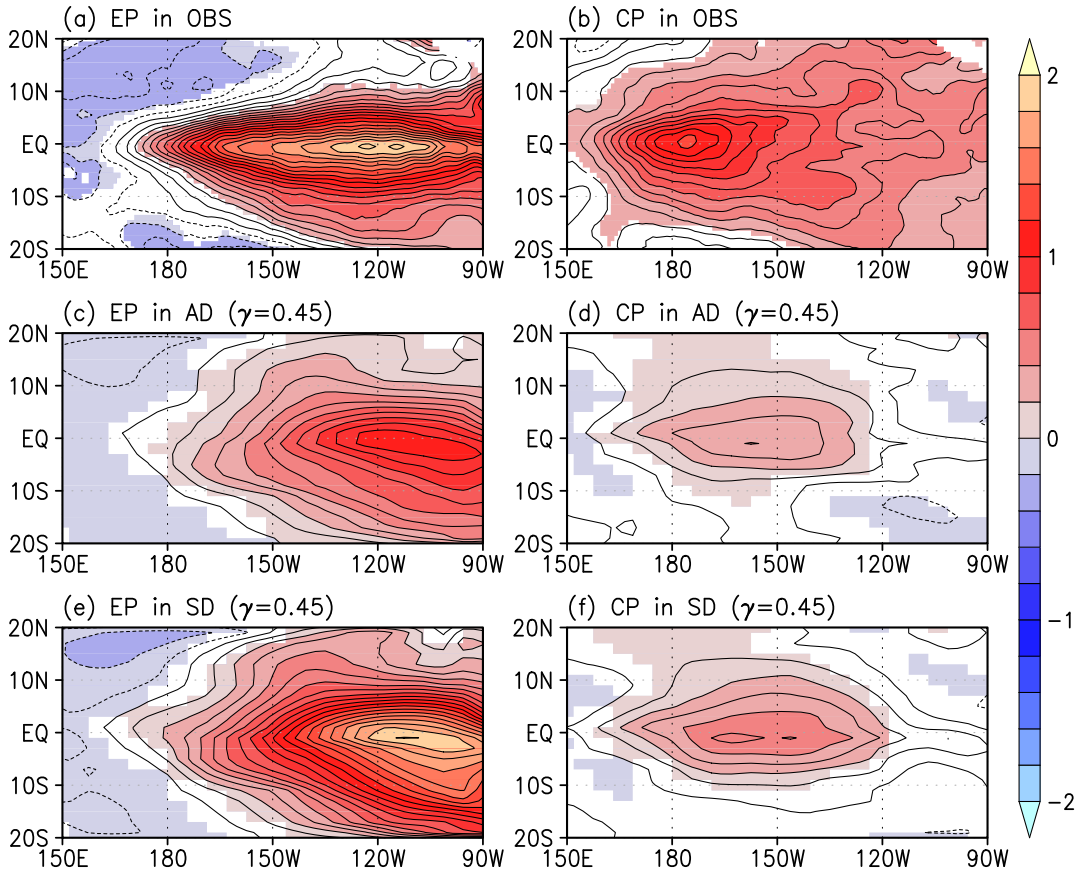

Figure 4.14: Composite of DJF averaged SST anomalies [contour intervals are 0.1 K] for EP and CP El Niños in (a, b) the observation, (c, d) AD, and (e, f) SD with $\gamma = 0.45$. Shaded areas indicate value exceeding 95% statistical confidence calculated by a two-tailed Student's t-test.

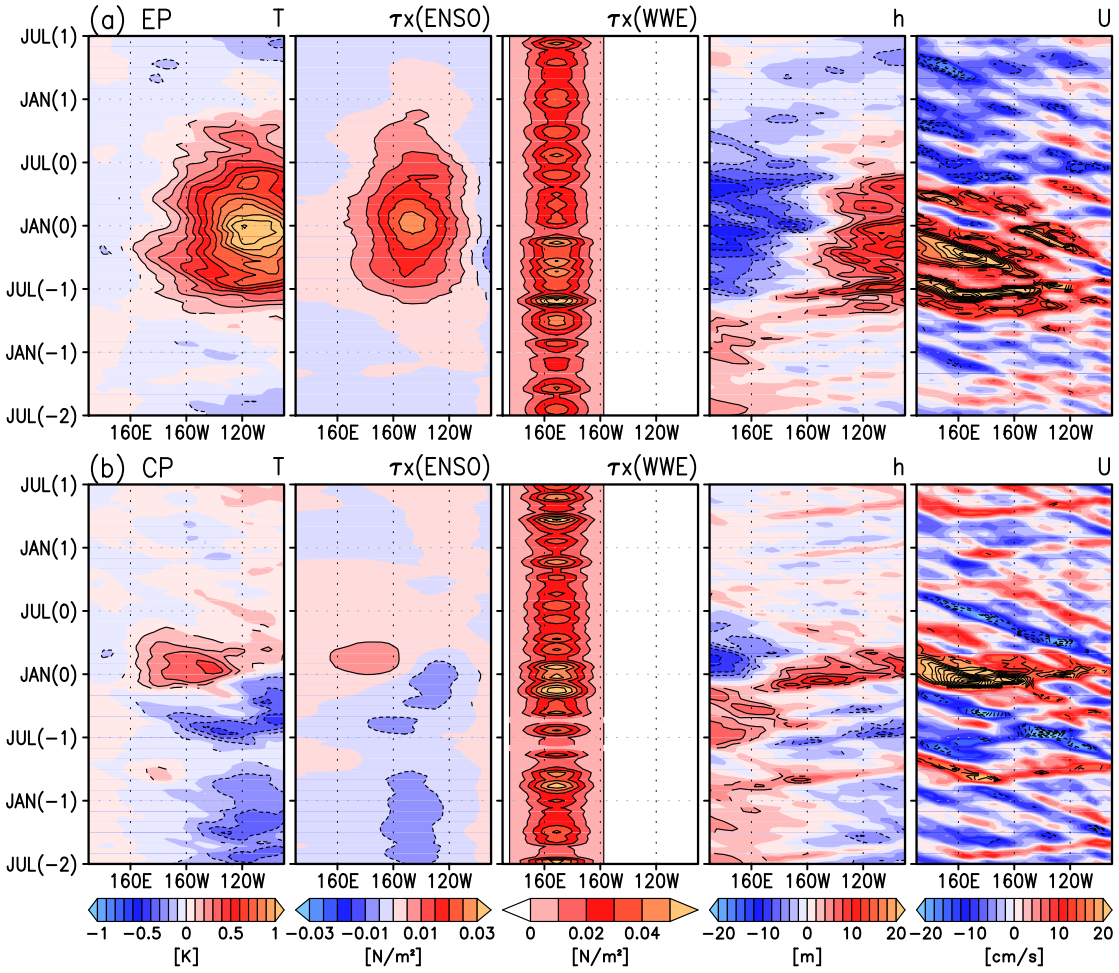

Figure 4.15: Lag composite of (a) EP El Niño and (b) CP El Niño for 3 years in AD with $\gamma = 0.45$, centered at the central day in January. From left to right, the SST anomaly [K], zonal wind stress anomaly associated with model's ENSO (τ_x^{ENSO}) [N m^{-2}], zonal wind stress of WWEs (τ_x^{WWE}) [N m^{-2}], anomalies of the thermocline depth [m] and surface zonal current [cm s^{-1}] averaged for 1 °S–1 °N. Contoured areas indicate value exceeding 95% statistical confidence calculated by a two-tailed Student's t-test.

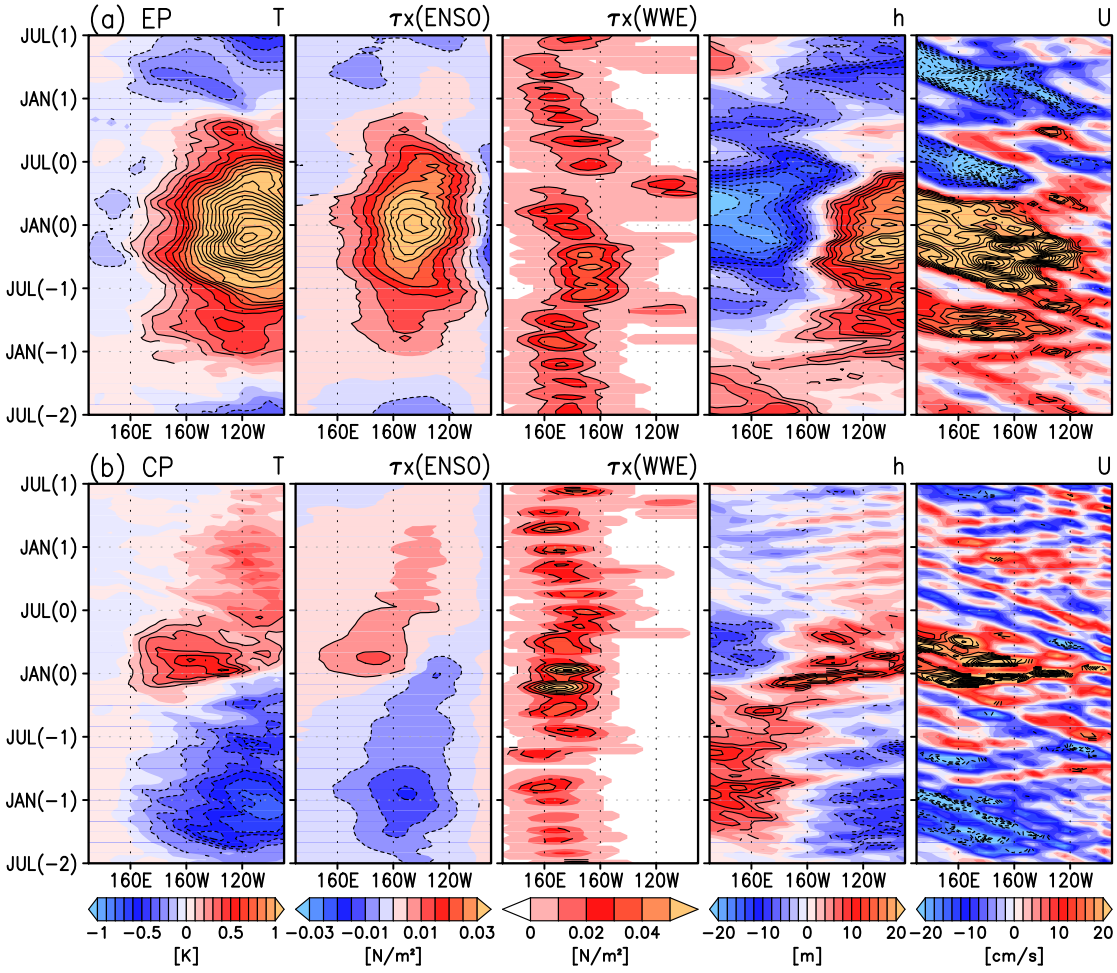

Figure 4.16: Same as Fig. 4.15, except for SD with $\gamma = 0.45$.

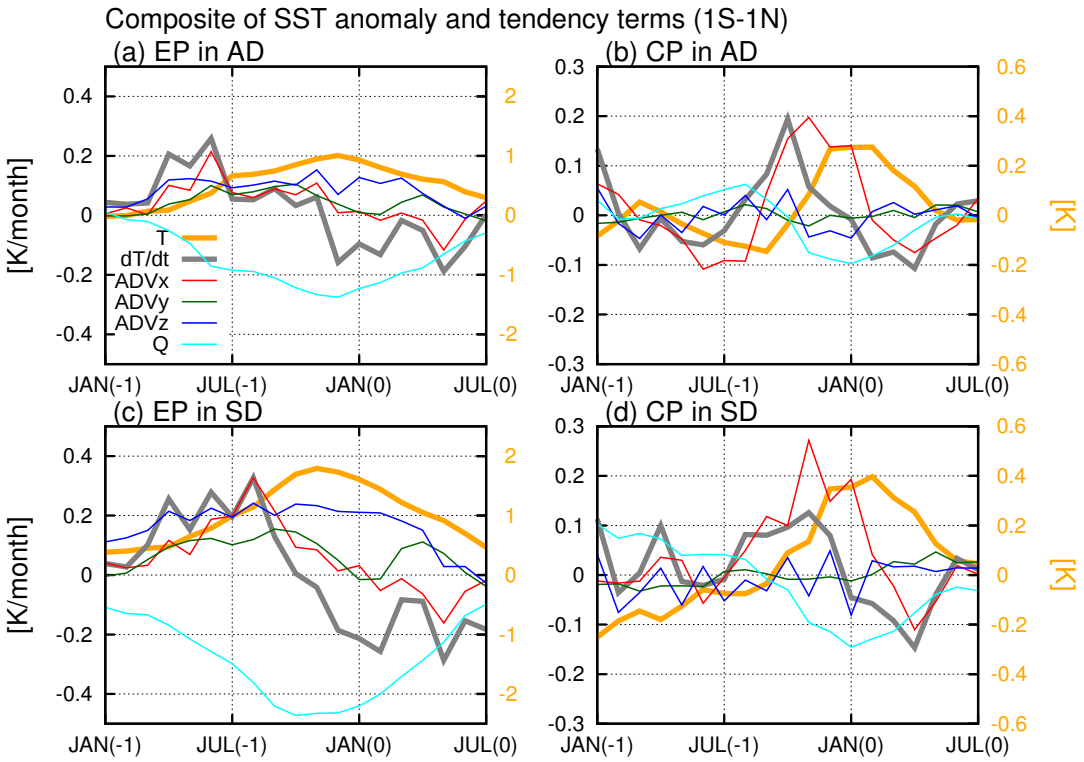

Figure 4.17: Lag composite of the SST anomalies [orange thick, K] and its tendency [gray thick, K month^{-1}] on (left column) EP El Niño and (right column) CP El Niño for 18 months in (a, b) AD and (c, d) SD. For EP (CP) El Niño, the values are averaged at the Niño3 (Niño4) region but 1 °S–1 °N in the meridional direction. Thin red, green, blue, and cyan lines show the zonal, meridional, and vertical adective terms and a damping term including the surface heat flux, respectively, in Eq. (4.2). The left and right vertical axes indicate the SST anomaly and its tendency terms, respectively.

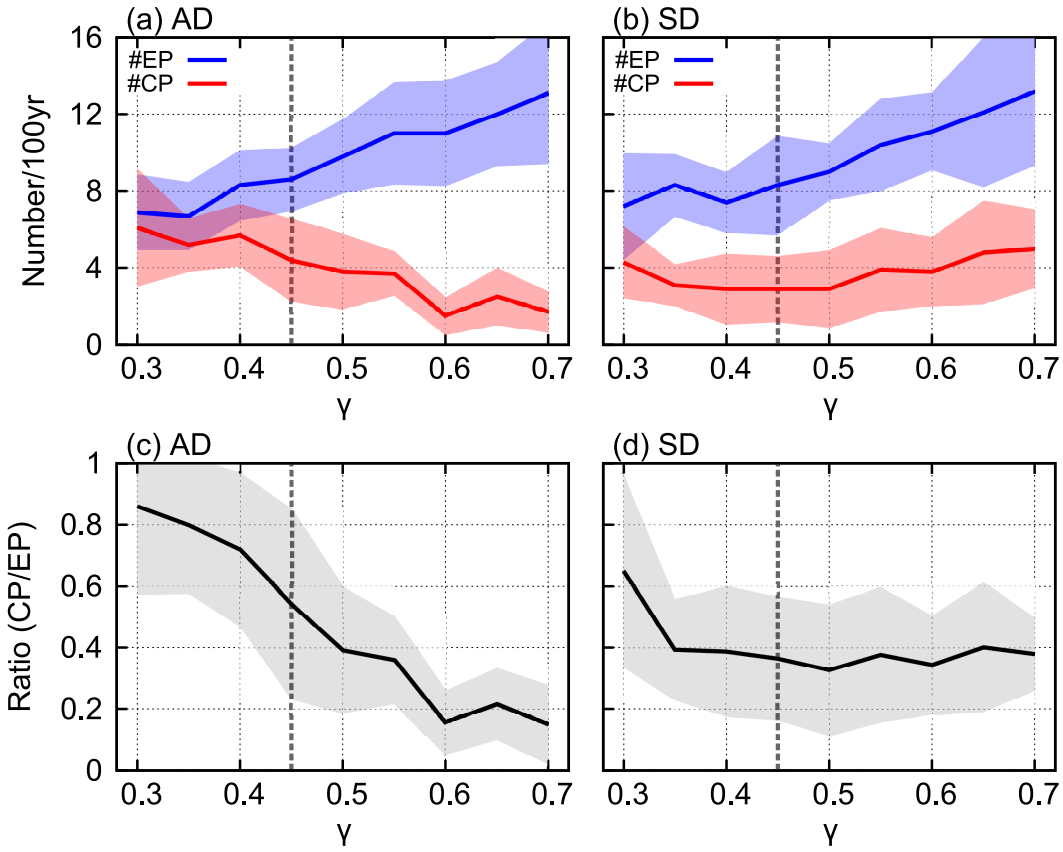

Figure 4.18: Dependency of the El Niño flavor on γ in (left) AD and (right) SD. Top panels show the numbers of (blue) EP and (red) CP El Niños for 100 years, and bottom panels show the ratio of the numbers of CP El Niño to that of EP El Niño. The mean and uncertainty (standard deviation) are calculated by dividing each 1000-year time series into ten 100-year periods. Vertical dashed lines denote $\gamma = 0.45$.

4.6 Summary and discussion

A coupled system between WWEs and ENSO and its dependence on the inherent ENSO stability were examined using an intermediate atmosphere-ocean coupled model, ZC-mLBM (Zebiak and Cane 1987; Watanabe and Jin 2003), which induces a periodic ENSO-like oscillation without external forcing. The annual cycles of both atmosphere and ocean are prescribed in the model given its importance on the ENSO cycle (Chapter 2). Additive and state-dependent WWEs, having a Gaussian shape centered at the equator, are probabilistically parameterized in the model. For the state-dependent case, likelihood of occurrence of WWEs increases for positive Niño4 SST anomaly and the location of WWEs depends of the eastern edge of the warm pool based on observations (Chapter 3). Roles of the state dependent WWEs on the model's ENSO are summarized as follows.

- Frequent occurrence of WWEs for the positive Niño4 SST anomaly increases the variance.
- The occurrence of WWEs at the warm pool edge increases the asymmetry.
- State dependence of WWEs ensures the existence of two types of El Niño.

The relationship between additive and state-dependent WWEs and the model's ENSO is schematically presented in Fig. 4.19. Without WWEs (Fig. 4.19a), the thermocline and zonal advective feedbacks drive an ENSO-like oscillation, and Niño3 and Niño4 SST anomalies are highly correlated, making it difficult to distinguish two types of El Niño. When additive WWEs are incorporated (Fig. 4.19b), the zonal advection due to WWEs (thick dashed arrow) simultaneously excites the central Pacific warming accompanied by the atmospheric response to the SST; then, the zonal advective feedback between the SST and atmospheric circulation induces CP El Niño. The additive WWEs also act to trigger EP El Niño through the downwelling Kelvin waves (thick bold arrow), which travel to the eastern Pacific in a few months. Since the thermocline feedback is effective in the eastern Pacific and increases with γ, the system favors EP El Niño for larger γ. When

the WWEs are state dependent (Fig. 4.19c), the positive Niño4 SST anomaly increases the probability of occurrence of WWEs (thick gray arrow), enhancing the zonal advective feedback to generate CP El Niño. Since the variance of the Niño4 SST anomaly increases with γ, the number of CP El Niño also increases owing to this feedback. Since the Niño4 region is located to the west of the Niño3 region, feedback between these regions is required to influence EP El Niño. First, WWEs induce the oceanic Kelvin waves associated with the deepening of the thermocline, resulting in the subsurface warming in the eastern Pacific where the mean thermocline depth is shallow. Then, the warm water is entrained into the surface layer due to the mean upwelling, and SST increases. The atmospheric response to the SST anomaly causes zonal advection to warm the Niño4 region, which is favorable for the subsequent occurrence of WWEs. In addition, WWEs rarely emerge during La Niña not to suppress the oscillatory system (Fedorov 2002). Therefore, the state-dependent WWEs increase the variance of the model's ENSO. The state-dependent WWEs also strengthen EP El Niño since they migrate to the east associated with the warm pool expansion, where zonal SST contrast is large, so that zonal advective warming is effective (cf. Gebbie et al. 2007). Thus, the ENSO-like oscillation becomes more asymmetric due to the state dependence of WWEs.

The ZC model has been used for El Niño forecasts (e.g., Chen et al. 1995), although it has several limitations in both the atmospheric and ocean components. For instance, Xie et al. (2015) applied thermal and dynamical modifications in the atmospheric component to reduce spurious convective heating anomalies and anomalous easterly bias over the eastern Pacific. In a similar spirit, Kirtman and Zebiak (1997) replaced the atmospheric model to an atmosphere general circulation model to improve the ENSO prediction. Since we coupled the mLBM (Watanabe and Jin 2003) to the ocean component, the atmospheric circulation driven by SST anomaly can be more realistic than the original one. Some previous studies also attempted to modify the ocean component of the ZC model. Kang and Kug (2000) parametrized the subsurface temperature based on the singular value decom-

position (SVD) of the thermocline depth and subsurface temperature based on observations, besides the use of an empirical atmospheric model. Then, the model resulted in the better performance in SST anomalies at the central Pacific due to the representation of subsurface temperature. In addition, Kug et al. (2005) introduced surface heat flux and vertical mixing into the SST equation to capture SST thermodynamics more realistically, especially at the western Pacific. These modifications provided better forecast skill not only at the western Pacific but also at the eastern and central Pacific. The modifications in the subsurface temperature and SST equation might present better performance in the ZC-mLBM.

Next, the WWE parameterization in this chapter is compared with previous studies. Perez et al. (2005) provided the dependence of noise variance on the Niño3 SST anomaly. However, the occurrence of WWEs does not depend on the SST anomaly in the eastern Pacific (Fig. B1b in Chapter 3). To assume relationship of occurrence of WWEs with the warm pool extent (Eisenman et al. 2005; Gebbie et al. 2007; Kapur and Zhang 2012; Lian et al. 2014; Chen et al. 2015) may be unrealistic since it greatly increases the noise variance (or likelihood of occurrence of WWEs) still after the mature phase of EP El Niño. Instead, the occurrence of WWEs is robustly dependent on the Niño4 SST anomaly (Chapter 3), consistent with dynamical amplification of high-frequency surface westerlies by low-level westerly (Seiki and Takayabu 2007b; Sooraj et al. 2009) and anomalous zonal contrast of SST and sea level pressure (Lengaigne et al. 2003; Yu et al. 2003).

Coupling between WWEs and ENSO is an aspect of multi-scale interaction in the equatorial Pacific. Since a seminal work by Eisenman et al. (2005), previous studies have confirmed the importance of the slow component (i.e., envelop) of atmospheric noise and WWEs on ENSO. Atmospheric noise is linearly uncorrelated with ENSO, but it is also partly deterministic due to the nonlinear interaction between high-frequency and interannual variability (e.g., Levine and Jin 2015). The modulation in the likelihood of occurrence of WWEs can be responsible for the deterministic and slow component. The pro-

cess to generate the slow component has also been investigated in Chapter 3, Lengaigne et al. (2003), Seiki and Takayabu (2007b), and many others. In this chapter, we compared the impacts of the additive and state-dependent components of WWEs on ENSO-like oscillations comprehensively, and showed significant roles of the state dependence in the statistics and flavor of the model's ENSO. Although, in nature, there are the other factors for modulating the ENSO cycle (e.g., An 2009), the state dependence of WWEs should be considered in ENSO dynamics to present its diverse behavior.

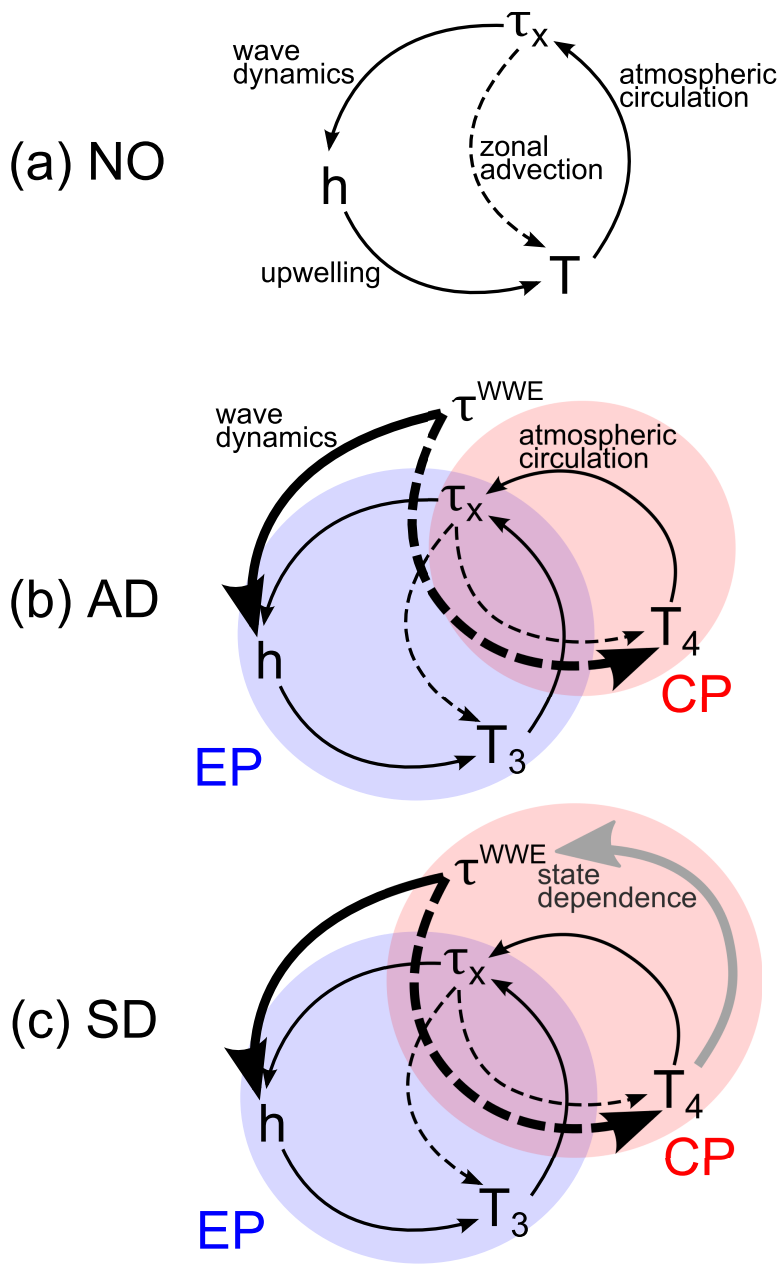

Figure 4.19: The main ENSO feedbacks in (a) NO, (b) AD and (c) SD, updated from Zelle et al. (2004). Here, τ_x, h, and T indicate the zonal wind stress associated with ENSO, thermocline depth, and SST anomalies. T_3 and T_4 are the SST anomalies in the Niño3 and Niño4 region, respectively. τ^{WWE} indicates the wind stress associated with additive and state-dependent WWEs in (b) and (c). Circles with blue and red shadings represent the feedbacks to produce EP and CP El Niños, respectively. All the dashed arrows indicate the zonal advection. Thick black solid and dashed arrows in (b) and (c) indicate the roles of τ^{WWE}, and a thick gray arrow in (c) represent the state dependence. See the text in the figure for the other arrows.

Chapter 5

General conclusions

The coupled system between westerly wind events (WWEs) and the El Niño-Southern Oscillation (ENSO) phenomenon has been examined in the present study using a hierarchy of coupled atmosphere-ocean models and observational data to clarify (i) processes responsible for the response of the atmosphere and ocean to WWEs in the presence of annual cycle, (ii) state dependence and asymmetry of WWEs and their easterly counterpart called easterly wind events (EWEs), and (iii) role of the state dependence of WWEs in generating the complexity of ENSO. Results in Chapters 2, 3, and 4 are summarized as follows.

- **In Chapter 2**, a coupled atmosphere-ocean response to WWEs was investigated using a coupled general circulation model (CGCM) with particular attention paid to the dependence on the seasonal timing of WWEs. Twelve sets of 20-member ensembles were made with an idealized WWE pattern imposed in different months from January to July and in different longitudes from 160 °E to 160 °W. The initial ocean states were set to be near neutral so that the lagged response to WWEs can be isolated.

  The results show that SST at the Niño3.4 region (170 °–120 °W, 5 °S–5 °N) increases largely and persistently when a WWE was imposed in May, which is fa-

vorable to El Niño growth. In contrast, a WWE imposed in March induces an SST increase only in the easternmost equatorial Pacific. In both cases, oceanic signal generated by the WWE in the subsurface propagates eastward and warms the surface in the eastern equatorial Pacific. When forced by the WWE in May, a positive SST anomaly appears in boreal summer when it can strongly interact with the atmospheric circulation and convective activity, which amplify the SST anomaly spreading toward the central equatorial Pacific. The above mechanism works conditioned by the seasonal march of both the atmosphere and ocean background states, and therefore the coupled response is sensitive to the timing of the WWEs. The above model experiments enable us to identify a favorable set of combinations of timing and location that maximize the role of WWEs in triggering El Niños in the subsequent winter. Other experiment sets with ocean initial states in El Niño and La Niña years showed that WWEs in May are efficient to amplify El Niño similar to the neutral case, while they are not efficient to suppress La Niña.

- **In Chapter 3**, the characteristics of WWEs and EWEs were examined. Their state dependence and asymmetry are analyzed by using observational daily data of atmosphere and ocean fields. We analyzed daily surface winds for 1982–2013 from which WWEs and EWEs were detected. Both types of events appear over the western Pacific warm pool, where SST is sufficiently high for active deep convection, with a similar seasonality, and they favorably occur with increasing Niño4 (160 °E–150 °W, 5 °S–5 °N) SST, indicating their state dependences. In addition, the occurrence of both WWEs and EWEs are highly related with the phase of the Madden-Julian oscillation (MJO). However, the occurrence frequency of EWEs is much less than that of WWEs, resulting in asymmetry in wind amplitude. This is confirmed from a comparison of their characteristics based on different criteria for the event detection. A high-frequency energy budget analysis indicated that, although the background low-level zonal winds similarly amplify WWEs and EWEs

locally, different local development processes caused by intraseasonal winds result in the asymmetry in the occurrence frequency between them. A linear model experiments showed that local and remote anomalous convections are equally important in exciting these events. These results can also be seen in wind stress anomalies, albeit obscured due to nonlinearity therein.

- **In Chapter 4**, a coupled dynamics between WWEs and ENSO was examined using an atmosphere-ocean coupled model with intermediate complexity that produces ENSO-like oscillations. WWEs are parameterized based on the results in Chapter 3 as a state-dependent stochastic noise to wind stresses in the model. Without the noise (experiment NO), the model produces an ENSO-like oscillation with a period of 6 years and its variance increased with respect to a parameter controlling the model's ENSO stability, γ. When additive (purely stochastic) noise are given to the model over the western Pacific (experiment AD), oscillations become irregular with the dominant period of about 5 years and the increase of its variance relative to NO depends on γ. When the state-dependent noise is incorporated (experiment SD), the oscillatory solution is also irregular besides its variance and asymmetry increase irrespective the value of γ.

  Both the additive and state-dependent noises produce two types of ENSO-like oscillation, corresponding to the eastern-Pacific (EP) and central-Pacific (CP) El Niños, although there is no such diversity in NO. EP El Niño is magnified in SD due to the eastward shift of the noise location caused by the warm pool expansion. CP El Niño is even favored by the state-dependent stochastic noise, which enhances the zonal advection to warm the central Pacific, and in turn the warmer Niño4 SST increases the probability of occurrence of the noise. This positive feedback ensures the existence of CP El Niño regardless of γ in SD, while the number of CP El Niño declines with larger γ in AD. The above results thereby suggest that the state dependence of WWEs may play a crucial role in the asymmetry and diversity of ENSO in nature.

This study showed crucial roles of the state dependence of WWEs and the interaction of response to WWEs with annual cycle of both atmosphere and ocean in the rich behavior of ENSO. Chapter 3 showed the observational characteristics of WWEs and EWEs, and the uneven occurrence probability of WWEs and EWEs, although they both have a similar state dependence, emphasizes the relative importance of WWEs on El Niño. As seen in Chapters 2 and 4, the atmosphere-ocean coupled response to WWEs is affected strongly by annual cycle. Chapter 4 showed that the state-dependent WWEs, based on the observational statistics in Chapter 3 as the basis, ensure the coexistence of CP and EP El Niños via the WWE-SST feedback. It is also found that the occurrence of the state-dependent WWEs at the warm pool edge plays a role to amplify EP El Niño and to cause the ENSO asymmetry.

Previous studies showed that the response to WWEs can be affected by the annual means of trade wind and thermocline depth (Fedorov 2002), annual cycle of the zonal SST gradient (Harrison and Schopf 1984), modulation of the tropical instability waves (Harrison and Giese 1988), and upper ocean heat content anomalies associated with the phase of ENSO (Fedorov 2002; Hu et al. 2014; Fedorov et al. 2015). Latif et al. (1988) implied the annual cycle in the background precipitation might affect the oceanic response to WWEs, although difference between responses to WWEs in January and July was not observed in their CGCM due to the unrealistic atmospheric seasonality. Chapter 2 showed that the atmospheric annual cycle also influences the response to WWEs in the atmosphere-ocean coupled system, and that WWEs in May are indeed favorable to trigger El Niño, as observed in extremely large El Niños in 1982/83, 1997/98, and 2015. This is consistent with the triggering role of the stochastic noise during early boreal summer in Chapter 4, where the annual cycles in both atmosphere and ocean were prescribed.

The state dependence of atmospheric noise has been considered in relation with the SST anomaly at the eastern Pacific in some previous studies (e.g., Vecchi and Harrison 2000; Perez et al. 2005; Levine and Jin 2015). However, as shown in appendix B of Chap-

ter 3, the noise robustly depends on the Niño4 SST instead of the Niño3.4 SST. This is reasonable since the Niño4 SST anomaly is highly correlated with the other indicators for occurrence of WWEs: warm pool expansion (Eisenman et al. 2005), the zonal gradients of background SST and sea level pressure (Lengaigne et al. 2003; Yu et al. 2003), and low-level westerly (Seiki and Takayabu 2007b; Sooraj et al. 2009; Chapter 3) at the western Pacific. Chapter 3 also clarified the asymmetry and state dependence of WWEs and EWEs, which has been debated in recent studies (Chiodi and Harrison 2015; Puy et al. 2015). Although both types of events have similar state dependence, their asymmetry in development process emphasizes the relative importance of WWEs on El Niño.

Chapter 4 showed that the state dependence of WWEs ensures the El Niño flavor regardless of the inherent model stability, and the time evolutions of CP and EP El Niño in the model resemble typical events in observations. Although Lian et al. (2014) and Chen et al. (2015) also showed the appearance of CP El Niño in an intermediate coupled model with a WWE parameterization, the necessity of the state dependence has not been clarified since they did not compare with experiments with stochastic additive noise. Besides, observational evidence lacks in their assumption that the occurrence location of WWEs propagates eastward with a constant speed. The impact of the state dependence of WWEs on EP and CP El Niños was examined by Lopez and Kirtman (2013) using CGCMs by parameterizing additive and state-dependent WWEs. Although they concluded that CP El Niño is not greatly enhanced by additive and state-dependent WWEs, their Fig. 4 indicates that the state dependence of WWEs magnifies CP El Niño, consistent with Chapter 4. Since low-order conceptual ENSO models generally have one variable of SST (e.g., Jin et al. 2007), the inclusion of a variable of Niño4 SST to assume the state-dependent noise may help to advance theoretical studies on coupling between the noise and ENSO.

CP El Niño events have been frequently observed since the late 1990's. From an analysis on the Coupled Model Intercomparison Project phase 3 (CMIP3) multi-model data

set (Meehl et al. 2007), Yeh et al. (2009) indicated that the increased frequency of CP El Niño in a changing climate was related to a shoaling of the thermocline depth to warm the central Pacific by enhancing the thermocline feedback. In contrast, an observational analysis by McPhaden et al. (2011) showed that the thermocline was on average deeper in the western and central Pacific during 2000–2010 compared to 1980–2000, implying that natural variations of ENSO might cause the decadal change in the background state. Although the mechanism responsible for such natural variations is still unclear, it is possible that the La Niña-like background state (e.g., Watanabe et al. 2014) reduces the warming response to WWEs in the eastern Pacific (cf. Chapter 2), resulting in frequent occurrences of CP El Niños during 2000–2010 via the state dependence of WWEs (Chapter 4). The cause for the change in the El Niño flavor requires further investigation.

The interaction between WWEs and ENSO was focused in Chapter 4. In previous studies, however, other processes responsible for the instability and asymmetry of ENSO have been examined, as reviewed by An (2009). For instance, Jin et al. (2003) and An and Jin (2004) showed that the nonlinear dynamic thermal advections (or the nonlinear dynamical heating, NDH) amplify (suppress) strong El Niño (La Niña) events through the vertical advective heating, suggesting that the eastward-propagating ENSO tends to be accompanied by large NDH (see also, Timmermann and Jin 2002; Timmermann et al. 2003; Duan et al. 2008). Although NDH is efficient for prescribed eastward-propagating wind stresses theoretically (An and Jin 2004), it is still unclear what causes the eastward propagation of ENSO. In observations, frequent WWEs resulted in eastward-propagating thermocline anomalies consecutively (e.g., McPhaden 1999), implying a possible role of WWEs for large NDH during El Niño. Although tropical instability waves (TIWs) affect the ENSO asymmetry (An 2008), the ocean response to WWEs is also influenced by the modulation of TIWs (Harrison and Giese 1988). The stability of ENSO can be affected by change in the mean state of the thermocline depth and zonal wind stress (e.g., Fedorov and Philandar 2001; Bejarano and Jin 2008), indicating the dependence of ENSO on Pacific

decadal variability and climate change (Fedorov and Philandar 2000; Collins et al. 2010). On the other hand, the impact of WWEs also depends on the mean state (Fedorov 2002), and the state-dependent noise itself shows a significant interdecadal change (Kug et al. 2008). A unified work for these possibilities can be a challenging future objective.

Some limitations in this study are discussed below. Although the CGCM used in Chapter 2 well reproduced the background annual cycle at the eastern Pacific, it still has the model bias (systematic model error) of SST in the western Pacific. Therefore, further studies by CGCMs having more realistic background state are needed to examine the dependence of atmosphere-ocean coupled responses to WWEs in the western Pacific on the annual cycle. The ocean component of the ZC model was used in Chapter 4. Kang and Kug (2000) suggested a modification in subsurface temperature of the ZC model based on statistical analysis to improve the skill of El Niño prediction. The Modification might influence the ENSO cycle in Chapter 4, although the observation-based parameterization will make the coupled system complex to interpret physically.

This study suggests that the background annual cycle, state-dependent high-frequency atmospheric disturbances, and interaction among them greatly influence the ENSO cycle in the coupled atmosphere-ocean system. It is also advocated that the WWE-SST feedback ensures the ENSO asymmetry and the existence of CP El Niño in nature. Although the operational El Niño prediction and future projection of ENSO are based on CGCMs (e.g., Hendon et al. 2009; Collins et al. 2010; Barnston et al. 2012; Taschetto et al. 2014; Imada et al. 2015), ENSO may be affected by the model bias not only in the mean state but also in the annual cycle through interacting with the atmospheric noise (Chapter 2; Harrison and Schopf 1984; Levine and McPhaden 2015) and ENSO itself (Stuecker et al. 2013, 2015a,b; Stein et al. 2014; Ren et al. 2015). Besides, the intraseasonal atmospheric variability like the MJO is not well simulated in CGCMs yet (Hung et al. 2013). Since the WWE activity is greatly controlled by tropical intraseasonal phenomena (Chapter 3; Hendon et al. 2007; Seiki and Takayabu 2007b; Puy et al. 2015), the better representation

of the intraseasonal and annual frequencies and the state dependence of atmospheric noise will increase the El Niño prediction skills and the reliability of future projection of ENSO in CGCMs.

References

Adler, R. F., G. J. Huffman, A. Chang, R. Ferraro, P.-P. Xie, J. Janowiak, B. Rudolf, U. Schneider, S. Curtis, D. Bolvin, A. Gruber, J. Susskind, P. Arkin, and E. Nelkin, 2003: The version-2 global precipitation climatology project (GPCP) monthly precipitation analysis (1979-present). *J. Hydrometeor*, **4**, 1147–1167.

An, S.-I., 2005: Interdecadal changes in the El Niño-La Niña asymmetry. *Geophys. Res. Lett.*, **31**, L23 210, doi:10.1029/2004GL021699.

——, 2008: Interannual variations of the tropical ocean instability wave and ENSO. *J. Climate*, **21**, 3680–3686.

——, 2009: A review of interdecadal changes in the nonlinearity of the El Niño-southern oscillation. *Theor. Appl. Climatol.*, **97**, 29–40.

——, Y.-G. Ham, J.-S. Kug, F.-F. Jin, and I.-S. Kang, 2005: El Niño-La Niña asymmetry in the Coupled Model Intercomparison Project simulations. *J. Climate*, **18**, 2617–2627.

—— and F.-F. Jin, 2004: Nonlinearity and asymmetry of ENSO. *J. Climate*, **17**, 2399–2412.

Ashok, K., S. K. Behera, S. A. Rao, H. Weng, and T. Yamagata, 2007: El Niño Modoki and its possible teleconnection. *J. Geophys. Res.*, **112**, C11 007, doi:10.1029/2006JC003798.

Barnston, A. G., M. K. Tippett, M. L. L'Heureux, S. Li, and D. G. DeWitt, 2012: Skill of real-time seasonal ENSO model predictions during 2002-11: Is our capability increasing? *Bull. Amer. Meteorol. Soc.*, **93**, 631–651.

Battisti, D. S. and A. C. Hirst, 1989: Interannual variability in a tropical atmosphere-ocean model: Influence of the basic state, ocean geometry and nonlinearity. *J. Atmos. Sci.*, **46**, 1687–1712.

Bejarano, L. and F.-F. Jin, 2008: Coexistence of equatorial coupled modes of ENSO. *J. Climate*, **21**, 3051–3067.

Belamari, S., J.-L. Redelsperger, and M. Pontaud, 2003: Dynamic role of a westerly wind burst in triggering an equatorial Pacific warm event. *J. Climate*, **16**, 1869–1890.

Cai, W., A. Santoso, G. Wang, S.-W. Yeh, S.-I. An, K. Cobb, M. Collins, E. Guilyardi, F.-F. Jin, J.-S. Kug, M. Lengaigne, M. J. McPhaden, K. Takahashi, A. Timmermann, G. Vecchi, M. Watanabe, and L. Wu, 2015: ENSO and greenhouse warming. *Nature Clim. Change*, doi:10.1038/nclimate2743.

Capotondi, A., A. T. Wittenberg, M. Newman, E. Di Lorenzo, J.-Y. Yu, P. Braconnot, J. Cole, B. Dewitte, B. Giese, E. Guilyardi, F.-F. Jin, K. Karnauskas, B. Kirtman, T. Lee, N. Schneider, Y. Xue, and S.-W. Yeh, 2015: Understanding ENSO diversity. *Bull. Amer. Meteorol. Soc.*, **96**, 921–938, doi:10.1175/BAMS-D-13-00117.1.

Chen, D., S. E. Zebiak, A. J. Busalacchi, and M. A. Cane, 1995: An improved procedure for El Niño forecasting: Implications for predictability. *Science*, **269**, 1699–1702.

——, T. Lian, C. Fu, M. A. Cane, Y. Tang, R. Murtugudde, X. Song, Q. Wu, and L. Zhou, 2015: Strong influence of westerly wind bursts on El Niño diversity. *Nature Geosci.*, **8**, 339–345, doi:10.1038/ngeo2399.

Chiodi, A. M. and D. E. Harrison, 2015: Equatorial Pacific easterly wind surges and the onset of La Niña events. *J. Climate*, **28**, 776–792.

——, ——, and G. A. Vecchi, 2014: Subseasonal atmospheric variability and El Niño waveguide warming: Observed effects of the Madden-Julian oscillation and westerly wind events. *J. Climate*, **27**, 3619–3642.

Collins, M., S.-I. An, W. Cai, A. Ganachaud, E. Guilyardi, F.-F. Jin, M. Jochum, M. Lengaigne, S. Power, A. Timmermann, G. Vecchi, and A. Wittenberg, 2010: The impact of global warming on the tropical Pacific Ocean and El Niño. *Nature Geosci.*, **3**, 391–397.

Drushka, K., H. Bellenger, E. Guilyardi, M. Lengaigne, J. Vialard, and G. Madec, 2014: Processes driving intraseasonal displacements of the eastern edge of the warm pool: The contribution of westerly wind events. *Clim. Dyn.*, 1–21, doi:10.1007/s00382-014-2297-z.

Duan, W., H. Xu, and M. Mu, 2008: Decisive role of nonlinear temperature advection in El Niño and La Niña amplitude asymmetry. *J. Geophys. Res.*, **113**, C01 014, doi:10.1029/2006JC003974.

Eisenman, I., L. Yu, and E. Tziperman, 2005: Westerly wind bursts: ENSO's tail rather than the dog? *J. Climate*, **18**, 5224–5238.

Fedorov, A. V., 2002: The response of the coupled tropical ocean-atmosphere to westerly wind bursts. *Q. J. R. Meteorol. Soc.*, **128**, 1–23.

——, S. L. Harper, S. G. Philander, B. Winter, and A. Witternberg, 2003: How predictable is El Niño? *Bull. Amer. Meteorol. Soc.*, **84**, 911–919.

——, S. Hu, M. Lengaigne, and E. Guilyardi, 2015: The impact of westerly wind bursts and ocean initial state on the development, and diversity of El Niño events. *Clim. Dyn.*, **44**, 1381–1401, doi:10.1007/s00382-014-2126-4.

—— and S. G. Philandar, 2000: El Niño changing? *Science*, **288**, 1997–2002.

—— and ——, 2001: A stability analysis of tropical ocean-atmosphere interactions: Bridging measurements and theory for El Niño. *J. Climate*, **14**, 3086–3101.

Fuchs, Z., S. Gjorgjievska, and D. Raymond, 2012: Effects of varying the shape of the convective heating profile on convectively coupled gravity waves and moisture modes. *J. Atmos. Sci.*, **69**, 2505–2519.

Gebbie, G., I. Eisenman, A. Witternberg, and E. Tziperman, 2007: Modulation of westerly wind bursts by sea surface temperature: A semistochastic feedback for ENSO. *J. Atmos. Sci.*, **64**, 3281–3295.

—— and E. Tziperman, 2009: Predictability of SST-modulated westerly wind bursts. *J. Climate*, **22**, 3894–3909.

Giese, B. S. and D. E. Harrison, 1991: Eastern equatorial Pacific response to three composite westerly wind types. *J. Geophys. Res.*, **96**, 3239–3248.

—— and S. Ray, 2011: El Niño variability in simple ocean data assimilation (SODA), 1871-2008. *J. Geophys. Res.*, **116**, C02 024, doi:10.1029/2010JC006695.

Gushchina, D. and B. Dewitte, 2012: Intraseasonal tropical atmospheric variability associated with the two flavors of El Niño. *Mon. Wea. Rev.*, **140**, 3669–3681.

Hansen, D. V. and C. A. Paul, 1984: Genesis and effects of long waves in the equatorial Pacific. *J. Geophys. Res.*, **89**, 10 431–10 440.

Harrison, D. E. and B. S. Giese, 1988: Remote westerly wind forcing of the eastern equatorial Pacific; some model results. *Geophys. Res. Lett.*, **15**, 804–807.

—— and P. S. Schopf, 1984: Kelvin-wave-induced anomalous advection and the onset of surface warming in El Niño events. *Mon. Wea. Rev.*, **112**, 923–933.

—— and G. A. Vecchi, 1997: Westerly wind events in the tropical Pacific, 1986–95. *J. Climate*, **10**, 3131–3156.

Hartten, L. M., 1996: Synoptic setting of westerly wind bursts. *J. Geophys. Res.*, **101**, 16 997–17 019.

Hendon, H. H., E. Lim, G. Wang, O. Alves, and D. Hudson, 2009: Prospects for predicting two flavors of El Niño. *Geophys. Res. Lett.*, **36**, L19 713, doi: 10.1029/2009GL040100.

——, M. C. Wheeler, and C. Zhang, 2007: Seasonal dependence of the MJO-ENSO relationship. *J. Climate*, **20**, 531–543.

Hu, S., A. V. Fedorov, M. Lengaigne, and E. Guilyardi, 2014: The impact of westerly wind bursts on the diversity and predictability of El Niño events: An ocean energetics perspective. *Geophys. Res. Lett.*, **41**, 4654–4663, doi:10.1002/2014GL059573.

Hung, M.-P., J.-L. Lin, W. Wang, D. Kim, T. Shinoda, and S. J. Weaver, 2013: MJO and convectively coupled equatorial waves simulated by CMIP5 climate models. *J. Climate*, **26**, 6185–6214.

Imada, Y., H. Tatebe, M. Ishii, Y. Chikamoto, M. Mori, M. Arai, M. Watanabe, and M. Kimoto, 2015: Predictability of two types of El Niño assessed using an extended seasonal prediction system by MIROC. *Mon. Wea. Rev.*, **143**, 4597–4617.

Ishii, M. and M. Kimoto, 2009: Reevaluation of historical ocean heat content variations with time-varying XBT and MBT depth bias corrections. *J. Oceanogr.*, **65**, 287–299.

——, A. Shoji, S. Sugimoto, and T. Matsumoto, 2005: Objective analyses of sea-surface temperature and marine meteorological variables for the 20th century using ICOADS and the Kobe collection. *Int. J. Climatol.*, **25**, 865–879.

Jin, F.-F., 1997a: An equatorial ocean recharge paradigm for ENSO. Part I: Conceptual model. *J. Atmos. Sci.*, **54**, 811–829.

——, 1997b: An equatorial ocean recharge paradigm for ENSO. Part II: A stripped-down coupled model. *J. Atmos. Sci.*, **54**, 830–847.

——, S.-I. An, A. Timmermann, and J. Zhao, 2003: Strong El Niño events and nonlinear dynamical heating. *Geophys. Res. Lett.*, **30**, 1120, doi:10.1029/2002GL016356.

——, L. Lin, A. Timmermann, and J. Zhao, 2007: Ensemble-mean dynamics of the ENSO recharge oscillator under state-dependent stochastic forcing. *Geophys. Res. Lett.*, **34 (3)**, doi:10.1029/2006GL027372.

Kalnay, E., M. Kanamitsu, R. Kistler, W. Collins, D. Deaven, L. Gandin, M. Iredell, S. Saha, G. White, J. Woollen, Y. Zhu, A. Leetmaa, R. Reynolds, M. Chelliah, W. Ebisuzaki, W. Higgins, J. Janowiak, K. C. Mo, C. Ropelewski, J. Wang, R. Jenne, and D. Joseph, 1996: The NCEP/NCAR 40-year reanalysis project. *Bull. Amer. Meteorol. Soc.*, **77**, 437–470.

Kang, I.-S., S.-I. An, and F.-F. Jin, 2001: A systematic approximation of the SST anomaly equation for ENSO. *J. Meteorol. Soc. Japan*, **79**, 1–10.

—— and J.-S. Kug, 2000: An El Niño prediction system using an intermediate ocean and a statistical atmosphere. *Geophys. Res. Lett.*, **27**, 1167–1170.

Kao, H.-Y. and J.-Y. Yu, 2009: Contrasting eastern-Pacific and central-Pacific types of ENSO. *J. Climate*, **22**, 615–632.

Kapur, A. and C. Zhang, 2012: Multiplicative MJO forcing of ENSO. *J. Climate*, **25**, 8132–8147.

——, ——, J. Zavala-Garay, and H. H. Hendon, 2012: Role of stochastic forcing in ENSO in observations and a coupled GCM. *Clim. Dyn.*, **38**, 87–107.

Karnauskas, K. B., 2013: Can we distinguish canonical El Niño from Modoki? *Geophys. Res. Lett.*, **40**, 5246–5251, doi:10.1002/grl.51007.

Kessler, W. S. and R. Kleeman, 2000: Rectification of the Madden-Julian oscillation into the ENSO cycle. *J. Climate*, **13**, 3560–3575.

Kiladis, G. N. and M. Wheeler, 1995: Horizontal and vertical structure of observed tropospheric equatorial Rossby waves. *J. Geophys. Res.*, **100**, 22 981–22 997.

Kimoto, M. and M. Ghil, 1993: Multiple flow regimes in the Northern Hemisphere winter. Part I: Methodology and hemispheric regimes. *J. Atmos. Sci.*, **50**, 2625–2644.

Kirtman, B. P. and S. E. Zebiak, 1997: ENSO simulation and prediction with a hybrid coupled model. *Mon. Wea. Rev.*, **125**, 2620–2641.

Kobayashi, S., Y. Ota, Y. Harada, A. Ebita, M. Moriya, H. Onoda, K. Onogi, H. Kamahori, C. Kobayashi, H. Endo, K. Miyaoka, and K. Takahashi, 2015: The JRA-55 reanalysis: General specifications and basic characteristics. *J. Meteorol. Soc. Japan*, **93**, 5–48, doi: 10.2151/jmsj.2015-001.

Kug, J.-S., F.-F. Jin, and S.-I. An, 2009: Two types of El Niño events: Cold tongue El Niño and warm pool El Niño. *J. Climate*, **22**, 1499–1515.

——, ——, K. P. Sooraj, and I.-S. Kang, 2008: State-dependent atmospheric noise associated with ENSO. *Geophys. Res. Lett.*, **35**, L05 701, doi:10.1029/2007GL032017.

——, I.-S. Kang, and J.-G. Jhun, 2005: Western Pacific SST prediction with an intermediate El Niño prediction model. *Mon. Wea. Rev.*, **133**, 1343–1352.

Larkin, N. K. and D. E. Harrison, 2005: Global seasonal temperature and precipitation anomalies during El Niño autumn and winter. *Geophys. Res. Lett.*, **32**, L16 705, doi: 10.1029/2005GL022860.

Latif, M., J. Biercamp, and H. V. Storch, 1988: The response of a coupled ocean-atmosphere general circulation model to wind bursts. *J. Atmos. Sci.*, **45**, 964–979.

Lengaigne, M., J.-P. Boulanger, C. Menkes, G. Madec, P. Delecluse, E. Guilyardi, and J. Slingo, 2003: The March 1997 westerly wind event and the onset of the 1997/98 El Niño: Understanding the role of the atmospheric response. *J. Climate*, **16**, 3330–3343.

——, ——, ——, S. Masson, G. Madec, and P. Delecluse, 2002: Ocean response to the March 1997 westerly wind event. *J. Geophys. Res.*, **107**, 8015, doi: 10.1029/2001JC000841.

——, ——, ——, and H. Spencer, 2006: Influence of the seasonal cycle on the termination of El Niño events in a coupled general circulation model. *J. Climate*, **19**, 1850–1868.

——, E. Guilyardi, J.-P. Boulanger, C. Menkes, P. Delecluse, P. Inness, J. Cole, and J. Slingo, 2004: Triggering of El Niño by westerly wind events in a coupled general circulation model. *Clim. Dyn.*, **22**, 601–620, doi:10.1007/s00382-004-0457-2.

Levine, A. F. Z. and F.-F. Jin, 2010: Noise-induced instability in the ENSO recharge oscillator. *J. Atmos. Sci.*, **67**, 529–542.

—— and ——, 2015: A simple approach to quantifying the noise-ENSO interaction. Part I: deducing the state-dependency of the windstress forcing using monthly mean data. *Clim. Dyn.*, doi:10.1007/s00382-015-2748-1.

—— and M. McPhaden, 2015: The annual cycle in ENSO growth rate as a cause of the spring predictability barrier. *Geophys. Res. Lett.*, **42**, 5034–5041, doi: 10.1002/2015GL064309.

Li, G. and S.-P. Xie, 2014: Tropical biases in CMIP5 multimodel ensemble: The excessive equatorial Pacific cold tongue and double ITCZ problems. *J. Climate*, **27**, 1765–1780.

Lian, T., D. Chen, Y. Tang, and Q. Wu, 2014: Effects of westerly wind bursts on El Niño: A new perspective. *Geophys. Res. Lett.*, **41**, 3522–3527, doi:10.1002/2014GL059989.

Liebmann, B. and C. A. Smith, 1996: Description of a complete (interpolated) outgoing longwave radiation dataset. *Bull. Amer. Meteorol. Soc.*, **77**, 1275–1277.

Lopez, H. and B. P. Kirtman, 2013: Westerly wind bursts and the diversity of ENSO in CCSM3 and CCSM4. *Geophys. Res. Lett.*, **40**, 4722–4727, doi:10.1002/grl.50913.

——, ——, E. Tziperman, and G. Gebbie, 2013: Impact of interactive westerly wind bursts on CCSM3. *Dyn. Atmos. Ocean*, **59**, 24–51, doi: 10.1016/j.dynatmoce.2012.11.001.

Luther, D. S., D. E. Harrison, and R. A. Knox, 1983: Zonal winds in the central equatorial Pacific and El Niño. *Science*, **222**, 327–330.

Madden, R. A. and P. R. Julian, 1971: Detection of a 40–50 day oscillation in the zonal wind in the tropical Pacific. *J. Atmos. Sci.*, **28**, 702–708.

—— and ——, 1972: Description of global-scale circulation cells in the tropics with a 40–50 day period. *J. Atmos. Sci.*, **29**, 1109–1123.

—— and ——, 1994: Observations of the 40–50-day tropical oscillation—A review. *Mon. Wea. Rev.*, **112**, 814–837.

Masuda, S., J. P. Matthews, Y. Ishikawa, T. Mochizuki, Y. Tanaka, and T. Awaji, 2015: A new approach to El Niño prediction beyond the spring season. *Scientific Reports*, **5**, doi:10.1038/srep16782.

McPhaden, M. J., 1999: Genesis and evolution of the 1997–98 El Niño. *Science*, **283**, 950–954.

——, 2002: Mixed layer temperature balance on intraseasonal timescales in the equatorial Pacific Ocean. *J. Climate*, **15**, 2632–2647.

——, 2004: Evolution of the 2002/03 El Niño. *Bull. Amer. Meteorol. Soc.*, **85**, 677–695, doi:10.1175/BAMS-85-5-677.

——, 2015: Playing hide and seek with El Niño. *Bull. Amer. Meteorol. Soc.*, C02024, doi:10.1029/2010JC006695.

——, H. P. Freitag, S. P. Hayes, B. A. Taft, Z. Chen, and K. Wyrtki, 1988: The response of the equatorial Pacific Ocean to a westerly wind burst in May 1986. *J. Geophys. Res.*, **93**, 10 589–10 603.

——, T. Lee, and D. McClurg, 2011: El Niño and its relationship to changing background conditions in the tropical Pacific Ocean. *Geophys. Res. Lett.*, **38**, L15 709, doi:10.1029/2011GL048275.

——, A. Timmermann, M. J. Widlansky, M. A. Balmaseda, and T. N. Stockdale, 2015: The curious case of the El Niño that never happened: A perspective from 40 years of progress in climate research and forecasting. *Bull. Amer. Meteorol. Soc.*, **96**, 1647–1665, doi:10.1175/BAMS-D-14-00089.1.

—— and X. Yu, 1999: Equatorial waves and the 1997–98 El Niño. *Geophys. Res. Lett.*, **26**, 2961–2964.

Meehl, G. A., C. Covey, T. Delworth, M. Latif, B. McAvaney, J. F. B. Mitchell, R. J. Stouffer, and K. E. Taylor, 2007: The WCRP CMIP3 multimodel dataset: A new era in climate change research. *Bull. Amer. Meteorol. Soc.*, **88**, 1383–1394.

Menkes, C. E., M. Lengaigne, J. Vialard, M. Puy, P. Marchesiello, S. Cravatte, and G. Cambon, 2014: About the role of westerly wind events in the possible development of an El Niño in 2014. *Geophys. Res. Lett.*, **41**, doi:10.1002/2014GL061186.

Min, Q., J. Su, R. Zhang, and X. Rong, 2015: What hindered the El Niño pattern in 2014? *Geophys. Res. Lett.*, **42**, doi:10.1002/2015GL064899.

Miyama, T. and T. Hasegawa, 2014: Impact of sea surface temperature on westerlies over the western Pacific warm pool: Case study of an event in 2001/02. *SOLA*, **10**, 5–9, doi:10.2151/sola.2014-002.

Perez, C. L., A. M. Moore, J. Zavala-Garay, and R. Kleeman, 2005: A comparison of the influence of additive and multiplicative stochastic forcing on a coupled model of ENSO. *J. Climate*, **18**, 5066–5085.

Picaut, J., M. Ioualalen, C. Menkes, T. Delcroix, and M. J. McPhaden, 1996: Mechanism of the zonal displacements of the Pacific warm pool: Implications for ENSO. *Science*, **274**, 1486–1489.

Puy, M., J. Vialard, M. Lengaigne, and E. Guilyardi, 2015: Modulation of equatorial pacific westerly/easterly wind events by the Madden-Julian oscillation and convectively-coupled Rossby waves. *Clim. Dyn.*, doi:10.1007/s00382-015-2695-x.

Qiao, L. and R. H. Weisberg, 1995: Tropical instability wave kinematics: Observations from the Tropical Instability Wave Experiment. *J. Geophys. Res.*, **100**, 8677–8693.

Ren, H.-L., J. Zuo, F.-F. Jin, and M. F. Stuecker, 2015: ENSO and annual cycle interaction: The combination mode representation in CMIP5 models. *Clim. Dyn.*, doi: 10.1007/s00382-015-2802-z.

Reynolds, R. W., T. M. Smith, C. Liu, D. B. Chelton, K. S. Casey, and M. G. Schlax, 2007: Daily high-resolution-blended analyses for sea surface temperature. *J. Climate*, **20**, 5473–5496.

Schopf, P. S. and M. J. Suarez, 1988: Vacillations in a coupled ocean-atmosphere model. *J. Atmos. Sci.*, **45**, 549–566.

Seiki, A. and Y. N. Takayabu, 2007a: Westerly wind bursts and their relationship with intraseasonal variations and ENSO. Part I: Statistics. *Mon. Wea. Rev.*, **135**, 3325–3345.

—— and ——, 2007b: Westerly wind bursts and their relationship with intraseasonal variations and ENSO. Part II: Energetics over the western and central Pacific. *Mon. Wea. Rev.*, **135**, 3346–3361.

Smyth, W. D., D. Hebert, and J. N. Moum, 1996: Local ocean response to a multiphase westerly wind burst: 1. Dynamic response. *J. Geophys. Res.*, **101**, 22 495–22 512.

Sooraj, K. P., D. Kim, J.-S. Kug, S.-W. Yeh, F.-F. Jin, and I.-S. Kang, 2009: Effects of the low-frequency zonal wind variation on the high frequency atmospheric variability over the tropics. *Clim. Dyn.*, **33**, 495–507.

Stein, K., A. Timmermann, N. Schneider, F.-F. Jin, and M. F. Stuecker, 2014: ENSO seasonal synchronization theory. *J. Climate*, **27**, 5285–5310, doi:10.1175/JCLI-D-13-00525.1.

Stuecker, M. F., F.-F. Jin, and A. Timmermann, 2015b: El Niño–Southern Oscillation frequency cascade. *PNAS*, **112**, 13 490–13 495.

——, ——, ——, and S. McGregor, 2015a: Combination mode dynamics of the anomalous northwest Pacific anticyclone. *J. Climate*, **28**, 1093–1111.

——, A. Timmermann, F.-F. Jin, S. McGregor, and H.-L. Ren, 2013: A combination mode of the annual cycle and the El Niño/Southern Oscillation. *Nature Geosci.*, **6**, 540–544, doi:10.1038/NGEO1826.

Takahashi, K., A. Montecinos, K. Goubanova, and B. Dewitte, 2011: ENSO regimes: Reinterpreting the canonical and Modoki El Niño. *Geophys. Res. Lett.*, **38**, L10 704, doi:10.1029/2011GL047364.

Takayabu, Y. N., T. Iguchi, M. Kachi, A. Shibata, and H. Kanzawa, 1999: Abrupt termination of the 1997–98 El Niño in response to a Madden-Julian oscillation. *Nature*, **402**, 279–282.

Taschetto, A. S., A. S. Gupta, N. C. Jourdain, A. Santoso, C. C. Ummenhofer, and M. H. England, 2014: Cold tongue and warm pool ENSO events in CMIP5: Mean state and future projections. *J. Climate*, **27**, 2861–2885.

Tatebe, H. and H. Hasumi, 2010: Formation mechanism of the Pacific equatorial thermocline revealed by a general circulation model with a high accuracy tracer advection scheme. *Ocean Modelling*, **35**, 245–252.

Taylor, K. E., R. J. Stouffer, and G. A. Meehl, 2012: An overview of CMIP5 and the experiment design. *Bull. Amer. Meteorol. Soc.*, **93**, 485–498.

Timmermann, A. and F.-F. Jin, 2002: A nonlinear mechanism for decadal El Niño amplitude changes. *Geophys. Res. Lett.*, **29**, 1003, doi:10.1029/2001GL013369.

——, ——, and J. Abshagen, 2003: A nonlinear theory for El Niño bursting. *J. Atmos. Sci.*, **60**, 152–165.

Trenberth, K., W. G. Large, and J. G. Olson, 1989: The effective drag coefficient for evaluating wind stress over the oceans. *J. Climate*, **2**, 1507–1516.

Tziperman, E. and L. Yu, 2007: Quantifying the dependence of westerly wind bursts on the large-scale tropical Pacific SST. *J. Climate*, **20**, 2760–2768.

——, S. E. Zebiak, and M. A. Cane, 1997: Mechanisms of seasonal–ENSO interaction. *J. Atmos. Sci.*, **54**, 61–71.

Vecchi, G. A. and D. E. Harrison, 2000: Tropical Pacific sea surface temperature anomalies, El Niño, and equatorial westerly wind events. *J. Climate*, **13**, 1814–1830.

——, A. T. Wittenberg, and A. Rosati, 2006: Reassessing the role of stochastic forcing in the 1997–1998 El Niño. *Geophys. Res. Lett.*, **33**, L01 706, doi:10.1029/2005GL024738.

Watanabe, M. and F.-F. Jin, 2003: A moist linear baroclinic model: Coupled dynamical-convective response to El Niño. *J. Climate*, **16**, 1121–1139.

—— and M. Kimoto, 2000: Atmosphere-ocean thermal coupling in the North Atlantic: A positive feedback. *Quart. J. R. Meteorol. Soc.*, **126**, 2247–2250.

—— and ——, 2001: Corrigendum. *Quart. J. R. Meteorol. Soc.*, **127**, 733–734.

——, H. Shiogama, H. Tatebe, M. Hayashi, M. Ishii, and M. Kimoto, 2014: Contribution of natural decadal variability to global warming acceleration and hiatus. *Nature Clim. Change*, **4**, 893–897.

——, T. Suzuki, R. O'ishi, Y. Komuro, S. Watanabe, S. Emori, T. Takemura, M. Chikira, T. Ogura, M. Sekiguchi, K. Takata, D. Yamazaki, T. Yokohata, T. Nozawa, H. Hasumi, H. Tatebe, and M. Kimoto, 2010: Improved climate simulation by MIROC5: Mean states, variability, and climate sensitivity. *J. Climate*, **23**, 6312–6335.

Wheeler, M. C. and H. H. Hendon, 2004: An all-season real-time multivariate MJO index: Development of an index for monitoring and prediction. *Mon. Wea. Rev.*, **132**, 1917–1932.

Wyrtki, K., 1975: El Niño—The dynamic response of the equatorial Pacific Ocean to atmospheric forcing. *J. Phys. Oceanogr.*, **5**, 572–584.

——, 1985: Sea level fluctuations in the Pacific during the 1982–1983 El Niño. *Geophys. Res. Lett.*, **12**, 125–128.

Xiang, B., B. Wang, and T. Li, 2013: A new paradigm for the predominance of standing central Pacific warming after the late 1990s. *Clim. Dyn.*, **41**, 327–340.

Xie, R., F.-F. Jin, and F. Huang, 2015: An improved atmospheric component of Zebiak-Cane model for simulating ENSO winds. *J. Meteorol. Soc. Japan*, **93**, 535–550.

Xie, S.-P., 1996: Westward propagation of latitudinal asymmetry in a coupled ocean-atmosphere model. *J. Atmos. Sci.*, **53**, 3236–3250.

—— and S. G. H. Philander, 1994: A coupled ocean-atmosphere model of relevance to the ITCZ in the eastern Pacific. *Tellus A*, **46**, 345–350.

Yang, G.-Y., B. Hoskins, and J. Slingo, 2007: Convectively coupled equatorial waves. Part I: Horizontal and vertical structures. *J. Atmos. Sci.*, **64**, 3406–3423.

Yeh, S.-W., J.-S. Kug, , and S.-I. An, 2014: Recent progress on two types of El Niño: Observations, dynamics, and future changes. *Asia-Pac. J. Atmos. Sci.*, **50**, 69–81.

——, ——, B. Dewitte, M.-H. Kwon, B. P. Kirtman, and F.-F. Jin, 2009: El Niño in a changing climate. *Nature*, **461**, 511–514, doi:10.1038/nature08316.

Yu, L., R. A. Weller, and W. T. Liu, 2003: Case analysis of a role of ENSO in regulating the generation of westerly wind bursts in the western equatorial Pacific. *J. Geophys. Res.*, **108(C4)**, 3128, doi:10.1029/2002JC001498.

Zavala-Garay, J., C. Zhang, A. M. Moore, and R. Kleeman, 2005: The linear response of ENSO to the Madden-Julian oscillation. *J. Climate*, **18**, 2441–2459.

Zebiak, S. E. and M. A. Cane, 1987: A model El Niño-Southern Oscillation. *Mon. Wea. Rev.*, **115**, 2262–2278.

Zelle, H., G. Appeldoorn, G. Burgers, and G. J. van Oldenborgh, 2004: The relationship between sea surface temperature and thermocline depth in the eastern equatorial Pacific. *J. Phys. Oceanogr.*, **34**, 643–655.

Zhang, C., 1993: Large-scale variability of atmospheric deep convection in relation to sea surface temperature in the tropics. *J. Climate*, **6**, 1898–1913.

——, 2005: Madden-Julian oscillation. *Rev. Geophys.*, **43**, RG2003, doi: 10.1029/2004RG000158.

Zhang, T. and D.-Z. Sun, 2014: ENSO asymmetry in CMIP5 models. *J. Climate*, **27**, 4070–4093.

Zhang, X., H. Liu, and M. Zhang, 2015: Double ITCZ in coupled ocean-atmosphere models: From CMIP3 to CMIP5. *Geophys. Res. Lett.*, **42**, 8651–8659, doi: 10.1002/2015GL065973.